Universidade do Minho
Escola de Ciências

Carolina Passos Rodrigues

An integrated liquid biopsy microfluidic device for the isolation, recovery, encapsulation and sorting of circulating cancer cells

december 2021

An integrated liquid biopsy microfluidic device for the isolation, recovery, encapsulation and sorting of circulating cancer cells

Carolina Rodrigues

UMinho | 2021

Universidade do Minho
Escola de Ciências

Carolina Passos Rodrigues

An integrated liquid biopsy microfluidic device for the isolation, recovery, encapsulation and sorting of circulating cancer cells

Master Thesis
Master in Biophysics and Bionanosystems

Work developed under the supervision of
Dr. Sara Abalde - Cela and
Prof. Dr. Ana Arminda Lopes Preto

december 2021

DIREITOS DE AUTOR E CONDIÇÕES DE UTILIZAÇÃO DO TRABALHO POR TERCEIROS

Este é um trabalho académico que pode ser utilizado por terceiros desde que respeitadas as regras e boas práticas internacionalmente aceites, no que concerne aos direitos de autor e direitos conexos.

Assim, o presente trabalho pode ser utilizado nos termos previstos na licença abaixo indicada.

Atribuição-NãoComercial-SemDerivações
CC BY-NC-ND

https://creativecommons.org/licenses/by-nc-nd/4.0/

[Esta é a mais restritiva das nossas seis licenças principais, só permitindo que outros façam download dos seus trabalhos e os compartilhem desde que lhe sejam atribuídos a si os devidos créditos, mas sem que possam alterá-los de nenhuma forma ou utilizá-los para fins comerciais.]

Acknowledgments

What's the point of all the finish lines we cross in life if there's no one there to celebrate with?

As I reach another finish line and complete one of the biggest stages of my life and academic journey, the moment has come to thank individually all the people who made this possible.

First, I would like to thank my supervisor, Dra. Sara Abalde-Cela for giving me the opportunity to work on this project and for all the assistance, guidance, and dedicated involvement in every step throughout the project, but above it all for being a great source of admiration and professionalism.

Similarly, I would also like to express my gratitude to my university supervisor, Dra. Ana Preto, for the availability and support, provided during the thesis.

Furthermore, I would like to manifest my deepest thanks to Dra. Lorena Díeguez for accepting me into her team and for providing the space and all the necessary resources, as well as all her expertise and helpful insights that contributed to overcoming the obstacles faced during the thesis. I´d also like to thank Paulina Piairo for the help with the biological samples and all the availability provided during this year.

I was very fortunate to work with brilliant people at INL, particularly Alexandra Teixeira and Adriana Carneiro. To you both, my sincere thanks for all the shared knowledge, all your unstinting support, infinite patience and availability, and for your friendship.

To my project colleague and friend, Madalena, thank you for all the support, companionship, and moments of relaxation.

I would also like to acknowledge my friends that I carried with me for life, for all the endless support, for all the advice, friendly words and, for being there to lift me in the bad moments.

Last, but most importantly, I would like to express my gratitude to my parents and brother. My parents, for all the unconditional love, for being my pillars of strength and support, for the education they provided me with, and for all the advice and words of encouragement and trust in the most difficult moments. My brother, for being my greatest pride, my best friend, and my source of admiration.

STATEMENT OF INTEGRITY

I hereby declare having conducted this academic work with integrity. I confirm that I have not used plagiarism or any form of undue use of information or falsification of results along the process leading to its elaboration.

I further declare that I have fully acknowledged the Code of Ethical Conduct of the University of Minho.

Dispositivo de microfluídica integrado de biopsia líquida para o isolamento, recuperação, encapsulamento e *sorting* de células tumorais circulantes

Resumo

Nos últimos anos, a medicina personalizada tem florescido no campo da oncologia. Neste âmbito, surgiu o conceito de biopsia líquida, como alternativa aos métodos de diagnóstico convencionais, baseando-se na análise de biomarcadores tumorais presentes nos fluidos corporais, tais como as células tumorais circulantes (CTCs). A quantificação e caracterização destes biomarcadores provou ser clinicamente valiosa para previsão e monitorização de tumores e, para a designação de tratamentos apropriados. Adicionalmente, para avaliar a heterogeneidade tumoral, é fundamental realizar estudos sobre a população de células tumorais a um nível de célula individual. As tecnologias baseadas na microfluídica são altamente aplicadas para estes ensaios de deteção e para estudos individuais a nível celular, pois permitem a manipulação individual de células com elevada seletividade e especificidade, e proporcionam uma fácil automatização e capacidade de paralelização.

Assim, com este projeto, pretendemos criar um sistema de microfluídica que integre o isolamento, recuperação, encapsulamento e separação de células tumorais. Para tal, utilizando o RUBYChip™, foi concebido e optimizado um protocolo de recuperação de células de uma linha celular de cancro colorectal (SW480) em tampão fosfato salino (PBS) e sangue, atingindo um máximo de recuperação de 51.4% e 48.4%, respetivamente. Posteriormente, foi fabricado um dispositivo de microfluídica composto por um gerador de microgotas e uma área de separação, inicialmente testado com diferentes valores de velocidade de fluxo para avaliar os tamanhos médios das microgotas, obtendo tamanhos que variam entre 74 e 160 μm. Após a escolha de uma combinação adequada de velocidade de fluxo, foram efetuadas experiências de encapsulamento e separação, com diferentes valores de densidades celulares, obtendo eficiências de separação entre 33 - 40%.

Uma vez selecionadas as melhores condições, foram realizadas algumas experiências preliminares, englobando o isolamento e recuperação das células, bem como o encapsulamento e separação das células recuperadas, para estabelecer a interface entre ambas as partes. Uma integração bem-sucedida destes módulos microfluidícos pode abrir caminho à realização de estudos detalhados da sua morfologia e composição molecular e fenotípica para obter um perfil detalhado das células tumorais e uma melhor compreensão do seu papel em cada paciente.

Palavras-chave: Microfluídica, CTCs, recuperação, encapsulamento, separação

An integrated liquid biopsy microfluidic device for the isolation, recovery, encapsulation and sorting of circulating cancer cells

Abstract

In recent years, personalised medicine has flourished in the oncology field. Within this scope, the concept of liquid biopsy has arisen as an alternative methodology of current diagnostic methods, focusing on the analysis of tumour biomarkers present in body fluids, such as circulating tumour cells (CTCs). The quantification and characterisation of these biomarkers proved to be clinically valuable for tumour prediction, monitoring and treatment designation. In addition, it is pivotal to perform studies of the tumour cell population at a single-CTC level to deepen the information about tumour heterogeneity. Microfluidic technologies have been widely applied for the manipulation and analysis of single-cells demonstrating high selectivity and specificity, while providing easy automation and parallelisation capabilities.

In this context, within this project, we aim to create a microfluidic system that integrates the isolation, recovery, encapsulation, and sorting of CTCs. For this, using the RUBYChip™, a recovery protocol for a colorectal cancer cell model (SW480) was designed and optimised in phosphate-buffered saline (PBS) and blood, achieving a maximum of 51.4% and 48.4%, respectively. Thereafter, a microfluidic device composed of a droplet generator and a passive sorting area was designed and fabricated. Different flow rates ratio values were used to assess the average droplet size and sorting efficiency of those devices, obtaining droplets with sizes ranging from 74 to 160 μm. After choosing a suitable flow rate combination, cell encapsulation and sorting experiments were conducted with distinct cell densities of colorectal cancer cell model (SW480), reaching sorting efficiencies between 33-40%.

Once the best performance conditions were selected, some preliminary experiments, involving the in-line isolation, recovery, encapsulation and sorting of cells were carried out to establish the interface between the different microfluidic modules. The successful integration of these microfluidic modules may pave the way towards the performance of downstream analysis to obtain a more detailed and in-depth profiling of cancer cells and a better understanding of their role of in each patient.

Keywords: Microfluidics, CTCs, recovery, encapsulation, sorting

Table of Contents

List of Abbreviations

AFM - Atomic Force Microscopy

AR - Androgen Receptor

BSA - Bovine Serum Albumin

C - Cystine

COPD- Chronic Obstructive Pulmonary Disease

CRC- Colorectal Cancer

CDXs - CTC- Derivated Xenografts

CTCs- Circulating tumour cells

ctDNAs- Circulating tumour nucleic acids

DAPI - Diamidino-2-phenylindole

DEP - Dielectrophoresis

DFF - Dean Flow Fractionation

DLD - Deterministic Lateral Displacement

DMEM - Dulbecco´s Modified Eagle Médium

DWL - Direct Write Laser

EGR - Early Growth Response Gene

EMT- Epithelial to Mesenchymal Transitions

FACS- Fluorescence-Activated Cell Sorting

FDA - Food and Drug Administration

GEDI - Geometrically Enhanced Differential Immunocapture

GO - Graphene Oxide

LPDE – Low Density Polyethlene

MBC- Metastic Breast Cancer

MET-Mesenchymal-Epithelial Transition

MPA - Micropipette Aspiration

MRD- Minimal Residual Disease

OS- Overall Survival

PBMCs – Peripheral Blood Mononuclear Cells

PBS - Phosphate Buffer Saline

PDMS - polydimethylsiloxane

PDX - patient-xenografts models

PFA - Paraformaldehyde

PFS- Progression-Free Survival

RBC- Red Blood Cells

SCLC- Small Cell Lung Cancer

T- Thymine

WBC - White Blood Cells

List of. Figures

List of Tables

1. Introduction

1.1 Cancer and metastasis

Worldwide, cancer is considered the second most leading cause of mortality whose prevalence has increased over the years. Statistically, men have a higher incidence of prostate, lung and bronchus, colon and rectum, and urinary bladder cancer types. Meanwhile, women are mostly affected by breast, lung, and bronchus, colon and rectum, uterine corpus, and thyroid types of cancer [1]. Cancer development at a cellular level is considered a multistep process that comprises the mutation and selection of cells that exhibit an increased ability for proliferation, survival invasion, and metastasis.

Metastasis is the principal cause of morbidity and mortality, being responsible for over 90% of cancer-related deaths. In the process, also known as the metastasis cascade, tumour cells are shed from the primary tumour site, entering the blood or lymphatic vessel, and migrate to distant organs forming a new tumour [2].

The localization of metastasis may vary according to the type of cancer. For instance, lung tumour cells tend to metastasize to the brain, meanwhile, breast tumour cells mainly spread to the bones. This evidence indicates that it may exist a signaling phenomenon between the tumour cells and the secondary tumour site, resulting in their next metastasis. The origin of these signals may be due to interactions between different cell types, mechanical characteristics of the invading tumour cells microenvironment, or chemokines released from the secondary tumour sites [3].

During the metastatic cascade, the irregular growth of cells, leads to a local invasion of the tissue, forming a primary tumour and, subsequently an intravasation, i.e., the process by which the cancer cells enter into the circulation. Cancer cells to undertake intravasation, they must undergo epithelial to mesenchymal (EMT) transitions, where the tumour epithelial cells lose some properties such as polarity and cell adhesion, gaining the ability to migrate and invade. Once in the circulatory systems, if the tumour cells manage to survive, they may get attached to the vascular walls of distant tissues, undertaking extravasation, i.e., the process by which the cancer cell exit the circulation and invade secondary sites. At this secondary site, the cancer cells can proliferate and colonise, forming new metastases [4].

Recent studies have evidenced that after colonization, cancer cells may remain dormant for many years until they are detected. This dormancy occurs due to the enrichment of the extracellular matrix with the type III-collagen. Moreover, the breaching of the dormant cells triggers a signal pathway that restores their proliferation[5].

1.2 Cancer diagnosis

1.2.1 Tissue Biopsy

Currently, the characterization of the tumour is obtained through a tissue biopsy. Tissue biopsy is an invasive procedure that involves a surgical intervention to remove a small part of a tumour for further analysis. As the current standard of care for cancer diagnosis, tissue biopsy provides relevant information about the histology and grade of the tumour, along with other characteristics that help to choose a suitable treatment[6]. However, this method presents certain inherent complications and limitations, such as (1) difficulties in accessing the tumour in some anatomical locations; (2) the quantity of sample of tumour extracted may not be enough to perform all the required tests; (3) some preservation methods, per example formalin fixation, may cause C (cytosine) > T (thymine) transitions resulting in false-positive results for genetic tests; and, (4) the portion of the tumour removed for analysis may not be representative of the whole genetic tumour profile. Moreover, the tumour high heterogeneity and its ability to change or acquire new mutations, especially after systematic drug treatment, hinders the stratification of patients to a specific targeted therapy [7].

Thus, for efficient evaluation and treatment of the illness, is essential to monitor the evolution of the tumour and, solid biopsies fail to provide a complete and real-time snapshot of the tumour status and progression. Therefore, emerging fields in oncology research are developing new methods to assess the molecular profile of cancers based on tumour biomarkers that circulate in the bloodstream [8].

1.2.2 Liquid Biopsy

Liquid biopsy is a new diagnostic approach based on the collection of blood samples consisting on the isolation of tumour-derived components from peripheral blood such as circulating tumour cells (CTCs), circulating tumour nucleic acids (ctNAs), and/or tumour-derived extracellular vesicles (EVs) for further genomic and proteomic analysis [8].

This approach stands out from the conventional tissue biopsies (Figure 1) due to its non-invasiveness and its ability to monitor the tumour heterogeneity both spatial and temporarily. It enables a complete comprehension of the tumour microenvironment, taking into account different clones present in all metastatic sites [9]. Additionally, liquid biopsies are very versatile, enabling their repetition with the desired frequency for close monitoring of subclonal evolution, cancer progress, and treatment efficacy [10].

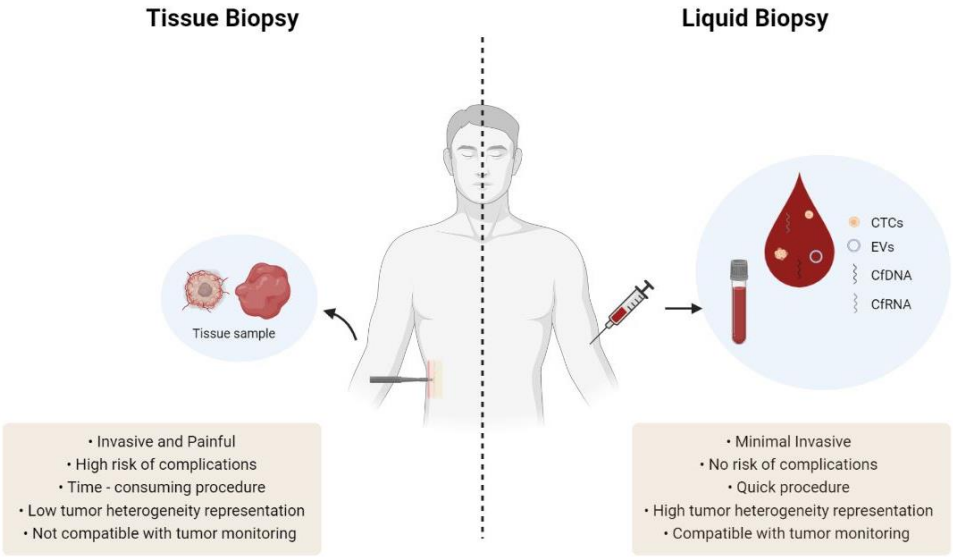

Figure 1- Main advantages of liquid biopsies versus tissue biopsies.(Adapted from [11])

Although blood is the most commonly used matrix in liquid biopsies, other biological fluids like saliva, urine, or cerebrospinal fluid also comprise a source of tumour-derived biomarkers [12].

The clinical significance of ctDNA has been widely reported in the literature. The ctDNA fingerprints the genetic profile of tumours, reflecting the mutations expressed in the primary and metastatic tumours. This way, their ability to detect specific mutations from various tumours has aroused much interest in its usage for cancer research. Nevertheless, given that this biomarker is found in small portions of the total sample and has a low half-life in circulation, its applicability is limited[13]. Likewise, EVs have also attracted some attention as a cancer biomarker, since they appear in greater number on the liquid biopsy samples, in comparison to CTCs and ctDNA. Furthermore, EVs possess a higher half-live and survival rate in circulation and prevent the degradation of proteins and nucleic acids encapsulated within their lipid shell. However, the isolation of EVs have significant technical challenges due to their variety of sizes which hinders their separation from the other blood components, impairing sample purity [14].

Despite all the tumour biomarkers that have been described and established in this field aim to a non-invasive real-time prognostic, predictive, and monitoring factor, the EVs area is still in a development stage. The analysis of ctDNA instead has proven to be more suitable for mutations detections, and it has made it through into the clinical practice [15][16][17]. However, the analysis of CTCs enables a broader assessment of whole cells, providing a genetic and protein-based molecular profiling.

1.3 Circulating Tumour Cells (CTCs)

Circulating Tumour Cells (CTCs) were first observed by Thomas Ashworth in 1860. However, their significant role in the metastatic process of different types of cancer was only assessed in the second half of the 20th century. The circulation of CTCs is considered an intermediate step of the metastatic process. CTCs are shed by a primary tumour and migrate into the circulatory system, enabling the development of distant metastases (Figure 2) [18].

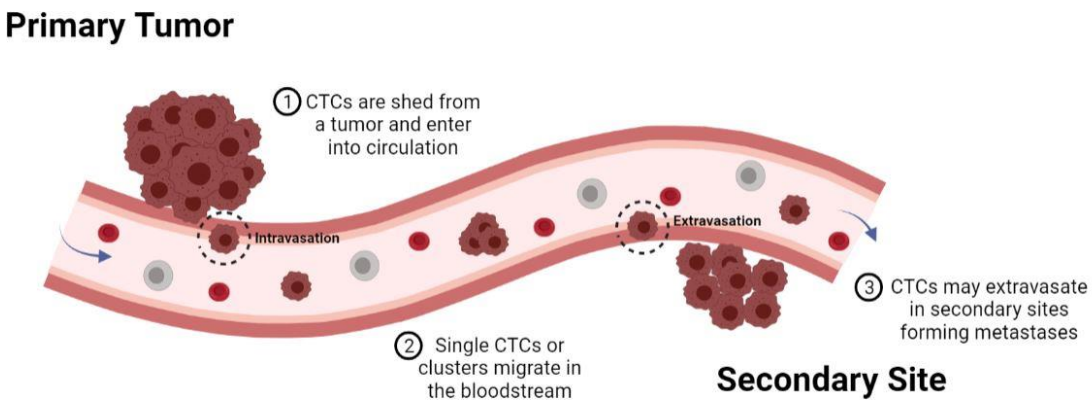

Figure 2- Schematic representation of the metastatic cascade. CTCs detach from a primary tumour proceeding with their intravasation into the bloodstream. Once reaching a distant site, they extravasate and originate new metastases.[Created in Biorender]

CTCs are found in a small percentage (usually 10 to 100 cells per 10 ml of blood) compared to other blood components and may exist in the form of individual cells or clusters. CTCs cluster display a faster extravasation, presenting a shorter half-life in circulation, in comparison to individual CTCs (6–10 min for clusters vs. 25–30 min for single cells), which aids in their survival and outgrowth. The survival rate of CTCs in the bloodstream is low due to the harsh conditions they are exposed to, such as physical stress (shear forces), fluid turbulences, anoikis, elimination by the immune system, and the absence of growth factors [19].

Like tumour cells, CTCs suffer EMT, which leads to phenotypic modifications, followed by a decrease of epithelial markers and acquisition of mesenchymal properties. This new phenotype enables the migration of the cells with the subsequent invasion through the basement membrane into the blood vessels. After the intravasation of CTCs and displacement throughout the bloodstream, they metastasise at a distant site. Thus, to form a secondary tumour, the cells must experience a reverse process of EMT-

mesenchymal-epithelial transition (MET), to recover their epithelial phenotype and capacity to disseminate and colonize distant organs [20].

1.3.1 The significance of CTCs: towards clinical utility and beyond

CTCs exhibit a promising potential as a biomarker for an early cancer diagnosis, prognosis, and to determine an appropriate treatment (Figure 3) [21]. This led to the emerging of new strategies for CTC counting and detection, in particular after the approval of the CellSearch® system. The CellSearch® operates through immunomagnetic particles coated with antibodies for the targeting of the epithelial cell-adhesion molecule (EpCAM). This system achieved clinical validation in metastatic breast cancer (MBC) colorectal cancer (CRC), and prostate cancer, in 2004, after a clinical testing program operated by Allard et al. [22]. In this study, blood samples from healthy patients and patients with diverse metastatic carcinomas were analysed. The presence of CTCs was detected in prostate cancers, breast cancers, ovarian cancers, CRCs, lung cancers, and other types of cancer in the percentage of 57, 37, 37, 30, 20 and 26 %, respectively. On the other hand, on the control sample, their existence was low or completely non-existent, proving that CTCs exhibit epithelial composition, which is characteristic of tumour pathologies [18][22].

The screening of patients prone to the development of cancer is a strategy used to accelerate the process of clinical validation. However, the low sensitivity and specificity of the CTCs make them limiting for screening. Nevertheless, a study by Ilie M Hofman et al. has shown that patients suffering from a chronic obstructive pulmonary disease (COPD), an indicator for lung cancer, presented CTCs 1-4 years earlier than what was evidenced in radiologic data obtained from a computed tomography scan.[19]

Moreover, the counting of CTCs in blood, while cancer patients are going through systemic therapies, serves as a prognostic factor for overall survival (OS) and progression-free survival (PFS) [21]. In an investigation conducted by Cristofanilli et al. [23], they found a correlation between the number of CTCs reported by CellSearch® essays and the survival rate of the patients. For this purpose, the data was collected from patients before the start of a new line of treatment and at the first follow-up visit. It was ascertained that patients with a high CTC count (≥5 CTCs) showed a median progression-free survival (PFS) of 2.7 months, versus 7 months for the patients with < 5 CTCs. Nonetheless, after the first follow-up, it was evidenced a decrease in the unfavorable group proportion, suggesting an improvement with the therapy implemented [18][23].

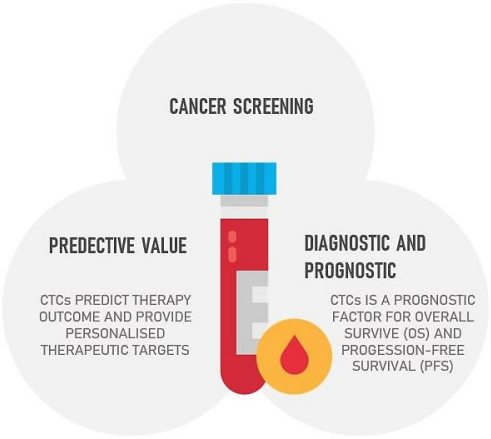

Figure 3 - Clinical Implications and Utilities of CTCs.

CTCs are a dynamic biomarker, in which its population is constantly being replaced by new circulating cells, mirroring the changes in systemic disease in real-time. In this context, numerous studies also demonstrated that CTCs enumeration can be helpful to determinate the risk of relapse and guide adjuvant therapy. A study by Lu, C.-Y., et al. [24] carried out in colon cancer patients exhibited that around 72.5 % of CTC- positive patients suffered a relapse after surgery, compared to 12 % of patients who have not detected CTCs. These results allowed the identification of patients with minimal residual disease (MRD), who were given adjuvant chemotherapy [19][24].

However, to complete the validation of CTCs as a major biomarker candidate for liquid biopsy, one should not only focus on single-cell analysis of CTCs in patients but also extend its studies for the development of in vitro and in vivo models to thoroughly characterize CTCs. [25]

In this context, Zhang et al. [26] were the first to accomplish a primary culture of CTCs isolated from blood samples of breast cancer patients. Through the use of fluorescence-activated cell sorting (FACS), they were able to isolate CTCs with the phenotype $CD45^{(-)}/ALDH1^{(+)}/EpCAM^{(+)}$, but some subpopulations did not express the $EpCAM^{(-)}$, only the $ALDH1^{(+)}$, revealing a propensity towards the formation of distant metastasis. Additionally, this CTC line was cultured for more than 21 days, and another FACS analysis indicated the presence of more indicators associated with brain tumour metastasis. In a follow up work, immunodeficient mice were subjected to the injection of these tumour cells, resulting in the development of tumours in the brain and lungs after 6 weeks. In this way, we may ascertain that, beyond enumeration essays, *in vitro* and *in vivo* studies are important steps for functional characterisation and understanding of CTCs and metastatic invasion mechanisms [25][26].

To overcome possible difficulties in establishing in vitro CTC lines very often researchers resort to the usage of patient-xenografts models (PDX). This approach consists of implementing tumour tissues samples directly in mice for their expansion. In comparison to cancer cell lines, these models enable the mimicking of the tumour molecular complexity and heterogeneity, and the evaluation of personalized therapies *in vivo*. Due to the challenges of obtaining a tissue sample, CTC-derived xenografts (CDXs) are widely applied [25].

For instance, in a work by Drapkin et al. [27] a PDX and CDX from patients with small cell lung cancer (SCLC) was reproduced, followed by the *in vivo* analysis of drug sensitivity to assess the development of resistance at different disease stages.

Currently, it still is not possible to state a more appropriate or accurate method, thus the ideal scenario is to combine distant experiment models to address specific research questions.

1.4 Microfluidic-based Technologies for CTCs Isolation and Detection

With the increasing popularity of research in the field of CTCs, there has been a high demand for innovative and effective techniques for CTCs isolation and detection.

The isolation technologies must follow three fundamental design objectives to obtain a high selectivity and specificity: (1) a high capture efficiency (must be able to isolate all the CTCs present on the blood sample); (2) a high isolation purity (should be able to distinguish the CTCs from the remaining blood components); and (3) high throughput performance (able to process a large volume of a blood sample in a short amount of time) [28].

Within this scope, microfluidic-based approaches are highly applied in investigations due to their advantages over conventional methods, such as density centrifugation and flow cytometry, concerning CTCs detection and isolation. For instance, microfluidics allows the handling of small volumes (10^{-6}–10^{-12} L), within their microchannels providing a highly sensitive method for capturing CTCs in low sample volumes. Thus, it offers an automated, miniaturised, and isolated environment for the analysis of CTCs, reducing significantly the processing time, as well as enabling the integration of other techniques improving the efficiency of the analysis of CTCs [2].

In general, CTCs isolation techniques may be categorised as biochemical (label-based) and biophysical (label-free) methods [27] .

1.4 .1 Comparison of Biophysical and Biomechanical Properties between CTCs and Normal Blood Cells

After several histological studies of CTCs, researchers were able to gather information about the modifications in cell cytoskeleton components and their structures that CTCs undergo to achieve a cancerous stage. It was evidenced that these cytoskeletal changes weigh on the mechanical properties of cells, such as higher nuclear/cytoplasm ratio, larger size, and distinct nuclear morphology compared to normal cells[29].

One important finding pointed to changes in their cellular biomechanics, like deformability, having an essential role in metastasis. For instance, CTCs endure adaptations on their cytoskeleton stiffness providing them with the ability of squeezing across small spaces in the extracellular matrix and endothelial cell-cell junctions and/or in small capillaries, improving their invasion capability. Moreover, the cell membrane of CTCs also alters its surface charge (electrical change) as an outcome of the hemodynamic forces and fluid shears that they must overcome within the blood vessel [29].

Thus, we may highlight three main physical differences between tumour cells and blood cells: size, deformability, and electrical properties.

1.4.1.1 Size

Cell size determinations are obtained by assessing several parameters, such as cell area, length, width, and shape. Regarding the size of blood components, red blood cells (RBC) exhibit a diameter of approximately 6 to 8 μm. The white blood cells (WBC) may be divided into two groups, granulocytes, and agranulocytes. The first group, whose neutrophils and eosinophils belong, present a diameter of 12 to 15 μm, meanwhile, cells from the agranulocytes groups like lymphocytes may vary between 7–10 μm for small lymphocytes and 14–20 μm for the bigger ones. In relation to leukocytes, monocytes have typically a diameter of 15 to 25 μm [29].

When comparing the size of these blood cells and that of the CTCs, the latter display a diameter ranging from 17 to 52 μm. These findings are supported by several studies that evidenced that CTCs were characterised with an elongated shape and with a larger size relative to leukocytes [29]. Similarly, a work by Park et al. [30] involving patients with prostate cancer, reported that the ruffled surface membrane of CTCs contributed to an increase of membrane surface area, therefore, showing a larger size in contrast to normal blood cells.

1.4.1.2 Deformability

The assessment of the tumour deformability of tumour cells is obtained through viscoelasticity. A variety of techniques such as atomic force microscopy (AFM), micropipette aspiration (MPA), magnetic twisting cytometry or automated methods like microfluid resonators and inertial focusing serve as tools to evaluate this mechanical property [29].

Generally, the cellular mechanical behaviour is evaluated by Young´s Modulus. This parameter allows the quantification of the stiffness of the cells, which is associated with the distribution of the Actin network within the cell cytoskeleton. Several studies resorted to the AFM technique to assess the viscoelastic properties of cultured cancer cells and blood cells. Their findings reveal that metastatic cells show lower levels of stiffness (Young's Modulus of 3.7 kPa–150 kPa), compared to a Young's Modulus of 0.2 kPa from the normal blood cells [29]. Besides, recent work by Byun et al. [31] using a suspended microfluidic resonator corroborates these results. This research consisted of tracking the velocity of the cells from a sample of blood spiked with human lung cancer cells, while they cross the constrictions regions of a device. The results showed that cancer cells show high cytoskeletal deformability since they required less time to deform and travel through the constriction zone than the normal blood cells.

Moreover, the examination of the viscoelasticity properties of the tumour cells undergoing metastasis enabled the establishment of a connection between cell deformability and cell malignancy. For this purpose, Mak and Erickson [32]and Mohammadalipou et al. [33] have conducted a study to determine the mechanical properties of both metastatic and benign breast cancer cell lines, concluding that the metastatic cells showed a longer aspiration length, resulting in a higher Young's modulus value. Following this line of thought, Chen et al. reported an AFM-based analysis performed with prostate cancer cells lines, which also pointed out that noncancerous cells present a lower elasticity value (Young´s modulus of 3.7 kPa), and that the highly metastatic cell line showed the higher Young´s modulus of 0.13 kPa [29].

1.4.1.3 Electrical Properties

Electric charges are responsible for the cell membrane selective permeability. The electrical potential surrounding the membranes is generated by the difference in concentrations of molecules on the inner and outer sides of the membrane. Theoretically, the cell membrane at physiological pH presents a negative charge, exhibiting a membrane potential ranging from -60 to -100mV. However, during tumourigenesis, the membrane charge may vary, as a result of abnormal metabolic transformation [29].

Studies on this field by Becker et al. [34], noticed that cancer lines of human breast show higher values of membrane capacitance (26 ± 4.2 mF/m2), in comparison to erythrocytes (9 ± 0.8 mF/m2) and T lymphocytes (11 ± 4.2 mF/m2). These differences in the conductivity are also evidenced throughout distinct stages of cancer, as Qiao et al.[35] discovered, showing that cancer cells at an early stage exhibit higher membrane capacitance (value of 5.58mS/cm and 3.94μF/cm^2), in contrast to cells on last stages of cancer (value of 3.97mS/cm and 1.10 μF/cm^2).

1.4.2 Biochemical Approach

Biochemical approaches are based on the specific affinity between antigens and antibodies. Throughout the metastatic cascade, CTCs express different surface markers. Currently, the epithelial cell adhesion molecule (EpCAM) is the most commonly used for CTC detection however, other specific tumour biomarkers are also used such as HER2neu and MUC1 in breast cancer, androgen receptor (AR), early growth response gene (EGR), and PSA in prostate cancer [10].

These affinity-based approaches may also be subcategorised as positive or negative selection strategies (Table 1). The first one is focused on the identification of specific tumour biomarkers meanwhile, the former one consists of the depletion of red and blood cells. [36] In particular, the CellSearch® system is the only CTC isolation platform that achieved clinical validation by FDA (Food and Drug Administration) for prognostic use in breast, prostate, and colorectal cancers. This technology enables the isolation of CTCs in whole blood due to the conjugation of anti-EpCAM antibodies with magnetic beads [28].

Besides biomarkers, these strategies may use a variety of nanomaterials such as carbon nanotubes, silicon, gold, and graphene oxide nanoparticles that have been widely applied in affinity techniques. Due to their high surface area/volume ratio, biocompatibility with antibody conjugation, and release capabilities they offer several improvements to the sensitivity and specificity for CTCs capture [2].

Table 1 - Label-dependent CTC isolation techniques divided into positive and negative selection.(Adapted from [37])

Positive selection				
Device	**Strategy**	**Tumour type**	**Observations**	**Ref**
Graphene oxide (GO) chip	EpCAM antibody-coated graphene oxide nanosheets	- Breast - Pancreatic - Lung	- Processing time: 1–3 mL/h - Sensitivity: 73 - 32.4 at 3–5 cells per mL of blood	[37]
Herringbone chip	8 microchannels patterned with herringbone to promote interactions between CTCs and a surface coated with EpCAM antibodies	Prostate	- Capture Efficiency of 91.8% - Processing Time:4.8 mL per hour	[37] [2]
GEDI (geometrically enhanced differential immunocapture) chip	Based on the collision between CTCs and micro-posts coated with anti-PSMA (prostate-specific membrane antigen)	- Breast - Prostate	- Reduced leukocyte adhesion - Efficiency of 97 ± 3 % at the flow rate of 1 mL h^{-1}. - Detection ratio and purity of captured CTCs reached 90 % and 62 ± 2 % in WB	[2]
NanoVelcro CTC chip	Silicon nanowire and patterned PDMS substrates	- Breast - Lung	- 93 % recovery rate of rare CTCs - More than 80 % capture efficiency high flow rate of 10 mL h−1	[38]
OncoCEE (cell enrichment and extraction) (Biocept)	Funcionalisation of the surface with antibodies cocktail targetting biotumour and mesenchymal markers	- Breast	- Sensitivity: 95 % - Specificity: 92 %	[37]
Negative selection				
$EasySep^{TM}$	Combination of an enrichment cocktail containing CD45 antibody and magnetic beads of different sizes.	- Pancreatic - Breast	-Mean log depletion of CD45+ cells of 2.9 ± 0.4 - Average capture of cancer cells of 42 ± 23 %	[2][39]
CanPatrol (CTC enrichment)	RBC lysis and depletion of CD45+ leukocytes using a magnetic bead separation followed by CTC size-based separation	- Lung - Breast - Colon - Esophageal	- Average WBCs depletion of 99.98 %; Recovery rate ranging from 83% to 89 %	[39]

1.4.3 Biophysical Approach

These platforms rely on the discrimination of CTCs from other cells due to their biophysical differences such as size, density, deformability, and electrical properties (Table 2). As described above (section 1.4.1) CTCs possess a greater nucleus/cytoplasm ratio, a larger size, and different nuclear morphology and electrical properties than the normal cells [37]. As a category of biophysical strategies, mechanical filtration through membranes enables a simple and high throughput separation of CTCs [2]. For instance, a platform designed by Desitter et all., Screencell, has a membrane with cylindrical pores (size of 6.5 μm), where the blood cells (red blood cells and leukocytes) flow through the pores meanwhile, the CTCs remain trapped and are collected [40]. However, these platforms usually need to be optimised because they may suffer clogging or leaking by microfiltration that may affect the purity and standardisation of the CTCs collection.

Moreover, other label-free methods focus on the application of inertial forces for the isolation of the CTCs. One commonly used strategy is dean flow fractionation (DFF) that exploits lateral forces such as shear-gradient and wall effect lift forces for CTCs isolation. The spiral shape of the microfluidic platform induces centrifugal forces that create dean double symmetrical vortices which drive the smaller cells towards the outer wall meanwhile, larger cells move into the inner wall due to the wall effect lift force [2]. For instance, the Vortex HT designed by Sollier E. et all [41] applies this principle. In the microfluidic chip, various reservoirs are distributed in series or in parallel generating multiple vortices to trap single cells.

Alternative detection methods may also use electrophysical properties to identify the targeted CTCs. The different conductivity behaviour of particles in a solution under the effect of an electric field is the basis for the separation of cells using dielectrophoresis (DEP)[37]. The ApoStream ™ system was the first commercialised microfluidic chip with DEP technology. A positive DEP force facilitates the isolation of CTCs in blood, while normal cells are subjected to a negative DPE that forwards them along the microchannel as waste [40].

Following this thematic, the Medical Devices group at INL has developed efficient microfluidic devices for the isolation of CTCs based on size and deformability. Several generations of the microfluidic system were refined, from the CROSS chip to the Mega chip and, most recently RUBYchip®. In the last years, various studies were conducted to validate the performance of the devices, reporting isolation efficiencies up to 70 % for the colorectal cancer and 56 % for breast cancer types, with an outstanding purity [42][43].

Table 2 - Label-independent CTC isolation techniques based on different biophysical properties.(Adapted from [37])

Density gradient separation				
Device	**Strategy**	**Tumour Type**	**Observations**	**Ref.**
AccuCyte	Automated system for CTC detection and isolation from a separated buffy coat	Adenocarcinoma	Capture Efficiency 90-91 %	[2][39]
OncoQuick	RBCs separation from CTCs using a porous barrier followed by density-grade centrifugation	- Gastrointestinal - Breast	25 mL of blood may be processed per tube Capture Efficiency 25-87 %	[37][40]
Filtration				
Device	**Strategy**	**Tumour Type**	**Observations**	
ISET	Blood samples flow through a porous membrane that enables the leukocytes removal	- Lung - Breast - Melanoma	Sensitivity: 76.37 % Specificity: 82.39 %	[37][2]
SmartBiopsy ™	Porous microfilter for CTC isolation	Lung	Capture Efficiency 82-86.7 %	[39]
Inertial Focusing				
Device	**Strategy**	**Tumour Type**	**Observations**	
ClearCell FX	CTCs separation using Dean Flow Fractionation (DFF)	Lung	Process 7.5 ml of Blood in 1 h Detection of 73.7-81.33 %	[39][40]
p-MOFF	Employment of hydrodynamic inertial forces for enrichment of CTCs	-Breast	Processing 7.5 ml of Blood in 30 min Capture Efficiency of 91.6 – 93.75 %	[40]
Dielectrophoresis				
Device	**Strategy**	**Tumour Type**	**Observations**	
DEPArray	The systems is composed by 16000 electrode cages to trap single cells	Breast	Allows the isolation of single CTCs for downstream gene analysis	[39][40]

1.5 Beyond Isolation: Recovery of Circulating Tumour Cells (CTCs)

Circulating tumour cells (CTCs) carry relevant information, enhancing the importance of their effective capture and analysis to investigate cancer progression and metastasis. Thus, apart from a specific and sensitive detection and isolation of CTCs is also essential a successful recovery of the CTCs for further downstream analysis. A feasible release of the CTCs is an important fulfilment to carry out ex-vivo CTC cultures and obtain morphological and phenotypic information. Nevertheless, the retrieval of CTCs from the capturing substrate offers many challenges. This way, researchers are channelling their efforts into the design of novel technologies for the recovery of viable CTCs [44].

In a study conducted by Hou et al. [45], the isolation of CTCs using Dean Flow Fractionation was reported. Their technology resorts to dean migration and inertial focusing to efficiently separate CTCs from blood. The dean migration leads the cells towards the inner channel of the platform and makes the smaller blood cells continuously flow along to the outer outlet as waste. Meanwhile, the larger cells are exposed to inertial lift forces preventing their migrating further along the channel, driving their collection in the inner outlet.

Additionally, Sarioglu et al. [46] developed a microfluidic chip, Cluster-Chip, that can isolate CTCs clusters from whole blood, as well as their retrieval from the chip. When processing the blood, single blood cells or CTCs pass through the chip, while the CTC clusters are retained within the device due to surface tension. In addition, the retrieval of CTCs is performed by reversing the flow and processing the samples at 4 °C, achieving a release efficiency of 80%. The usage of low temperatures reduces non-specific cell adhesion, leading to fewer leukocyte contamination and, therefore improving the purity of the processed samples.

Most recently, Miller et all. [47] created a semiautomated microfluidic-based approach, the Parsortix™ Cell Separation System for the capture and retrieval of rare cells, i.e CTCs, from body fluidics. The separation cassette design has structured steps and a critical gap, where the cells are captured. For the recovery step, the flow was also reversed and the cells trapped between the gaps later released and collected into a vessel.

1.6 Single-cell Analysis

In the field of cancer research, there has been a great demand for alternatives and technologies that enable the study and analysis of single cells from a heterogeneous tumour population. The analysis of tumour cell populations as a bulk provides inaccurate information, as it only measures an averaged data about the population. This way, some relevant evidence about subpopulations, which may be responsible for the behaviour of the whole population, may be lost (Figure 4) [48].

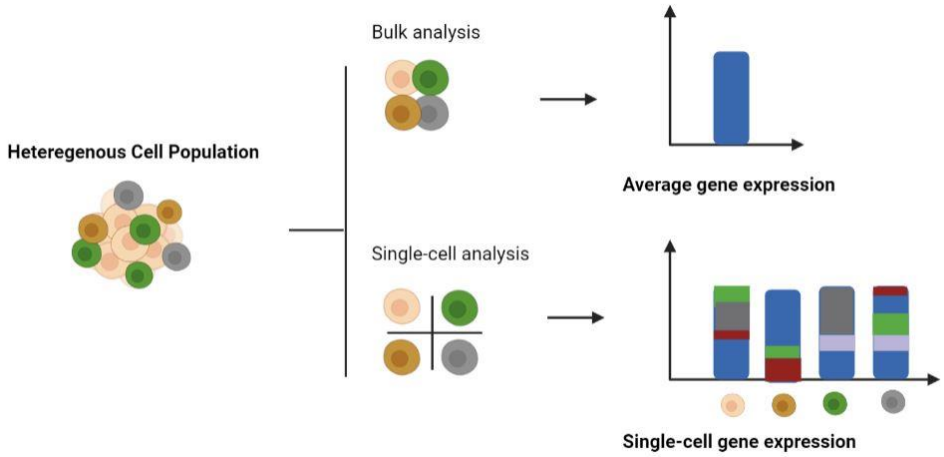

Figure 4 - Schematic representation of single-cell analysis importance. Tumour heterogeneity scrutiny at a single level enables the revelation of cell subpopulations and their different gene expressions. Reproduced from [49].

Cancer develops due to a complex interrelation of mutations, selection, and clonal expansion, resulting in a set of distinct subclones within a single tumour. Consequently, such heterogeneity is the most significant cause that leads to cancer treatment failure and disease recurrence. Variations of tumour biomarkers at the intra- and intermolecular levels may introduce significant challenges and condition the efficiency and success of biomarker-driven clinical trials if the biomarker used to both predict the therapeutic response and stratify the patients into subgroups shows spatial variability. Likewise, metastatic lesions undergo divergent progressions in different microenvironments, contributing to possible changes in the expression of biomarkers initially identified in the primary tumour [50].

Methods for single-cell analysis can comprise a variety of assays, such as the measurement of the physical properties of cells, protein analysis, decoding cell signalling, and sequencing of DNA/RNA. Through the progress of these examinations, is enabled the identification and detection of rare tumour cells like CTCs or the study of cancer stem cells, leading to a better understanding of disease progression and treatment selection [51].

In the early days, single-cell analysis was achieved with cytometric analysis, consisting of the screening of fluorescently labelled cells in a flow. Currently, emerging techniques of microfabrication for cell studies have been developed. For instance, microfluidic devices allow the integration of various individual analytical operations in a single microfluidic chip for the study of single cells. One promising tool for single-cell manipulation and analysis is droplet microfluidics [51].

1.6.1 Droplet-based Microfluidics for Single-Cell Analysis

For the accurate characterisation and evaluation of the heterogeneity among single cells, it is crucial to develop systems with high throughput and sensitivity. These two requirements were the driving force that stimulated the development of microfluidic systems for single-cell analysis.

In particular, droplets microfluidics consists of the convergence between an aqueous phase with an immiscible fluid generating droplets to encapsulate single cells. This type of technology has a handful of characteristics, such as parallelisation where multiple identical units can be generated in a short time allowing parallel processing; miniaturisation, since the size of the droplets may range from nanoliter to picoliters; and compartmentalization, in which each droplet functions as an independent microreactor [52].

The generation of droplets requires the existence of two immiscible phases, where the first one, designated as the continuous phase, is the medium in which the droplets are formed, while the second one is referred to as the dispersed phase. The size of the microdroplets may be manipulated by variating the flow rate of the two phases, their interfacial tension, and by modifying the geometry of the channels [53]. The three most commonly used geometries for droplets generation are T-junction, flow-focusing, and co-flowing (Figure 5).

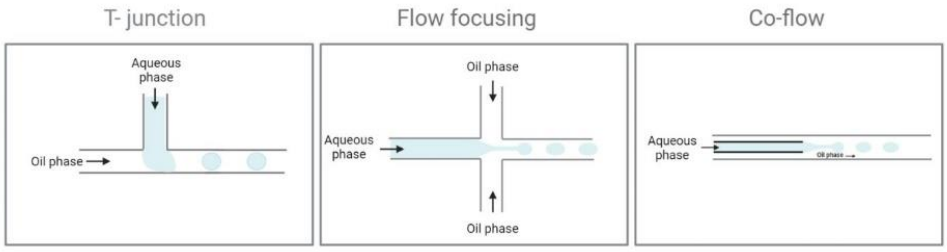

.

Figure 5 - Droplets generation can be performed using microfluidic devices with three different geometries: T-junction, flow focusing, and co-flow. Reproduced from [54]

In the co-flow geometry, the continuous and disperse phase merge in parallel streams [55]. However, the T-junction geometry is the most commonly used one among the community due to formation of droplets with the lowest polydispersity ratio. The channel containing the dispersed phase intersects the continuous phase channel with a specific angle, as the junction section may be in the shape of a T or a Y. When the two fluidics merge, the neck of the dispersed phase splits the stream into a droplet. Moreover, the flow-focusing configuration enables the formation of droplets through the effect of symmetrical shear forces applied by the continuous phase on the dispersed phase [49].

Droplets microfluidics is a very appealing tool that allows high-throughput screening and sampling, being applied for single-cell analysis, genomics, transcriptomics, imaging, drug delivery, antibody screening, toxicity screening, and diagnostics. Due to their biocompatible and isolated environment, these platforms provide the ideal conditions to study and identify cell subsets, to quantify the secretion of signaling molecules from single cells, and investigate cell to cell communication [56].

1.6.2 Single-cell encapsulation in microdroplets

Droplet- microfluidics techniques enable a high throughput culture, manipulation and analysis of encapsulated cells. Cells and molecules of interest secreted by the cells remain trapped inside the droplets, reaching detectable concentrations due to the small volume of the droplets enabling rapid detection. In addition, the encapsulated cells may be manipulated or used for subsequent molecular assays, providing a link between genotype and phenotype screening [57].

Single-cell encapsulation entails the dispersion of cells in an aqueous solution, the generation of droplets, and finally a random delivery of cells to droplet nozzles (Figure 6). Thus, the distribution of cells in the droplets is still not precise and, we may encounter droplets with more than one cell and others empty. The distribution of single cells in the droplets naturally follows the Poisson distribution [52].

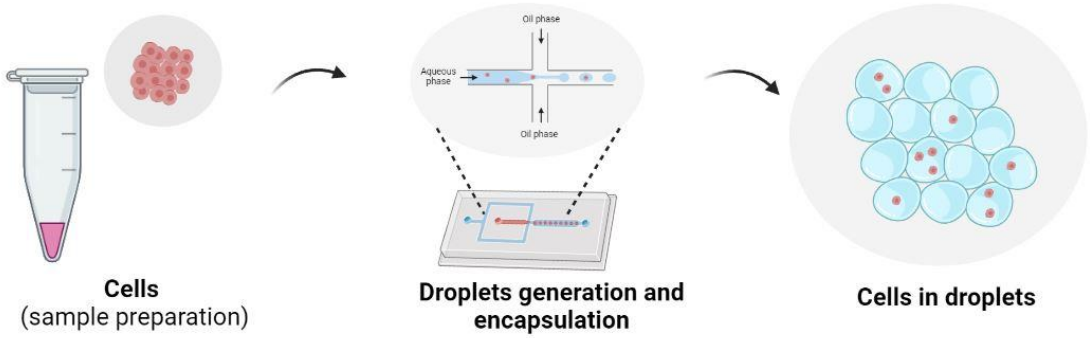

Figure 6 - Schematic illustration of single-cell encapsulation in droplets.[Created in Biorender]

The Poisson distribution (equation 1) gives the probability $P(X = x)$ of finding x cells (or beads) per droplet, where λ represents the average number of cells in the volume of each droplet. Thus, variations in cell density in the aqueous phase allow the adjustment of the droplet occupancy [57].

$$P(X = x) = \frac{e^{-\lambda}\lambda^{x}}{x!} \qquad \text{(equation 1)}$$

However, this is a process difficult to control, since according to the Poisson distribution the probability of a droplet only containing one cell is 36.8 %, while the possibility of pairing two distinct cell types in a droplet corresponds to 13.5 %. In an attempt to overcome the confinement of two cells within the droplet, the cell suspension may be diluted, however, this results in a larger number of empty droplets [58]. As the high throughput of droplet formation is very high (in the range of thousands droplets per second), the target droplets containing the single cells will be amongst many empty droplets (≈ 70 % of the whole droplet population generated). As defined above, if we have tenths to thousands of CTCs, it is extremely difficult to find the droplets having those CTCs. Hence, strategies to select the droplet subpopulation containing the single cells are needed.

1.7 Droplets Sorting

For cell analysis, an effective and fast sorting of cells of interest is highly important. Cell sorting consists of the separation of target cells from a complex and heterogeneous population based on properties or type differences. This process is usually used to sort cells for subsequent downstream analysis or to purify cells into well-defined populations[59](Shen et al., 2019). In order to select the cells of interest after encapsulation in droplets, the selection of cell containing droplets is necessary.

The sorting of droplets can be divided into two types, active sorting and passive sorting. Active methods function with external sources to apply forces to accomplish the sorting, such as electrophoresis, acoustrophoresis, magnetism and fluorescence. The most common methodologies used are FADS and dielectrophoresis (DEP). FADS relies on a fluorescent reporter substrate, whereas DEP is based on the permeability of the droplet in relation to the fluid, the droplets are fowarded to positive or negative channels[60]. Several studies have demostrated DEP´s ability for droplet sorting, i.e. a work conducted by Thomas et al. [61] reported the sorting of fluorescent labeled cells in microelectrode arrays using DEP. The incidence of a negative dielectrophoresis creates a "dielectrophoretic virtual channel", in which by changing the polarity of the electrodes, the virtual channel suffers reconfigurations, directing the particles through different paths. Despite exhibiting higher sorting efficiencies, this type of methods require expensive set-ups, as well as as expert operators.

On the other hand, the passive sorting is based on the separation of the droplets into different carriers due to hydrodynamic interactions between the channel geometries and the intrinsic properties of the droplets [62]. For instance, Griffiths et al.[63] designed a size-based sorting system. Larger and smaller droplets flow together along the channel until they reach a branch that consists of a central wide main channel and two narrowing side channels. Given the size differences between the droplets, the larger ones rest on the main channel, whereas the smaller droplets enter the side channels.

Microfluidics passive sorting methods commonly explore the different sizes of the droplets and their ability to deform in techniques such as mechanical filtration, inertial microfluidics, and the deterministic lateral displacement (DLD). Mechanical filtration approaches rely on the usage of arrays with pores or funnels for separation [64].

Another possible sorting process through inertial microfluidics recurs to the action of Dean drag forces and inertial lift forces on the droplets. Likewise, DLD is a widely used method for cell sorting based on size. In this approach, the criterion for the separation relies on the geometrical features of the microchannel, such that droplets with a diameter larger than the critical diameter will follow a diagonal streamline, meanwhile smaller droplets will go through the centre streamline [64].

2. Objectives

Several technologies are under development to be validated for clinical applications and to be used as potential platforms for liquid biopsy. In particular, circulating tumour cells (CTCs), cells shed by an active tumour into the bloodstream, can be used as a real snapshot of the cancer status. Thus, the development of a variety of microfluidic-based detection and analysis platforms for the analysis of CTCs is key towards a more precise diagnosis and monitoring of patients.

Likewise, single-cell analysis enables more detailed and in-depth profiling of cell populations and unveils rare cell subpopulations**.** In this context, droplet-based microfluidics systems are widely used for this purpose. Each droplet is equivalent to a reaction flask, which can be loaded with a single cell for further high-throughput analysis.

Therefore, the main objective of this project will be to develop the interface for the recovery of the CTCs from the already developed isolation chip to the single-cell encapsulation chip (Figure 7). For this integration to be successful and achieve the main goal of the project, the following specific objectives have been defined:

1. Development of a modular microfluidic device capable of: (a) isolation of CTCs; (b) recovery of isolated CTCs from module 1; (c) encapsulation of CTCs in microdroplets and (d) sorting of droplets containing CTCs from empty droplets.

2. Optimisation of the microfluidic platform with cancer cell lines and analysis of recovery, encapsulation, and sorting efficiencies.

3. Validation of the technology with real samples from cancer patients.

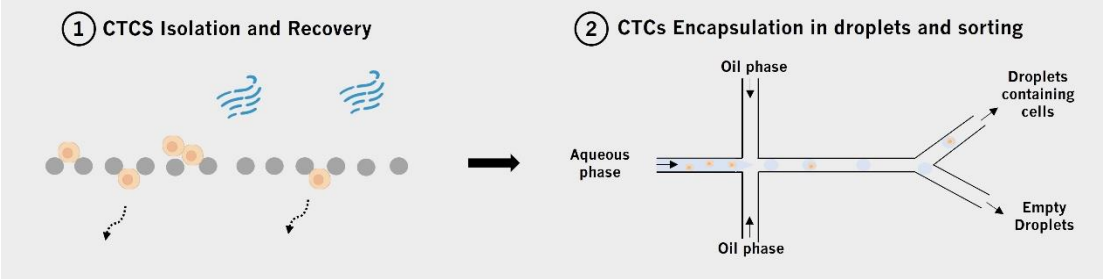

Figure 7 - Schematic representation of the overall objectives and workflow of the project.[Created in Biorender]

3. Materials and Methods

This chapter describes in detail the fabrication techniques and procedures used throughout the different parts of this project. Unless otherwise stated the materials and reagents used were purchase from Merck.

3.1 Isolation/Recovery Experiments

3.1.1 Device fabrication

For the isolation experiments, the microfluidic device used was the RUBYchip™ (Figure 8), already developed by the research team, which allows the capture of CTCs based on cell size and deformability. [43]I[44]The RUBYchip™ is constituted by two main rows with four modules each that contain a filtration area with a single row of micropillars distanced in 5 μm from each other [65].

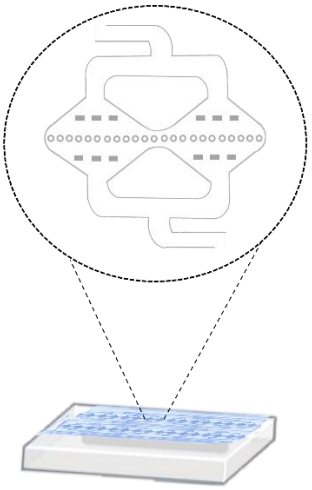

Figure 8 - Schematic representation of the RUBYchip™ design. Each module has a filtration area, which is constituted by micropillars, distanced from each other in 5μm.[Created in Biorender]

The masters of the chip were designed in AutoCAD software and built on a 200 mm silicon wafer by photolithography and deep reactive ion etching [42]. The microfluidic structure was prepared in polydimethylsiloxane (PDMS) by soft lithography.

3.1.2 PDMS replica preparation

The microfluidic structure was made of PDMS. The PDMS mixture was prepared by weighing the pre-polymer in a 1:10 ratio (4g crosslinker: 40 g PDMS polymer, SYLGARD™ 184 Silicone Elastomer, Dow Chemical Company) into a plastic cup. The resulting mixture was either used as prepared or stored in the freezer for further use.

For the replica fabrication, the PDMS mixture was poured into the master, and placed on the desiccator under vacuum to remove any remaining bubbles. Finally, the replicas were cured in the oven at 65 °C for at least 2 h or left overnight.

Following, using a scalpel the replicas were cut from the master mold and peeled off gently. Finally, holes for the inlet/outlet were created using biopsy punchers (1.25 mm).

3.1.3 Bonding and Passivation of the device

To create a closed structure the PDMS replicas were irreversibly bonded to glass slides (25×75 mm^2, ThermoFisher Scientific), previously cleaned with Hellmanex (Hellmanex III, Hellma Analytics). To do this, the surfaces of the glass slide and the pattern face of the replica were activated with oxygen plasma (Plasma Cleaner PDC-002-CE, Harrick Plasma). Then, the two elements were bonded together with the help of tweezers. To ensure the appropriate bonding the samples were placed in the oven for 15 min.

For the passivation of the microfluidic channels, 30 cm of ethyl vinyl acetate microtube (51×0.5mm ID×1.5mm OD EVA, ColeParmer) were inserted in the inlet and outlet holes, and the inlet was connected to a syringe pump (NE-1200, New Era Syringe Pumps) using a blunt needle (LS22K Luer Stub, Instech).

First, a 350 μL washing step with ethanol at 100 μL min-1 was performed to increase the wettability of the surface. Then, the device was rinsed with 350 μL of 10 mM phosphate buffer saline (PBS) at 120 $\mu L\ min^{-1}$, and lastly, 4000 μL of 1 % Pluronic F-127 was pumped at 140 $\mu L\ min^{-1}$ to passivate the surface and to test the device with a volume of the same magnitude as the blood sample to ascertain the device performance and the success of the fabrication.

3.1.4 Cell Culture and Maintenance

For the experiments conducted the colorectal cancer cell line used was SW480 (ATCC, CCL-228). The SW480 cells were cultured in Dulbecco´s modified eagle medium (DMEM) with the supplementation of 1 % Penicillin/Streptomycin (PS) and 10 % fetal bovine serum (FBS). The flasks were kept in an incubator at 37 °C and with a 5 % CO_2 humidified atmosphere. Routinely, for the maintenance of the cells, the medium was renewed every 2-3 days, until a confluence of 80-90 % when they were sub-cultured.

3.1.5 Cell Spiking for Isolation Experiments

First, cells were trypsinised by removing the medium and adding 500 μL of 0.25 % (w/v) Trypsin-0.53 mM EDTA solution and put into incubation for 5 min at 37 °C. To neutralise the trypsin-EDTA/cell suspension, 4.5 mL of complete growth medium was incorporated into the flask. Then, the cell density was estimated by mixing 10 μL from the cell suspension with 10 μL of Trypan blue and added to a haemocytometer. The calculations to determinate the number of cells on the flask were performed as follows:

$$\frac{counted\ cells}{number\ of\ quadrants\ counted} \times dillution\ factor \times 10^4 \qquad \text{(equation 2)}$$

For the staining, the volume equivalent to 6×10^5 cells was transferred to a new falcon tube, and the remaining volume was made up with sterile 0.01M PBS to achieve a total of 1 mL. This suspension was centrifuged at 1200 rpm for 5 min and, during this time, the 4,4-diamidino-2-phenylindole (DAPI) solution was prepared to contain 40 μL of DAPI and 360 μL of sterile 0.01M PBS. After the centrifugation, the resultant pellet was resuspended with the DAPI solution and incubated at 37 °C for 30 min.

Once the incubation time was finished, several washing steps took place by adding 1600 μL of complete growth medium (DMEM) to fulfill a final volume of 2 mL in the falcon, followed by centrifugation at 1200 rpm for 5 min. This process was repeated three times. After the final centrifugation, an additional cell counting was performed to assess the number of cells in the stock cell suspension. Then, a series of dilutions were prepared to obtain a final cell suspension of 1000 cells.

3.1.6 Processing and Isolation Experiments

Initially, the protocol was performed using PBS. To help design the recovery protocol, different cell targets were used (1000 and 200 cells). Thus, for the spiking experiments (Figure 9), 7.5 mL of PBS were spiked with 200 μL of SW480 cells and aspirated into 10 mL syringes using a 20G needle, and the syringes were placed in the pump and connected with the device inlet tube. Once the parameters were all set up, the sample was processed with a syringe pump (NE- 115 1200, New Era Syringe Pumps) at a flow rate of 100 μL min^{-1}.

In the end, 350 µL of 2 % Bovine Serum Albumin (BSA) in PBS was pumped at 100 µL min^{-1} to wash the device, followed by 350 µL of 4 % Paraformaldehyde (PFA) with an incubation of 20 min to fix the cells inside the device. Then, the device was rinsed with filtered 700 µL of 0.01M PBS. Finally, the ends of tubing were sealed off to allow microscopic analysis.

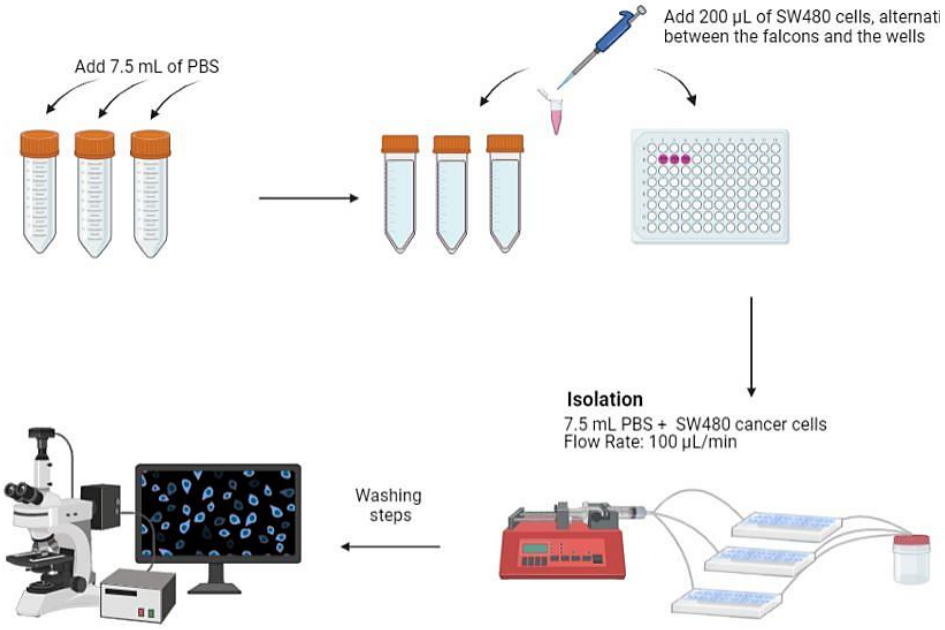

Figure 9- Processing and isolation protocol: (A) 7.5 mL of PBS is transferred to three falcons (50 mL). (B)200 µL of SW480 cells are added alternatively to the falcons and their control wells. (C) PBS spiked with the SW480 cells is processed at a flow rate of 100 µL min^{-1}. (D) In the end, the devices are sealed and taken to the microscope for analysis. [Created in Biorender]

The devices containing the isolated cells were taken to the Nikon Ti-5 microscope for analysis. Using NIS Elements analysis software (Nikon) the filtration areas of the microfluidic chip were examined using Bright Field and Fluorescent Blue and the DAPI (cell nuclei staining) positive trapped cells were counted (Figure 10).

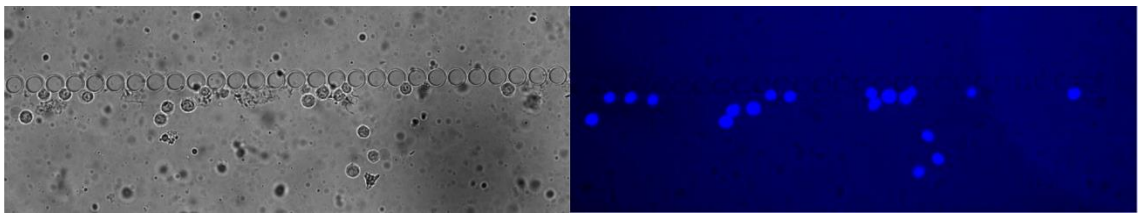

Figure 10- Microscopic images obtained using the NIS- elements analysis software. During analysis, the bright-field and fluorescent blue filters are employed for the identification of the cells.

This value was then compared to the total number of spiked cells to determine the capture efficiency, as follows:

$$\textbf{Capture Efficiency (\%)} = \frac{Number\ of\ cells\ counted\ on\ the\ device}{Mean\ of\ initial\ total\ cells} \quad \text{(equation 3)}$$

3.1.7 Recovery Protocol

3.1.7.1 Discover Method

To perform the recovery of cells, three methods were tested to inquire the most suitable one (Figure 11). The first one consisted of using the pumping mode, with the flow going in the same direction as the isolation step. In the second approach, the withdraw mode from the syringe pump was applied, so that the content within the device was aspirated back to the syringe. Finally, the third attempt was carried out using the pumping mode, but this time the connectors were shifted from the inlet to the outlet, and the chip was inverted so that the pumping was done in the reverse flow direction. For these series of trials, the parameters used were the same, where three rounds of PBS injections were performed (350 µL each round) at the flow rates of 100, 200, 200 µL min^{-1}, respectively.

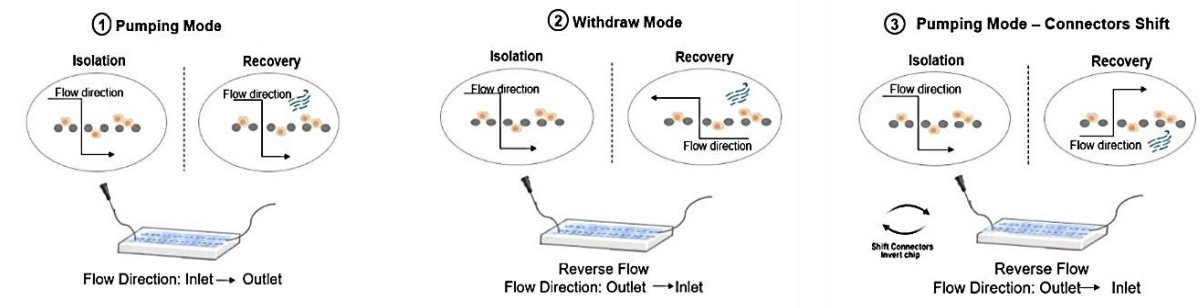

Figure 11- Schematic representation of three recovery methods: (1) Recovery in pumping mode: the flow goes in the same direction as the isolation; (2) Withdraw mode: the flow direction is reversed in relation to the isolation; (3) Pumping mode: the connectors shift, the chip is inverted and, thereby the flow is also reversed. [Created in Biorender]

For the assessment of the recovery success, two parameters were considered:

$$\textbf{Retrieval Efficiency (\%)} = \frac{Number\ of\ cell\ recovered}{Number\ of\ cells\ trapped} \quad \text{(equation 4)}$$

$$\textbf{Recovery Efficiency (\%)} = \frac{Number\ of\ cell\ recovered}{Number\ of\ total\ initial\ cells} \quad \text{(equation 5)}$$

In the literature [66], the recovery rate is calculated based on the number of spiked cells extracted from the system. However, it is not specified what they consider spiked cells to be, the total number of cells that are initially placed or whether it is the spiked cells that get trapped in the device. Thus, we decided to use both formulas to evaluate the recovery performance.

3.1.7.2 Flow Rate, Fluid Volume, and Number of Repetitions Influence

To improve the success of the recovery efficiency, the best method from the protocol previously described was used to test different flow rates: 200, 220, 240, 260, 280, and 300 μL min^{-1}.

Moreover, once the ideal flow rate was established, the most adequate fluid for the recovery was evaluated. In order to do so, experiments with BSA at different concentrations in PBS (2.5, 5, and 10 %) were conducted.

Additionally, after determining the most suitable fluid, we also found it relevant to investigate the influence of the number of repetitions executed, so for that, we carried out experiments to determine the minimum number of pumping operations that need to be performed to obtain the most cells out of the device.

Table 3 - Summary of all the parameters tested and optimised in the isolation and recovery in PBS

Isolation	Target Cells	Recovery Fluid	Number of Pumping Operations		Flow Rates (μL min^{-1})
PBS	1000	PBS	3		300
		BSA (2.5, 5 and 10%)	3	6	
	200	BSA 10%	6		

All these experiments (Table 3) were performed in triplicates, and at the end, the devices were examined in the fluorescent inverted microscope to assess the capture and recovery efficiencies (Eq. 4 and 5).

3.1.7.4 Optimisations in Whole Blood

Once the recovery protocol was optimised, the spiking experiments started to take place using whole blood samples (7.5 mL) from healthy donors, following the procedure described above. Likewise, for the first recovery experiments, the optimal parameters achieved with the PBS experiments were used.

Furthermore, the previously defined recovery protocol was subjected to new assessments to further improved the recovery efficiency. For instance, two distinct washing steps: 1) an additional 2 mL pumping of BSA 10 % at 200 μL min^{-1} before the pumping operations of the recovery; 2) 2 mL of PBS at 100 μL min^{-1} as the washing step in the isolation process, were tested to check their influence on the recovery.

Similarly, the effect of the change of new connectors at different time points of the procedure was also evaluated. All the conditions tested along the experiments are summarised in the tables below (table 4 and 5).

Table 4 - Summary of all the parameters tested and optimised in the isolation and recovery in PBS. The ideal conditions defined with experiments with PBS (in green) were used in the firts attempt with blood.

Isolation	Target Cells	Recovery Fluid	Number of Pumping Operations		Flow Rates (μL min^{-1})
PBS	1000	PBS	3		300
		BSA (2.5, 5 and 10%)	3	6	
	200	BSA 10%	6		
Blood	200	BSA 10%			

Table 5- Summary of all the parameters tested and optimised in the isolation and recovery with blood.

Isolation	Target Cells	Recovery Fluid	Washing step	Number of Pumping Operations	Flow Rates (μL min^{-1})	
Blood	200	BSA 10 %	2mL of BSA 10%	6	200	300
			2mL of PBS		100	

3.1.8 Additionally Tested Approaches

In order to assess the obstruction problem of red blood cells, additional strategies were tested to check for possible improvements in the recovery efficiency.

3.1.8.1 Isolation and Extraction of PBMCs

For the extraction of peripheral blood monuclear cells (PBMCs), we started with the dilution of the blood sample in PBS- FBS 2 % in a 1:1 ratio. Following, the blood sample diluted was transferred to a falcon with histopaque in a proportion of 2:1 and, centrifuged at 400×g for 30 min. Then, the PBMCs were recollected and placed into a 15 mL falcon and two rounds of washing steps with PBS- FBS 2 % and centrifugations at 300×g for 10 min were performed. In the end, the number of cells were counted using a Neubauer haemocytometer.

Simultaneously, the SW480 cells were prepared following the steps already described in the spiking experiments section. Thereafter, 1 mL of PBMCs spiked with 200 μL of SW480 cells were processed at 100 μL min^{-1}, rinsed with BSA 2 %, followed by a change of connectors and a washing step of 1 mL of PBS at 100 μL min^{-1}. Then, to carry out the recovery, the flow was reversed by shifting the connectors, and 6 pumping operations of BSA 10 % (350 μL) were performed at 300 μL min^{-1}.

3.1.8.2 Double Isolation Protocol

The isolation part was conducted according to the procedure described in section 3.1.6, using blood samples. However, in the washing step of PBS, the connectors were changed to new ones and 2 mL of PBS were rinsed at 100 μL min^{-1}. Then, the connectors were shifted so that the fluid would flow in the reverse direction and 2 mL of BSA 10 % was pumped at 300 μL/min^{-1} to an Eppendorf. Subsequently, the direction of the flow was once again changed, and the 2 mL collected at 100 μLmin^{-1} was processed. Finally, the flow was reversed, and 6 rounds of pumping (350 μL per each) were performed with BSA 10 % at 300 μL min^{-1} and the recovered cells were collected into a 96-well plate.

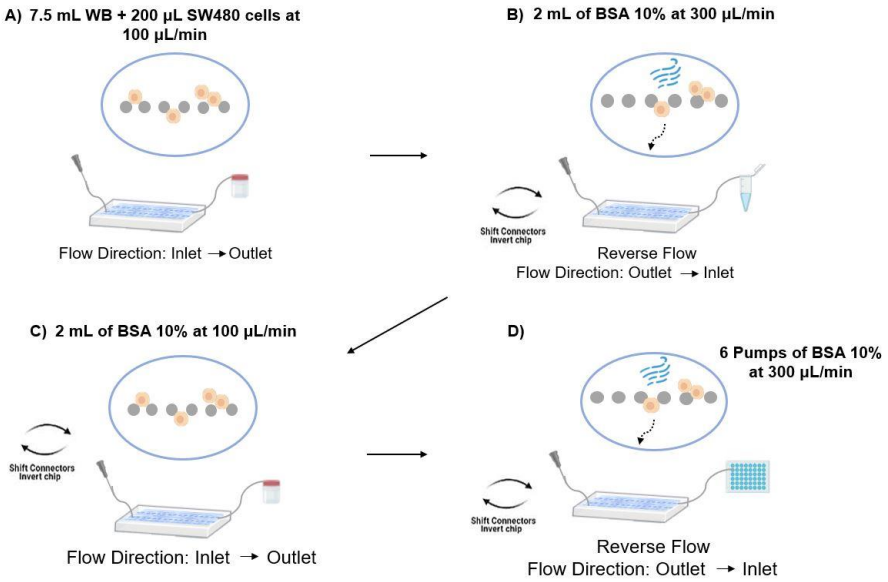

Figure 12 – Schematic representation of the double isolation protocol. [Created in Biorender]

3.8.1.3 Red Blood Cell Lysis Protocol

For the spiking and processing of the blood, we followed the steps described in section 3.1.6 and, the device was washed with 350 µL of BSA 2 %, preceeded by the change of connectors and the injection of 2 mL of PBS at 100 µL min^{-1}. Then, 700 µL of Lysis Buffer 1X was pumped at 100 µL min^{-1} and was incubate for 3-5 min. Afterwards, the connectors were shifted and 6 pumping rounds of 350 µL each were performed at 300 µL min^{-1}.

3.2 Cell Encapsulation and Passive Sorting

3.2.1 Device Fabrication

Two types of microfluidic designs were needed: (1) module 1 for the encapsulation of cells in droplets and passive sorting (Figure 13) of empty cells from cell containing cells and (2) a droplet reservoir for imaging. Both modules were designed in AutoCAD and PDMS soft lithography was cast over a silicon master mould at the Clean Room of INL (Class 100/1000). Features on this mold were etched down to 80 µm using a SF6/C4F8 plasma and a 1µm SiO2 patterned mask. Mask patterned was obtained using standard photolithography on a direct write laser (DWL) and SiO2 etching performed with a C4F8 etching

chemistry. The depth chosen for the cell encapsulation/sorting module and for the reservoirs for imaging was 80 µm and 100 µm, respectively.

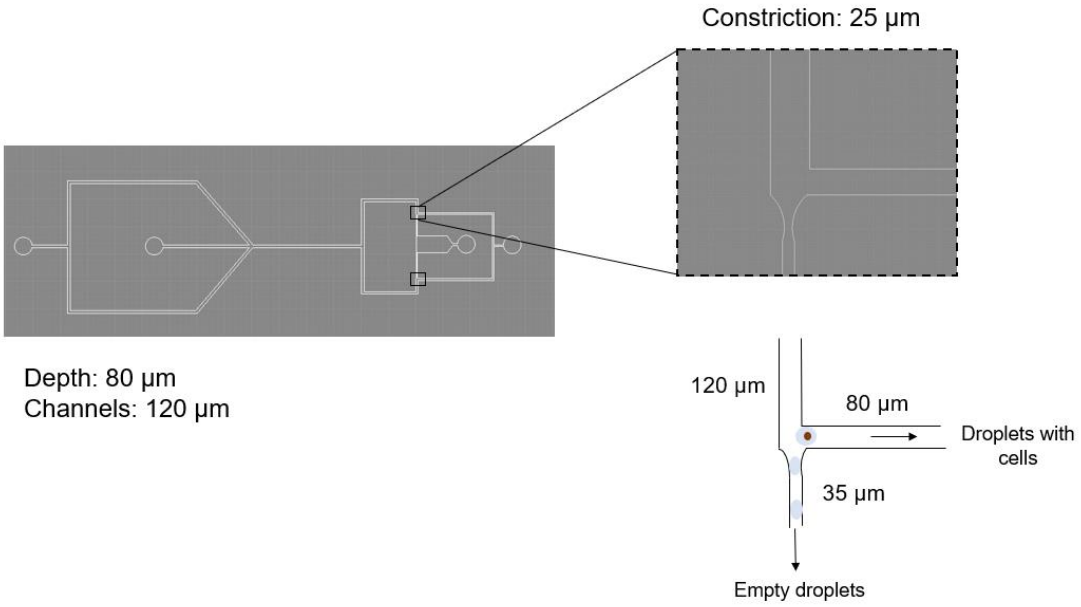

Figure 13- Device design in AutoCAD software, as well as its dimensions and characteristics detailed (zoomed region). The device is composed by a droplet generator and a sorting region. The sorting is carried out through a constriction, where the empty droplets manage to shrink and pass the constriction, while the droplets with cells are diverted to the other channel. [Created in Biorender]

For the replica the fabrication, the master moulds were placed in petri dishes and used for further casting with PDMS for replication. Then, the PDMS replicas preparation went according to the procedure described in the section 3.1.2. Afterward, the replicas were cut with a scalpel and peeled off manually, and the inlet/outlet holes were opened using a 1 mm diameter biopsy puncher (Kai Medical). To complete the fabrication, the PDMS replicas were bounded to glass slides through surface activation by resorting to an oxygen plasma chamber (Plasma Cleaner PDC-002-CE, Harrick Plasma).

Next, the devices were functionalised with Aquapel, to increase the hydrophobicity of the channels that are in contact with the continuous phase (fluorinated oil), using a 1 mL syringe, a syringe needle and a small portion of low density polyethylene (LPDE) (Scientific Commodities, Inc.) tubing, followed by injections with FC40 oil to remove the Aquapel from the channels to prevent the formation of crystals.

3.2.2 Optimisation and Calibration of Droplet Size and Flow Rate

For the droplets generation process, Mili-Q water was chosen as the disperse phase (Qd), and a solution of 2 % FC-40 + Pico-Surf™ 1 (PS-1, Sphere Fluidics, Ltd.) as the continuous phase (Qc). The solutions were respectively added to 1 mL syringes with syringe needles (0.5 mm inner diameter), with the tips connected to a portion of tube (LDPE). For the setup (Figure 14), the two syringes were placed in two different syringes pumps (New Era Pump), and the tubes were connected to the two inlets for the continuous and dispersive phases. Portions of tube were also inserted into the two outlets, one connected to a 2 mL Eppendorf for waste collection, and the other one connected to the inlet of a droplet reservoir. The outlet of the reservoir was also connected to a 2 mL Eppendorf. The syringe pumps were programmed, defining a flow rate of 100 μL h^{-1} for the dispersive phase, and a range of flow rates (500; 1000; 1500; 2000; 2500 μL h^{-1}) for the continuous phase.

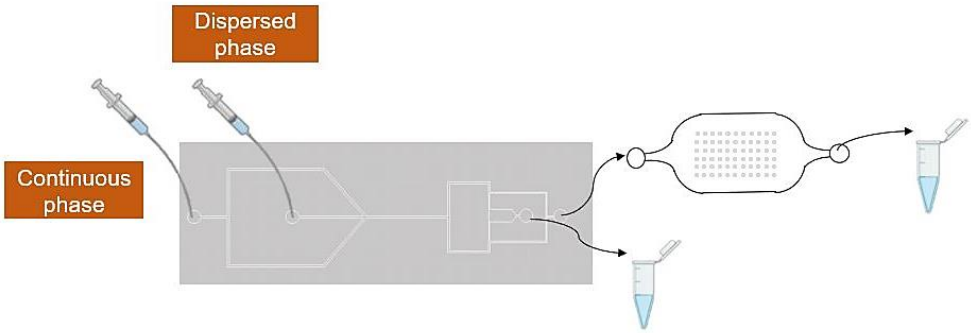

Figure 14 - Schematic representation of the droplets size determination experiments.[Created in Biorender]

Droplet formation was monitored under an inverted optical microscope (Nikon ECLIPSE MA200) with a 5× objective. Moreover, to seal the reservoirs, the tips of a tweezer were heated using a lighter and tubes were contracted to the inlet and outlet, closing the holes.

When sealed, pictures from the reservoirs were taken under the microscope (Nikon Eclipse Ti-E), using the NIS Elements analysis software. Afterwards, the images were analysed in ImageJ to determine the average droplet diameter. A total of 150 droplets were consider for the average size calculations.

3.2.3 Encapsulation and sorting process

In the droplets encapsulation experiments, the continuous phase (Q_{oil}) consisted of a solution of 2 % FC-40 + Pico-Surf™ 1 (PS-1, Sphere Fluidics, Ltd.) and as the dispersed phase (Q_{cells}) we used SW480 cells at different densities (1 million cells mL^{-1} and 2 million cells mL^{-1}). Likewise, the values of flow rates established for these experiments were those which ratio between the continuous and dispersed phases (Q_{oil}/Q_{cells}) corresponding to 10, 15, and 20.

Thus, the syringes corresponding to the continuous and dispersed phase were connected to both inlets and the outlets were connected to two reservoirs, one destined to the empty droplets and the other one to collect the droplets with cells. Both outlets from the reservoirs were connected to Eppendorfs (Figure 15).

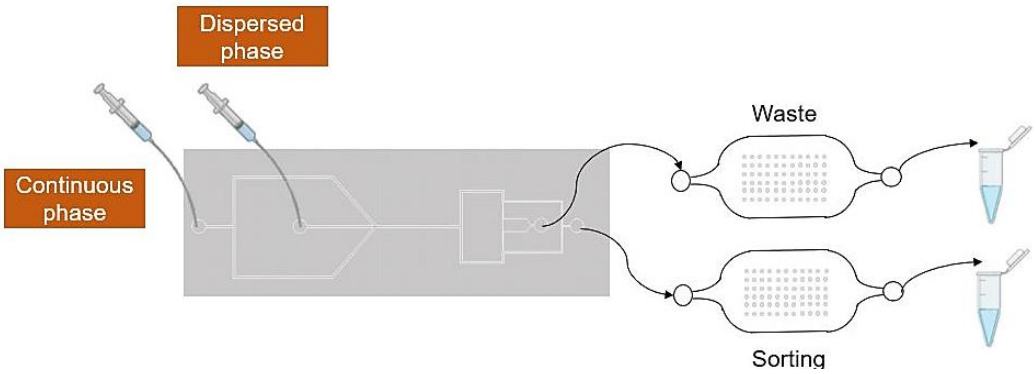

Figure 15 - Schematic representation of the cell encapsulation and sorting experiments.[Created in Biorender]

Afterwards, the devices were sealed and taken to the Ti-E microscope to acquire images from the reservoirs. The images were analysed using ImageJ to assess the sorting efficiency of the device. All the droplets in each reservoir that having the size corresponding with the flow rate used were accounted for the calculations. For the calculation, the following two equations were used:

$$\textbf{Waste Efficiency} = \frac{Empty\ Droplets}{Total\ droplets} \times 100 \qquad \text{(equation 5)}$$

$$\textbf{Sorting Efficiency} = \frac{Droplets\ with\ cells}{Total\ droplets} \times 100 \qquad \text{(equation 6)}$$

4. Results and Discussion

A breakdown of all the results obtained throughout every step of the thesis work follows in this section. The two main challenges of the thesis were to develop an efficient recovery protocol of cells from the isolation device, and also optimise the passive sorting of cell containing droplets from empty droplets.

4.1 Recovery optimisation

A set of different conditions have an influence on the efficiency of the recovery of cells from the isolation device. The recovery of viable cells at high efficiencies is very relevant because of the scarcity of CTCs and their prognostic importance. Most of the efforts of the CTC community were focused on developing efficient isolation methods. However, when it comes to the recovery and accessibility to CTCs for their genetic or functional analyses there is still plenty of room for improvement. [29][44]. In this first part of the project, a set of conditions were varied in order to define the best recovery protocol of CTCs from the RUBYchip™ (Figure 16).

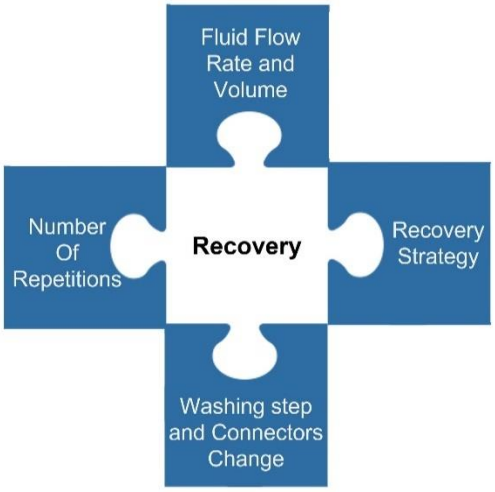

Figure 16 - Illustrative scheme of all the parameters tested for the recovery.[Created in Biorender]

4.1.1 Isolation and Recovery Experiments with PBS

As these initial experiments were to serve as trials, it was decided to use PBS instead of blood in order to ease the design and optimisation of a recovery protocol, and to get acquainted with the technologies, protocols and instrumentations used for this aim.

4.1.1.1 Optimisation of the Recovery Protocol

In the first set of experiments regarding the isolation process, the standard protocol described in 3.1.6 was followed. As per the recovery, three potential methods were tested: (1) the pumping mode; (2) the withdraw mode and (3) the pumping mode with the connectors shift (section 3.1.7.1). All the three experiments were carried out under the same condictions, which comprised a round of three pumps of PBS, 350 μL each, at the flow rates of 100, 200 and 200 μL min^{-1}, respectively. Overall, the capture efficiencies (Figure 17) obtained were consistent with each other, registering the values of 46 %, 34.4 % and 41 %, respectively. Lopes et al.[43] reported isolation efficiencies of 53% and 59 % for MCF-7 and MDA-MB-435 breast cancer cell lines, repectively. Carneiro et al.[67] used the RUBYchip™ for the isolation of CTCs and after the optimisation with the SW480 cell line the authors reported an isolation efficiency of 60 to 70 %. The difference compared to the efficiency we report here is due to the use of PBS as isolation fluid, which is less dense than blood, as well as due to the learning curve the operator has to undergo to perform the isolation protocol.

Relatively to the recovery (Figure 17), the recovery and retrieval efficiencies were assessed. The recovery efficiency takes into the account the number of cells recovered in relation to the number of spiked cells, whereas the retrieval efficiency refers to the number of cells recovered relative to the number of cells trapped inside the device. The highest recovery and retrieval efficiency (25.4 % and 62.5 %, repectively) was achieved with the pumping mode with the connectors shift, followed by the pumping mode (2.6 % and 6.3 %) and the withdraw mode (0.2 % and 0.7 %), which results are considered negligeble.

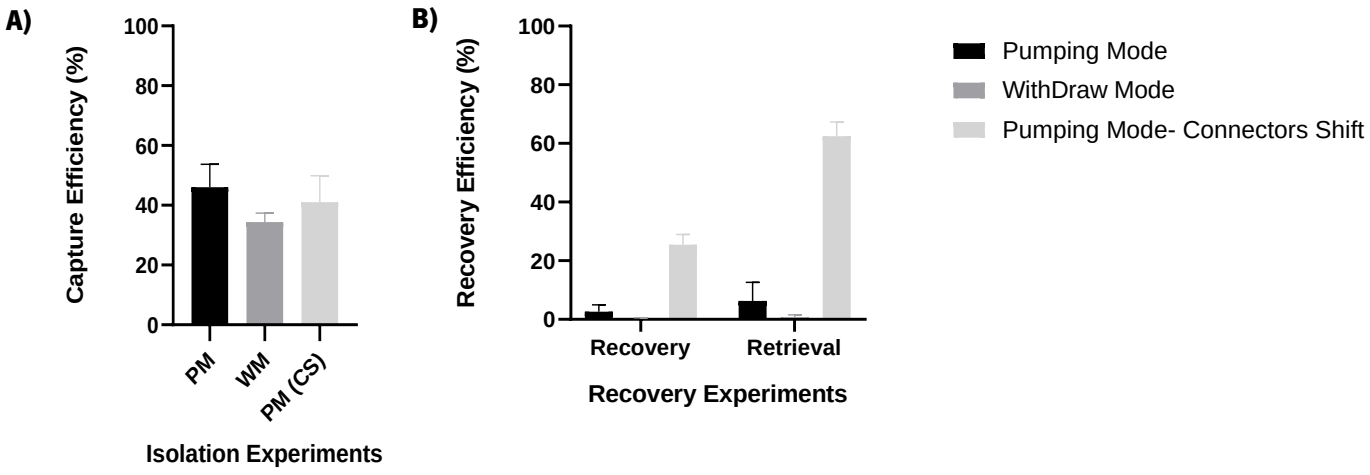

Figure 17- Graphic representation of the results achieved for A) capture Efficiency and B) recovery and retrieval Efficiency of three different recovery methods. The highest recovery and retrieval efficiency was achieved by the Pumping mode with the

connectors shift, followed by the pumping mode and the withdraw mode. Bars represent Mean±Standard Deviation between three biological replicates (n=3).

In pumping mode, when applying the same flow direction as the isolation, taking into account the design of the device, there is an added difficulty in the exit of the cells, because they have to be able to pass through the pillars, which may have contributed to the poor performance of this method. Likewise, a low efficiency with the withdraw mode may also be due to the absence of coating in the syringes to aid suction.

Thus, we can conclude that the methodology that produced the best results and efficiency was the pumping mode with the connectors shift. A recovery strategy using a reverse flow for the release of captured cells in a microfluidic device was also reported by Miller et al. [47]. Their system allowed the recovery of the trapped cells into a small volume of 100–210 μL of buffer, like PBS, achieving an average of recovery rate of 74 %. Despite their higher efficiency, their method exhibits higher isolation steps and processing time, due the usage of the flow rate of 5 mL hr^{-1} (∼83 μL min^{-1}), in contrast to your processing time of 75 minutes at a flow rate of 100 μL min^{-1}.

4.1.1.2 Optimisation of the Flow Rates

Once we had the method chosen, we decided to optimise the flow rate conditions for the recovery. Therefore, we repeated the experiments following all the parameters defined previously, but in the recovery part, the three pumping operations were performed using the same flow rate of 200 μL min^{-1}. The capture efficiency obtained was 41.1 % and, the recovery efficiency assessed was 28.1 %.

After that, we carried out another experiment intending to discover the maximum flow rate that could be applied without causing the cell bursting or any damage to the cell integrity. With this purpose, several pumping operations ranging from 200 to 300 μL min^{-1}, rising in intervals of 20 were performed under the microscope to observe the cells inside the chip and evaluate their integrity. The results (Annex 2 – Table 7) demonstrated that at all flow rates tested (maximum flow rate tested was 300 μL min^{-1}) viable cells could be recovered.

Therefore, another experiment was executed in which at the recovery step for the three pumping operations of PBS, with 350 µL each, the flow rate of 300 µL min^{-1} was used, obtaining a recovery efficiency of 27.67 %.

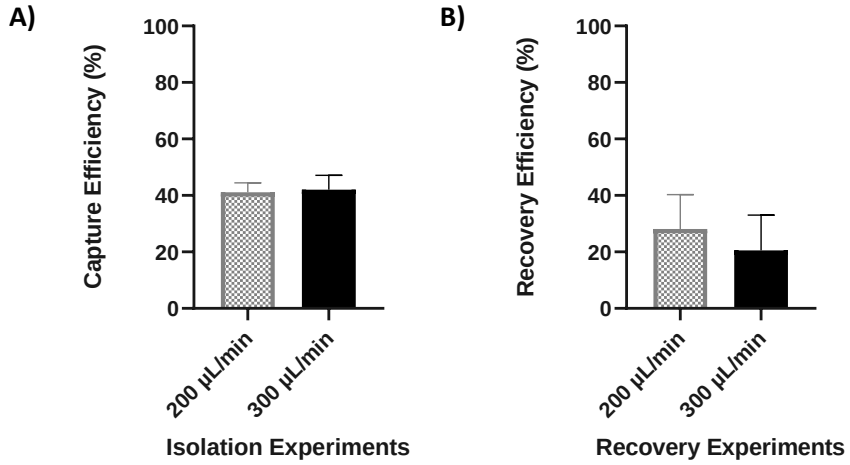

Figure 18 - Graphic with the results of A) Capture Efficiency and B) Recovery Efficiency with two different flow rates. Bars represent Mean±SD between three biological replicates (n=3).

Although the flow rate was increased, there was no evidence of improvement in the recovery efficiency (Figure 18).

4.1.1.3 Optimisation of the Washing Fluid Volume

In order to focus on the recovery protocol optimisation and decrease the interval time between isolation and recovery, in the next experiments the isolation efficiency was assumed to be 42 %. This value was inferred by calculating the average of the capture efficiencies from the previous isolation experiments performed. In this way the lag time between one step and the other is decreased, in views of accelerating the process to recover as many viable CTCs as possible when transferring the protocols into real samples.

Based on the results obtained previously, for the next experiments, we opted to only use 1 mL of PBS for the isolation instead of 7.5 mL. Moreover, the fluid used for the recovery was changed to be bovine serum albumin (BSA) added to PBS, since it is denser than the PBS and is already used for washing steps in the protocol. For this purpose, we tested three different concentrations (2.5, 5, and 10

%) (Figure19). Regarding the recovery procedure, the usual three pumping operations were carried out at 300 μL min^{-1}.

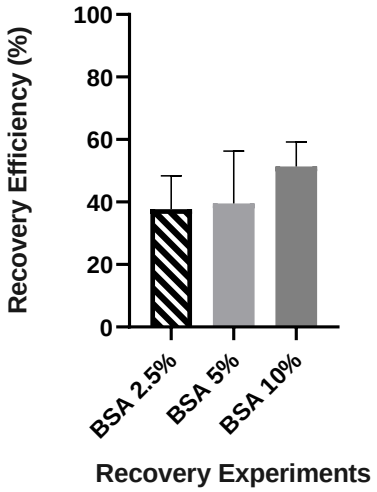

Figure 19 - Graphic with the results of the Recovery Efficiency obtained using three different BSA concentrations. As the concentration of BSA increases, the recovery Efficiency also gets higher. Bars represent Mean±SD between three biological replicates (n=3).

Indeed, the usage of BSA in PBS reflected better efficiencies results, in comparison to the previous experiments with PBS. Moreover, we also observed the highest recovery efficiency (51.4 %) with a higher concentration of BSA (10 %), meanwhile, the efficiencies for the other concentrations (2.5 and 5 %) were considerably close, 37.7 and 39.5 %, respectively.

4.1.1.4 Optimisation of the Number of Repetitions

To test the recovery protocol designed, and to adjust it to the conditions used for the processing with blood, we started to perform our experiments with a total of target 200 cells. Additionally, we also intended to ascertain the number of repetitions that we could execute, where nearly all the cells came out of the device.

For this trial, in the isolation we processed 1 mL of PBS spiked with the SW480 cells and didn´t evaluate the capture efficiency. As for the recovery, we performed several pumping operations and noted that the minimum number of repetitions, where there is no longer an outflow of cells, was six pumping

operations. (Annex 2- Table 7). Thus, after these several optimisations, we were able to gather a set of ideal parameters (Table 6) to follow up with the experiments using whole blood samples.

Table 6 - Summary of the optimal parameters gathered with the recovery experiments in PBS.

Method	*Flow Rate* ($\mu L\ min^{-1}$)	*Fluid*	*No. of Pumping Operations*
Pumping Mode – Shift connectors	300	BSA 10 %	6

4.1.2 Isolation and Recovery Experiments with Whole Blood

On our first attempt with blood, the procedure went according to as described in section 3.1.6 of the Materials and Methods. Likewise, for the recovery we used the parameters optimised in PBS, so for that, six pumping operations of 350 μL each were performed at 300 $\mu L\ min^{-1}$, using BSA 10 %. As result (Figure 20.A), we got an average of 52 % for the capture efficiency, while for the recovery we attained an efficiency of 5.4 %.

Since this was our first trial using blood, naturally we would not be able to immediately replicate the results obtained with PBS. Therefore, we repeated the experiment but, this time we double the number of repetitions to see if more pumping operations would improve the efficiency. The results (Figure 20.B) for the capture efficiency were consistent, obtaining an average of 52,6 %, however, the recovery efficiency was still low about 3.4 %.

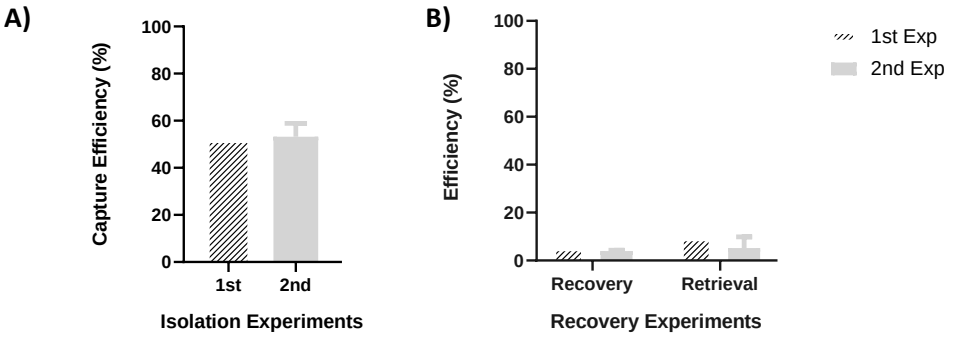

Figure 20 - Graphic representation of the A) Capture Efficiency and B) Recovery Efficiency obtained in the first experiment with blood samples. First experiment bar represent mean between two replicas (n=2). Second experiment bars represent Mean±SD between three biological replicates (n=3).

When we examined the wells from the first attempt (Figure 21), we observed that they were full of red blood cells, so the existence of cells or any events were not perceptible.

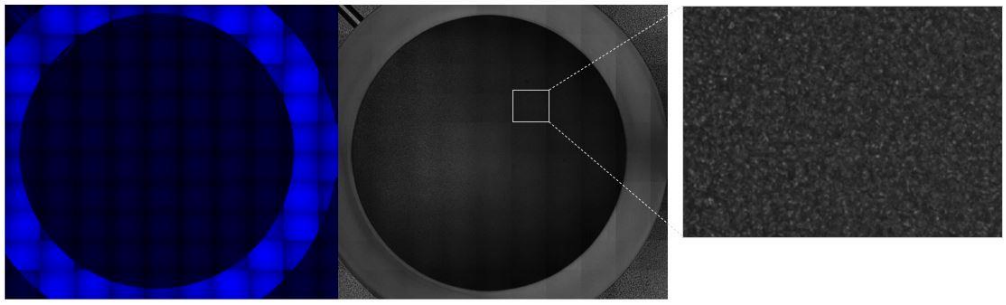

Figure 21 - Images captured of the wells obtained from the experiments with blood. The analysis of the wells shows that they are full of red blood cells and no SW480 cells can be seen.

This was also the case in the second attempt (Annex.3 – Figure 37 and 38), where we were enabled to observe any cells on either pump, which led us to add another modification in the protocol.

4.1.2.1 Optimisation of the Washing step and Connectors

For this reason, before proceeding with the recovery, we decide to implement a washing step with BSA 10 % at 200 μL min^{-1} for an Eppendorf, in order to remove and clean the device from red blood cells (Annex 4 – Figure 39). Then, the 6 pumping operations of BSA 10 % at 300 μL min^{-1} are applied and collected into a 96-well plate.

Despite this, the efficiency of the recovery did not improve, so this experiment was repeated and run under the microscope to inspect the potential problems. We discovered that the cells were not coming out of the pillar area and that in some regions they were obstructed by waste and other cellular components. Similarly, we also noticed that with the pumps only the erythrocytes were being expelled.

Given this, it was hypothesised that the difficulty in removing the cells and the blockage by other components could be due to the cell fixation process, which may be fixing the remaining components in addition to the SW480 cells. Additionally, after isolation, sedimentation of red blood cells was observed in the connectors. Since the very same connectors are used for the recovery, this may also explain the fact that only red blood cells exited the device.

In order to tackle these issues some modifications were implemented. First, in the isolation step the cells were not fixed and in the recovery step new connectors and reverse flow for the 2 mL washing step with BSA 10 % was used before the six pumps. Likewise, this time the content of the Eppendorf for the recovery efficiency was also analysed to rule out the possibility of not being reckoning cells recovered present in the Eppendorf (Annex 4 – Figure 40). On our first attempt, we only assessed the recovery efficiency attaining an average of 34.4 %. For our second repetition, we estimated the capture efficiency getting an average of 62 % and we evaluated the success of the recovery by determining both recovery and retrieval efficiency, achieving 48.4 and 75.6 %, respectively.

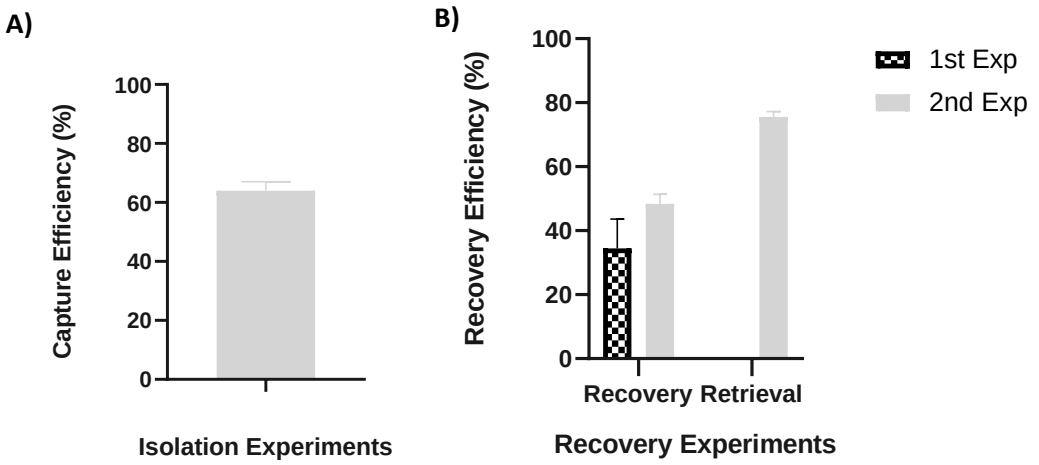

Figure 22 - Graphic with the results of the A) capture efficiency and B) recovery and retrieval efficiency assessed in the experiments with the introduction of a washing step of 2 mL of BSA 10 % at 300 μL min^{-1}. Bars represent Mean±SD between three biological replicates (n=3).

The capture efficiency obtained in blood, with the SW480 cells, was in accordance with the values of 60-70 %, reported by Carneiro et al. [67].

Despite the results obtained, the replication of these achievements using a smaller volume for the recovery was considered pertinent to try. Taking this into account, we decided to increase the PBS washing step of the isolation to 2 mL in hopes that it has the same effect as the 2 mL BSA 10 % pumping, and change the connectors in this step and, then proceed with the recovery, performing 6 pumping operations of BSA 10 %. The results (Figure 23) with this variation revealed a recovery efficiency of 22.8 %.

Moreover, we interrogated if the moment at which we change connectors in the protocol may influence the efficiency. Thus, we experimented to confront this hypothesis where, contrary to what was

done in the previous experiment, the connectors were changed right before the recovery procedure. In turn, the recovery efficiency obtained was 17.4 %.

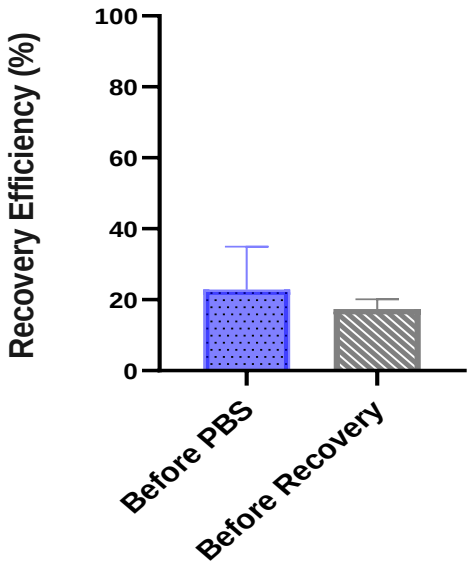

Figure 23- Graphic depicting the recovery efficiency results obtained in two different experiments carried out to compare the shift of connectors in distinct steps in the protocol. Bars represent Mean±SD between three biological replicates (n=3).

Based on the results changing the connectors before the PBS washing step contributes to better Efficiency. However, we have to take into consideration that the total initial cells from the experiment with the change of connectors before the recovery were higher than the former one (Annex 2- Figure 41), which led to slightly lower efficiency.

4.1.3 Alternative Methods

For this parallel experiment, we followed the protocol described in section 3.1.8 for the extraction and isolation of PBMCs, and the processing in the device. The capture efficiency assessed was 46.8 %. Regarding the recovery, the procedure involved the change of connectors at the 1 mL PBS washing step and the 6 pumping operations of BSA 10 % at 300 μL min^{-1}, resulting in a recovery efficiency of 21.6 %.

As an alternative, a double isolation protocol was also tested, with the steps described in detail in section 3.1.8. With this approach, we attained an average of 22.1 % for the recovery efficiency.

Finally, a third method was attempted that consisted of the regular protocol involving a red blood cells lysis step, to tackle the issues with the red blood cells influence, in which we obtained a recovery efficiency of 7.6 %.

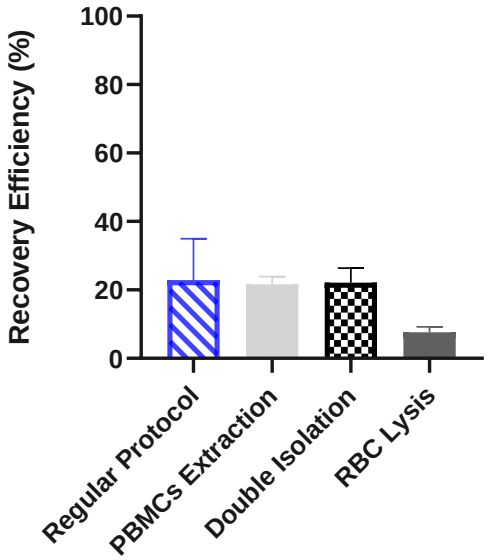

Figure 24 - Graphic illustrating the recovery efficiencies obtained using different methods for isolation and recovery. Bars represent Mean±SD between three biological replicates (n=3).

Comparing all the methodologies (Figure 24), the PBMCs extraction and isolation procedure and the double isolation protocol presented recovery efficiencies close to the regular designed and optimised recovery protocol. The red blood lysis was the method that achieved the lowest recovery efficiency.

The alternative of extracting and isolating PBMCs has been proposed as an attempt to minimise the contamination of other cellular components, such as RBCs and other PBMCs constituents, in order to promote the ideal conditions for subsequent downstream analysis. Despite exhibiting a recovery efficiency similar to the regular protocol, the recovery with the PBMCs strategy misses the purpose of the RUBYChip™ that is to process whole blood samples.

Moreover, the double isolation protocol also exhibit certain disadvantages, in comparison to the regular protocol. Firstly, it adds more lag time between the two steps. Secondly, after the first isolation and the collection of the 2 mL of 10 % BSA, the second processing performed in the isolation direction

with the Eppendorf content, enables possible recovered cells to get trapped in the pillars again. Additionally, this step also contradicts the intention of cleaning the device, as we are putting the waste mostly red blood cells, back into the device, making the recovery more challenging.

Similarly, the red blood cell lysis method, although it might be favourable considering the problem of red blood cell contamination, it may not be very suitable for our purpose, since it has been reported that treatments with red blood cell lysis might cause the loss of CTCs, leading to a reduction of the capture efficiency [10] and consequently the recovery efficiency.

Therefore, we can conclude that the regular protocol is the one that better fits the intention of increasing the purity of the sample, with the depletion of other cellular components of the blood, while maintaining a good recovery efficiency.

4.2 Droplet Experiments

Having finished the optimisations of the isolation and recovery experiments conducted with PBS and whole blood samples, using the RUBYChip™, we decided to move foward into the droplets encapsulation and sorting part of the project. For this, our droplet microfluidic device was tested for droplet encapsulation and our passive sorting system was evaluated for the efficient and selective sorting of the droplets.

4.2.1 Optimisation of the droplet size

Formation of microdroplets is ruled by various factors, such as surface tension, microfluidic geometry, viscosity, flow rate, among others. Concerning the size of the droplets, the flow rate influence is the most prominent, being associated with the ratio between the flow rates of the continuous and the dispersive phases [68][69].

Thus, our first objective was to test several flow rates combinations to enquire the size of the droplets that we were able to obtain with our device. For that purpose, the experimental setup was prepared, as described in section 3.2.2. After initiating the droplet generation process, a few minutes were waited to the microdroplets stabilize. Once they achieve monodispersity, a tube from one of the outlets was connected to the inlet of the reservoir. When a significant number of droplets is reached inside the reservoir, the reservoir is sealed and taken to the microscope to acquire pictures. The images captured were analysed using the ImageJ program. To determine the size of the droplets in ImageJ, we first set a

scale, using the distance between the pillars of the reservoirs. Then, a straight line was drawn in each droplet, and using the "Measure" option, the diameter value was obtained (Figure 25).

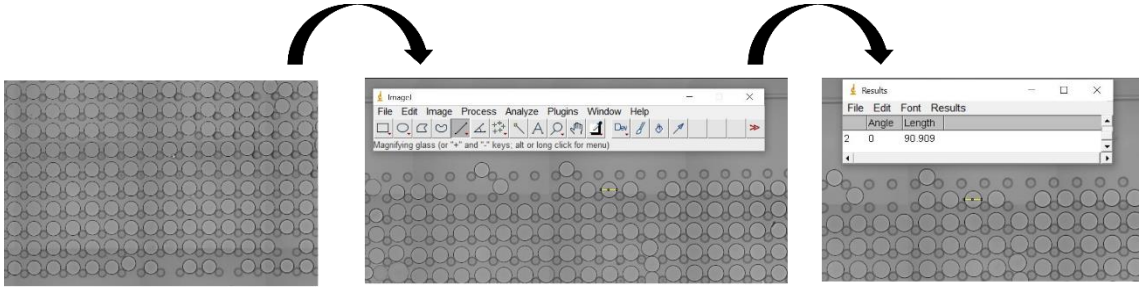

Figure 25 – Bright field images corresponding to the step-by-step schematic representation of the analysis process in the ImageJ program for the droplets size determinations. Once the scale is set, a straight line is drawn in each droplet, and using Ctrl+M the size measurements are presented. In the end, the values are transferred to an excel sheet. A total of 150 droplets are considered for these assessments. Small circles in each bright-field image are pillars, and the large circles are the droplets.

For these experiments, reservoirs with a distance between pillars of 100 and 80 µm were used. The results of the droplets size can be seen in figures 26, 27, 28 and Annex 5. Depending on the Q_c/Q_d ratio, the sizes vary ranging from 74 to 160 µm.

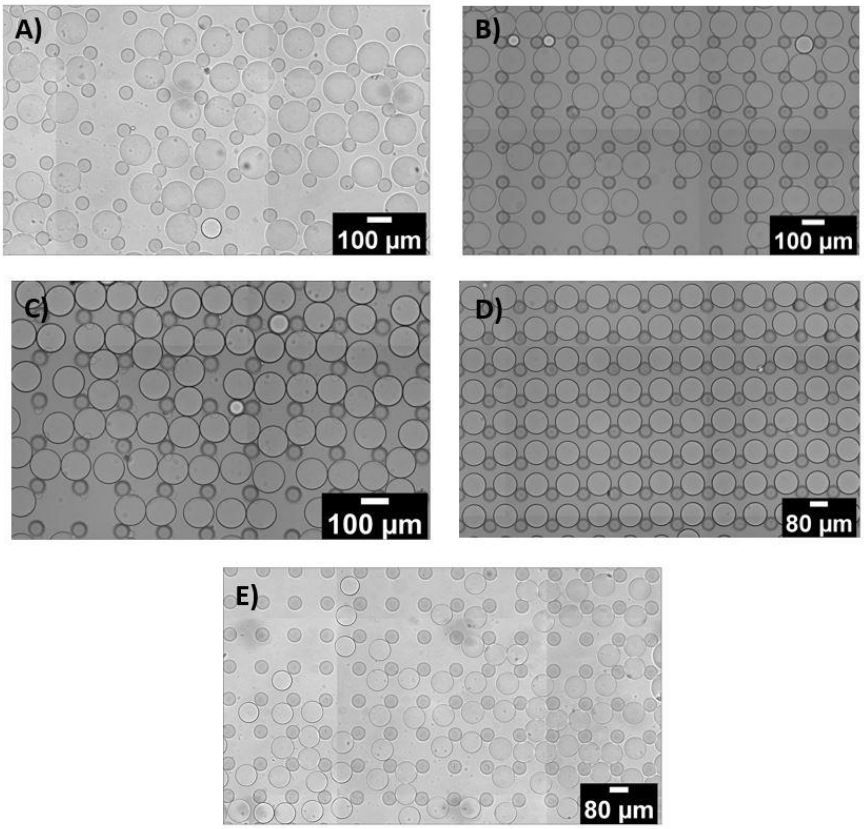

Figure 26- Bright-field images of the microdroplets contained within reservoirs of 100 and 80 µm, at different ratio values between the continuous and dispersive phases: A) 5, B) 10, C) 15, D) 20 and, E) 25, for the droplets size experiments.

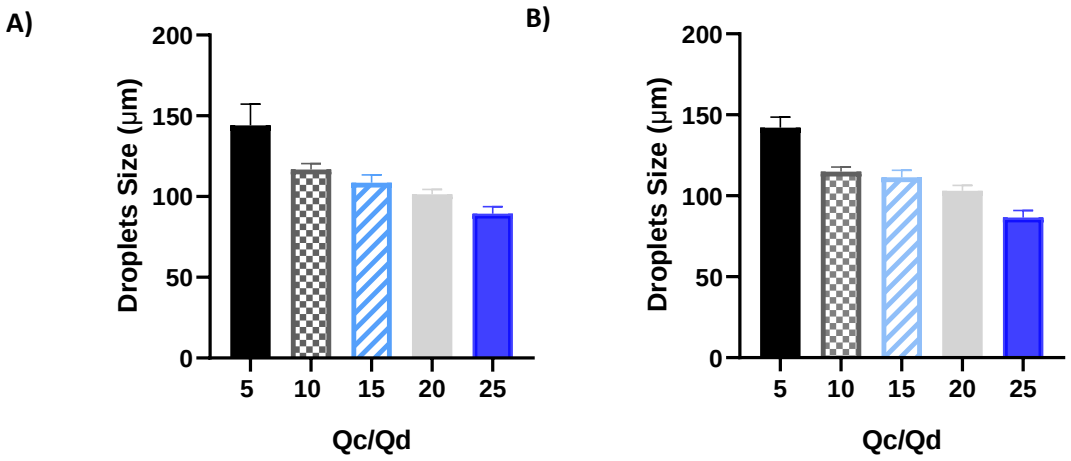

Figure 27 - Graphs with the results of droplets size experiments using A) Reservoir 1 (100 and 80 µm) and B) Reservoir 2 (100 an 80 µm) at different Qc/Qd ratios. A higher ratio corresponded to lower droplet size and viceversa. Bars represent Mean±SD between a total of 150 droplets (n=150).

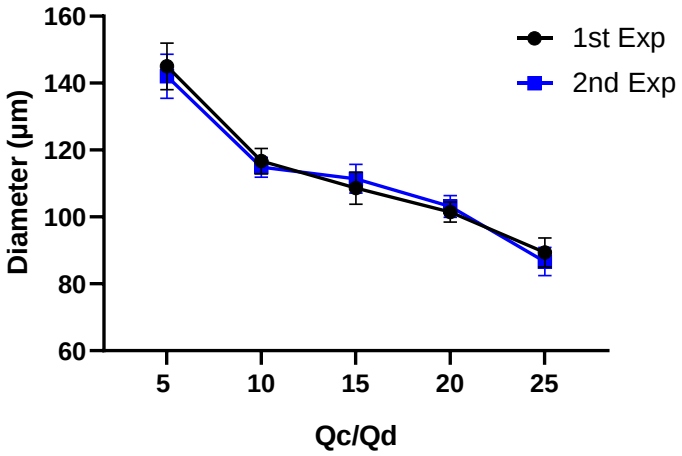

Figure 28 - Graph illustrating the variation of the average size of the droplets at different flow rate ratio values (Qc/Qd). Bars represent Mean±SD between a total 150 droplets per flow rate ratio value. (n=150).

The results evidenced that the higher the Qc/Qd ratio, the smaller the diameter of the droplets obtained, matching the information described in the literature. [70]

4.2.2 Passive Sorting Efficiency

Passive sorting methods do not demand the usage of automated external tools, exploiting the properties of the droplets and the fluids, as well as the geometry of the microfluidic chip or shear forces that act on the droplets [71].

Our approach is based on the droplets capability to shrink. For this purpose, the device design has a bifurcation where one of the channels has a constriction so that the empty droplets can squeeze and pass, while the droplets with cells follow through the other channel. Several similar studies of this type have been described in the literature, namely droplets separation based in deformation [64] and size [72].

Hence, experiments were conducted to ascertain the efficiency of our device relative to the sorting. For this set of experiments, SW480 cells were considered as the dispersed phase, and two values of cell density (1 million cells mL^{-1} and 2 million cells mL^{-1}) were tested. Based on the results from the microdroplets size optimisations, the flow rates chosen were the ones in which the Qc/Qd ratio was 10, 15, and 20. The procedure went according to as described in section 3.2.3. Once the droplets stabilised, the outlets were connected to two different reservoirs (100 μm), one to collect the empty droplets (waste), and the other one to gather the droplets with cells (sorting).

Regarding the analysis of the reservoirs, given their polydispersity, the microdroplets were counted individually and we only considered for the waste and sorting efficiencies determinations the droplets that have the size corresponding to the flow rate that we used. This criterion was applied in all experiments. In addition, to determine the efficiency, two equations were considered, already presented in section 3.2.3 of the Materials and Methods.

4.2.2.1 Results from 1st Set

The results from the experiments are displayed in figures 29, 30 and Annex 6.1. Based on the results, we can firstly mention that it was possible to perform the sorting of the droplets with the device. Secondly, we can note that the efficiency of the waste reservoir was higher than the sorting reservoir. This means that, relative to the number of total droplets counted in each reservoir, the number of empty droplets in the waste reservoir was greater than the number of droplets with cells in the sorting reservoir.

Moreover, by comparing the two cell densities, a better sorting efficiency was attained with a higher number of cells (2 million cells mL^{-1}). This is in agreement with the expected, since it was already reported by Jenifer Clausell-Tormos et al. [73], that higher cell densities have more probability of cell encapsulation (multiple cells per droplet). In opposition, low cell densities are more likely to only have one cell per droplet or having more empty droplets. This factor may also justify, why in the experiments with lower cell density (1 million cells mL^{-1}) exhibit higher waste efficiencies[52].

Additionally, we can add that with the Qc/Qd ratio of 15 we achieved a higher efficiency of sorting than the one with 20.

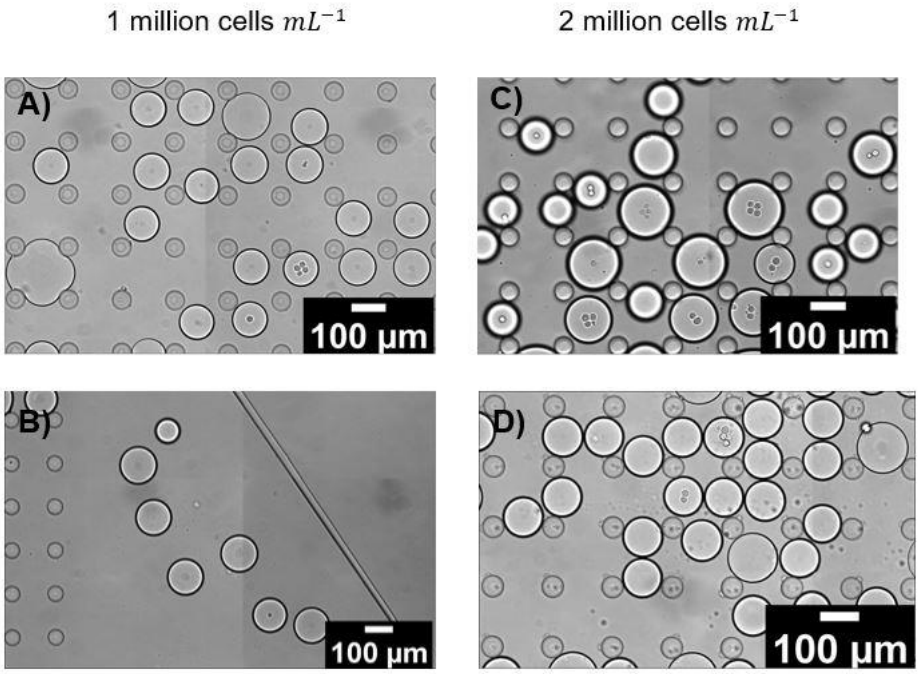

Figure 29 – Bright-field images of the microdroplets from the sorting reservoir (Reservoir 2). The sorting experiments were carried out using two different cell densities at different flow rates ratio values of 15 (A and C) and, 20 (B and D).

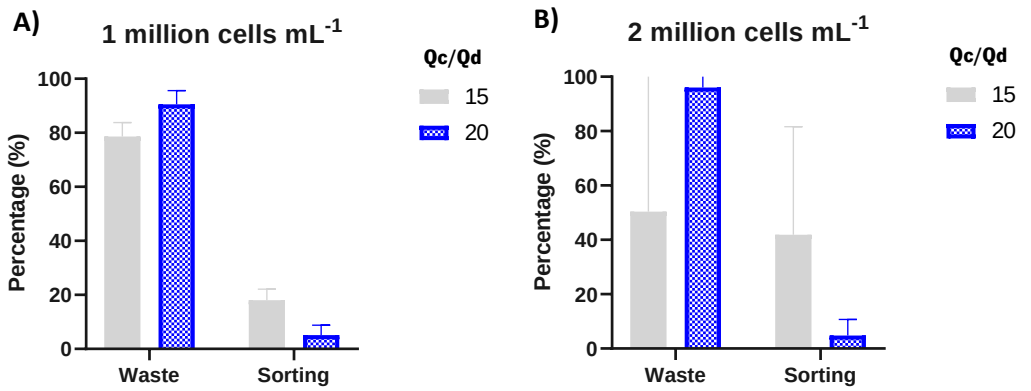

Figure 30 - Graphic depicting the results of the sorting experiments at different flow rate ratio values (Qc/Qd) using the cell densities of A) 1×10^6 and B) 2×10^6. The waste and sorting efficiency were assessed for both cell densities. Bars represent Mean±SD between three replicates (n=3).

4.2.2.2 Results from the 2nd Set

For this second set of experiments, the Qc/Qd ratio of 10 was also tested, in addition to the 15 and 20. The results obtained, figure 31, 32 and Annex 6.2, corroborated some remarks from the first set, particularly it was highlighted a higher sorting efficiency with a greater number of cells (2 million cells mL^{-1}), contrary to the waste high efficiency obtained by the lower cell density (1 million cells mL^{-1}) and, by comparing the three flow rates the 20 was the one with the lowest efficiency.

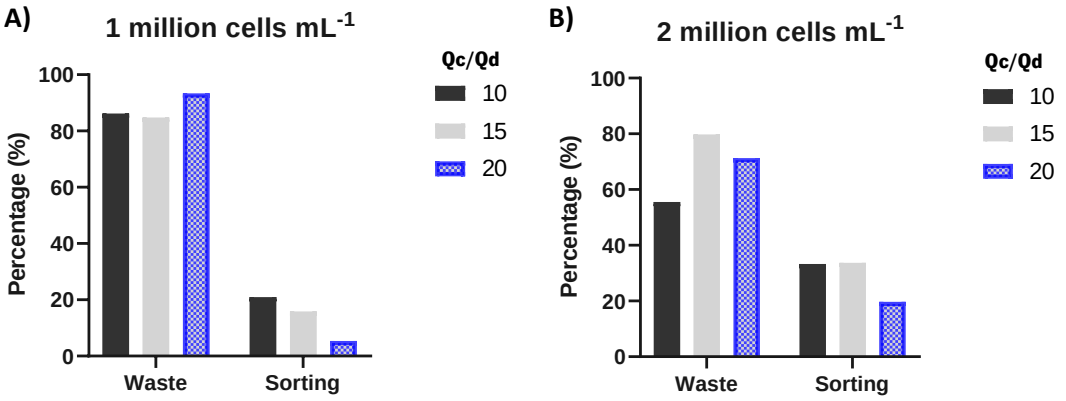

Figure 31 – Results of the sorting experiments at different flow rate ratio values (Qc/Qd) using the cell densities of A) 1×10^6 and B) 2×10^6. The waste and sorting efficiency were assessed for both cell densities

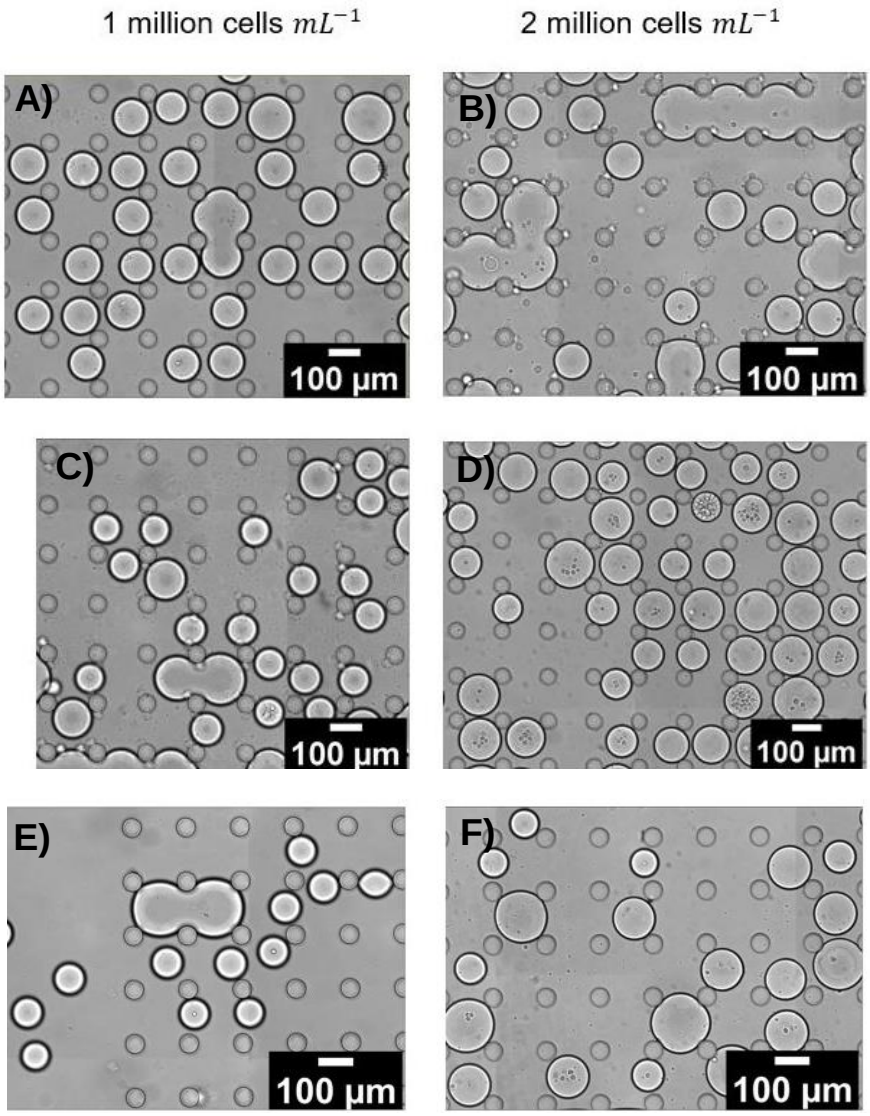

Figure 32- Bright field images of the microdroplets from the sorting reservoir (Reservoir 2). The sorting experiments were carried out using two different cell densities at different flow rates ratio values of 10 (A and B) and, 15 (C and D), and 20 (E and F).

From an overall perspective, we can state that taking into account the values from the waste and sorting Efficiency, the Qc/Qd ratio of 15 was the one who stood out and achieved the best results.

Comparing our passive sorting system to a size-based sorting microfluidic device for hydrogel droplets published by Li, Ming et all [72], regarding the capacity to discriminate the empty droplets, our device achieved efficiencies of 90%, matching the efficiencies reported of 83.3 % - 92.4 %.

On the other hand, comparing the values obtained for sorting efficiency, we managed a maximum of 41.9 %, in reference to the 88.2 % and 93.6 % attained by their system. However, we must bear in

mind that our strategy consists of droplet induced shrinking based on a constriction from the device design, meanwhile their methodology involves the encapsulation of metabolically active cells which induce size changes in droplets during cell growth. This way, their method can be more controlled, but it is only feasible after a few days of incubation of the cells. Most reported works base their sorting systems in active systems, such as dieletrophoresis or fluorescence activated sorting, among others. The reported sorting efficiencies for those works also range from 80-95 % sorting efficiencies, though they need from external instrumentation and controls [74][75]. It is worth highlighting that this work is, to the best of our knowledge, the first development based on passive sorting of empty droplets from cell-containing droplets, having droplets of the same size.

Thus, we may conclude that our device allows a selective separation of the droplets. Nevertheless, since we observed that some droplets with cells follow the constriction channel, future optimisations are still needed to improve efficiency.

4.3 Proof of Concept

As an ultimate goal, we intended to establish the interface between the isolation and recovery of CTCs with the encapsulation and sorting in microdroplets. For this, we performed two global experiments with the number of target cells of 1000 and 200 cells, as a proof of concept of the whole project.

For the isolation, 7.5 mL of whole blood spiked with SW480 cells was processed at 100 μL min^{-1}. Then the device was rinsed with BSA 2 %, the connectors are changed to new ones and, a washing step of 2 mL of PBS at 100 μL min^{-1} was completed. Thereafter, the connectors were shifted and the flow reversed and, the recovery process took place with 6 pumps of BSA 10%, a volume of 350 μL each, at a flow rate of 300 μL min^{-1}. In the end, the devices and the 96-well plate were taken to the microscope for assessment of the recovery efficiency.

Following, the recovery content from the wells was collected to a 10 mL falcon to be used as the dispersed phase in the droplets experiments. As the continuous phase, 2 % FC-40 + Pico-Surf™ 1 was used and, the setup was prepared as described in section 2.3.3. For these experiments, we selected the flow rate of 1000 μL hr^{-1}, since it exhibited a better sorting efficiency with lower cell density values. Once the formation of the droplets stabilised, the outlet tubes were connected to two reservoirs to collect the droplets for further image acquisition in the Ti-E microscope.

The results from the recoveries are presented in figure 33, and the images analysed from the reservoirs are in Annex 7.

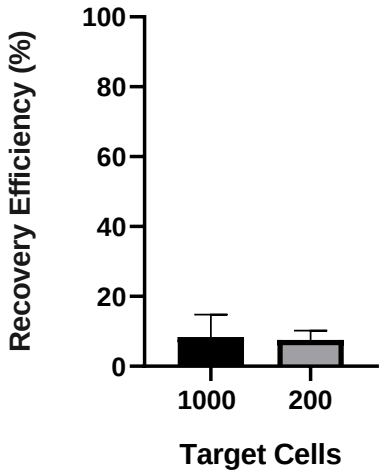

Figure 33 - Results of the recovery efficiencies from the global experiments carried out with an initial total number of cells of 1000 and 200. Bars represent Mean±SD between three biological replicates (n=3).

Regarding the droplets sorting, we were not able to observe any recovered cells encapsulated in droplets, in none of the experiments. Despite using a high value of target cells, in both experiments, we obtained low values of recovery efficiencies. In addition, we also have a large volume of the dispersed phase, 6 mL of BSA 10 % with the recovered cells, which makes the encapsulation process more difficult.

5. Conclusions and Future Perspectives

Circulating tumour cells research has had a major impact on the oncology field, leading to the development of novel CTC detection technologies based on microfluidics. In our work, the RUBYChip™, developed at the Medical Devices group of INL, was assessed in terms of isolation and detection efficiency and its potential to allow the recovery of the trapped cells.

Following the sequential order of the thesis, we can initially mention that we were able to reproduce the previously systematically tested capture efficiency results, achieving an average of 62.6 %.

In addition, an efficient recovery protocol was designed and optimised, first on PBS and then in blood, allowing the retrieval of viable model cancer cells trapped inside the device. In this part, a maximum average of recovery efficiency of 51.4 % and 48.4 %, in PBS and blood were achieved, respectively. For this, several parameters were tested and evaluated, such as flow rates, the number of pumping rounds or the fluid volume for recovery. Likewise, in blood experiments, it was fiund that the minimisation of contamination with red blood cells favoured the recovery process and contributed to a higher purity of the retrieved cells, being an essential requirement for further downstream analysis.

Additionally, single-cell studies of heterogeneity among CTCs are key for detailed characterisation and a better understanding of the causes and progression of the tumour. Only by assessing tumour heterogeneity clinicians will be able to provide an accurate identification of molecular prognostic/prediction markers and designation of suitable therapies [40]. In particular, new tools based on droplets microfluidics have emerged intending to encapsulate single cells in microdroplets for high-throughput analysis with high sensitivity and selectivity [76].

Thus, for the second part of the project, a microfluidic device for droplet generation and sorting was designed. In the sorting region, the channels have a constriction so that the empty droplets are able to go through this constriction meanwhile, the droplets with cells follow through the so-called sorting channel. The device was first optimised to achieve a suitable droplet average size, showing results consistent with previous literature [54]. Flow rates were also optimised to ease the choice of a fitting set of flow rate ratio values (Qc/Qd) for the next steps. Moreover, with the sorting experiments, the device also exhibited good functioning, being capable of selectively separating empty from filled droplets.

As such, some global experiments were carried out in order to explore the interface of the different modules: isolation and recovery module to of cell encapsulation and droplet sorting. In the experiments

performed we have not yet been able to integrate the two parts, as we were unable to verify the encapsulation of the recovered cells in the droplets. However, by having optimised both modules, promising perspectives by implementing some adjustments have been planned:

- Testing of the droplet sorting with lower cell densities, to replicate the real conditions;
- Fabrication of new designs created during this thesis with different constriction geometries and distances (20 and 30 μm) and with traps.

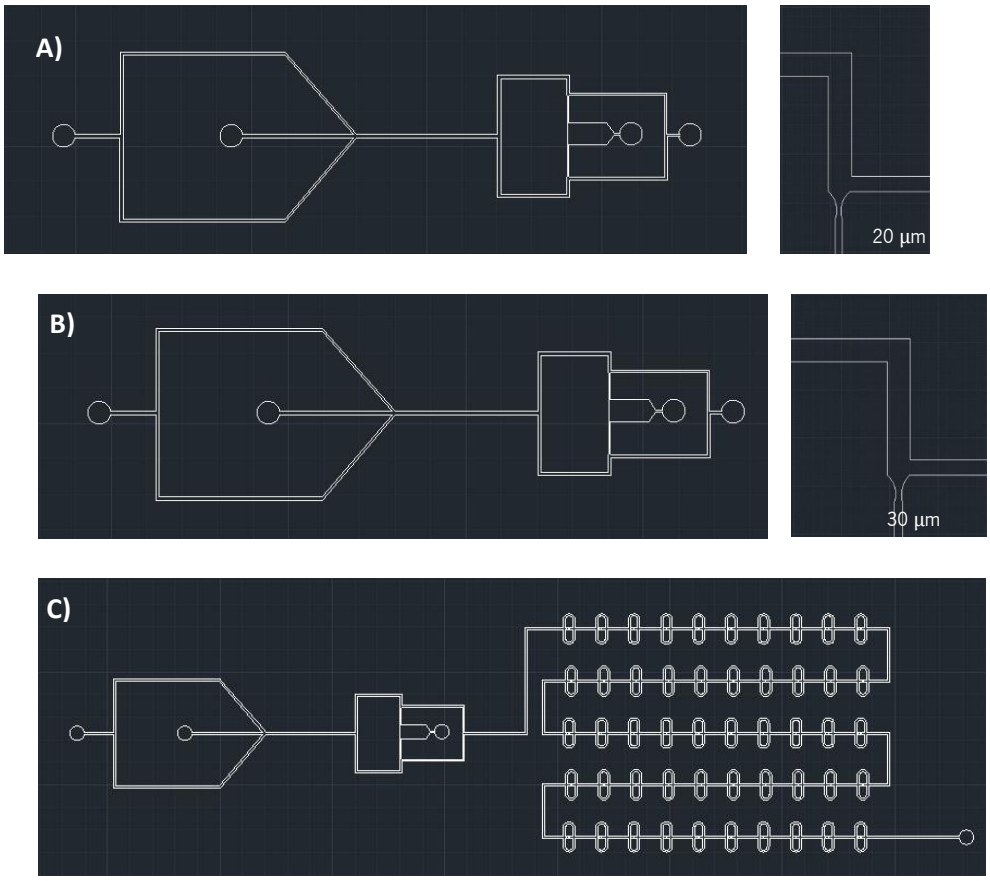

Figure 34 - Device design in AutoCAD software. A) Droplet generator and passive sorter region with a constriction of 20 μm. B) Droplet generator and passive sorter region with a constriction of 30 μm. B) Droplet generator and passive sorter region with a constriction of 25 μm, and with traps.

References

[1] Hassanpour, S. H., & Dehghani, M. (2017). Review of cancer from perspective of molecular. *Journal of Cancer Research and Practice*, *4*(4), 127–129. https://doi.org/10.1016/j.jcrpr.2017.07.001

[2] Lin, Z., Luo, G., Du, W., Kong, T., Liu, C., & Liu, Z. (2020). Recent Advances in Microfluidic Platforms Applied in Cancer Metastasis: Circulating Tumor Cells' (CTCs) Isolation and Tumor-On-A-Chip. *Small*, *16*(9), 1–21. https://doi.org/10.1002/smll.201903899

[3] Xu, H., Liu, X., & Le, W. (2018). Recent advances in microfluidic models for cancer metastasis research. *TrAC - Trends in Analytical Chemistry*, *105*, 1–6. https://doi.org/10.1016/j.trac.2018.04.007

[4] Mittal, V. (2018). Epithelial Mesenchymal Transition in Tumor Metastasis. *Annual Review of Pathology: Mechanisms of Disease*, *13*, 395–412. https://doi.org/10.1146/annurev-pathol-020117-043854

[5] Di Martino, J. S., Nobre, A. R., Mondal, C., Taha, I., Farias, E., Fertig, E., ... Bravo-Cordero, J. J. (2021). A tumor-derived type III collagen-rich ECM niche regulates tumor cell dormancy. In *Nature Portfolio*. Retrieved from https://doi.org/10.21203/rs.3.rs-580847/v1

[6] Corcoran, R. B. (2020). Liquid biopsy versus tumor biopsy for clinical-trial recruitment. *Nature Medicine*, *26*(12), 1815–1816. https://doi.org/10.1038/s41591-020-01169-6

[7] Brock, G., Castellanos-Rizaldos, E., Hu, L., Coticchia, C., & Skog, J. (2015). Liquid biopsy for cancer screening, patient stratification and monitoring. *Translational Cancer Research*, *4*(3), 280–290. https://doi.org/10.3978/j.issn.2218-676X.2015.06.05

[8] Palmirotta, R., Lovero, D., Cafforio, P., Felici, C., Mannavola, F., Pellè, E., ... Silvestris, F. (2018). Liquid biopsy of cancer: a multimodal diagnostic tool in clinical oncology. *Therapeutic Advances in Medical Oncology*, *10*, 1–24. https://doi.org/10.1177/1758835918794630

[9] Guibert, N., Pradines, A., Mazieres, J., & Favre, G. (2020). Current and future applications of liquid biopsy in nonsmall cell lung cancer from early to advanced stages. *European Respiratory Review*, *29*(155). https://doi.org/10.1183/16000617.0052-2019

[10] Bankó, P., Lee, S. Y., Nagygyörgy, V., Zrínyi, M., Chae, C. H., Cho, D. H., & Telekes, A. (2019). Technologies for circulating tumor cell separation from whole blood. *Journal of Hematology and Oncology*, *12*(1), 1–20. https://doi.org/10.1186/s13045-019-0735-4

[11] Alba-Bernal, A., Lavado-Valenzuela, R., Domínguez-Recio, M. E., Jiménez-Rodriguez, B., Queipo-Ortuño, M. I., Alba, E., & Comino-Méndez, I. (2020). Challenges and achievements of liquid biopsy technologies employed in early breast cancer. *EBioMedicine*, *62*. https://doi.org/10.1016/j.ebiom.2020.103100

[12] De Rubis, G., Rajeev Krishnan, S., & Bebawy, M. (2019). Liquid Biopsies in Cancer Diagnosis, Monitoring, and Prognosis. *Trends in Pharmacological Sciences*, *40*(3), 172–186. https://doi.org/10.1016/j.tips.2019.01.006

[13] Campos, C. D. M., Gamage, S. S. T., Jackson, J. M., Witek, M. A., Park, D. S., Murphy, M. C., ... Soper, S. A. (2018). Microfluidic-based solid phase extraction of cell free DNA. *Lab on a Chip*, *18*(22), 3459–3470. https://doi.org/10.1039/c8lc00716k

[14] Weng, J., Xiang, X., Ding, L., Wong, A. L. A., Zeng, Q., Sethi, G., ... Goh, B. C. (2021). Extracellular

vesicles, the cornerstone of next-generation cancer diagnosis? *Seminars in Cancer Biology*, *74*(May), 105–120. https://doi.org/10.1016/j.semcancer.2021.05.011

[15] Kwapisz, D. (2017). The first liquid biopsy test approved. Is it a new era of mutation testing for non-small cell lung cancer? *Annals of Translational Medicine*, *5*(3), 1–7. https://doi.org/10.21037/atm.2017.01.32

[16] Leighl, N. B., Page, R. D., Raymond, V. M., Daniel, D. B., Divers, S. G., Reckamp, K. L., ... Papadimitrakopoulou, V. A. (2019). Clinical utility of comprehensive cell-free DNA analysis to identify genomic biomarkers in patients with newly diagnosed metastatic non-small cell lung cancer. *Clinical Cancer Research*, *25*(15), 4691–4700. https://doi.org/10.1158/1078-0432.CCR-19-0624

[17] Woodhouse, R., Li, M., Hughes, J., Delfosse, D., Skoletsky, J., Ma, P., ... Dennis, L. (2020). Clinical and analytical validation of foundation one liquid CDx, a novel 324-Gene cfDNA-based comprehensive genomic profiling assay for cancers of solid tumor origin. *PLoS ONE*, *15*(9 September), 1–18. https://doi.org/10.1371/journal.pone.0237802

[18] Abalde-Cela, S., Piairo, P., & Diéguez, L. (2019). The Significance of Circulating Tumour Cells in the Clinic. *Acta Cytologica*, *63*(6), 466–478. https://doi.org/10.1159/000495417

[19] Lozar, T., Gersak, K., Cemazar, M., Kuhar, C. G., & Jesenko, T. (2019). The biology and clinical potential of circulating tumor cells. *Radiology and Oncology*, *53*(2), 131–147. https://doi.org/10.2478/raon-2019-0024

[20] Lianidou, E., & Pantel, K. (2019). Liquid biopsies. *Genes Chromosomes and Cancer*, *58*(4), 219–232. https://doi.org/10.1002/gcc.22695

[21] Cho, H., Kim, J., Song, H., Sohn, K. Y., Jeon, M., & Han, K. H. (2018). Microfluidic technologies for circulating tumor cell isolation. *Analyst*, *143*(13), 2936–2970. https://doi.org/10.1039/c7an01979c

[22] Allard, W. J., Matera, J., Miller, M. C., Repollet, M., Connelly, M. C., Rao, C., ... Terstappen, L. W. M. M. (2004). Tumor cells circulate in the peripheral blood of all major carcinomas but not in healthy subjects or patients with nonmalignant diseases. *Clinical Cancer Research*, *10*(20), 6897–6904. https://doi.org/10.1158/1078-0432.CCR-04-0378

[23] Cristofanilli, M., Budd, G. T., Ellis, M. J., Stopeck, A., Matera, J., Miller, M. C., ... Hayes, D. F. (2004). Circulating tumor cells, disease progression, and survival in metastatic breast cancer. *New England Journal of Medicine*, *351*(8), 781–791. https://doi.org/10.1056/NEJMoa040766

[24] Lu, C. Y., Uen, Y. H., Tsai, H. L., Chuang, S. C., Hou, M. F., Wu, D. C., ... Wang, J. Y. (2011). Molecular detection of persistent postoperative circulating tumour cells in stages II and III colon cancer patients via multiple blood sampling: Prognostic significance of detection for early relapse. *British Journal of Cancer*, *104*(7), 1178–1184. https://doi.org/10.1038/bjc.2011.40

[25] Cortés-Hernández, L. E., Eslami-S, Z., & Alix-Panabières, C. (2020). Circulating tumor cell as the functional aspect of liquid biopsy to understand the metastatic cascade in solid cancer. *Molecular Aspects of Medicine*, *72*(July), 0–1. https://doi.org/10.1016/j.mam.2019.07.008

[26] Zhang, L., Ridgway, L. D., Wetzel, M. D., Ngo, J., Yin, W., Kumar, D., ... Marchetti, D. (2013). The identification and characterization of breast cancer CTCs competent for brain metastasis. *Science Translational Medicine*, *5*(180). https://doi.org/10.1126/scitranslmed.3005109

[27] Drapkin, B. J., George, J., Christensen, C. L., Mino-Kenudson, M., Dries, R., Sundaresan, T., ... Farago, A. F. (2018). Genomic and functional fidelity of small cell lung cancer patient-derived xenografts. *Cancer Discovery*, *8*(5), 600–615. https://doi.org/10.1158/2159-8290.CD-17-0935

[28] Lei, K. F. (2020). A review on microdevices for isolating circulating tumor cells. *Micromachines*, *11*(5), 1–19. https://doi.org/10.3390/mi11050531

[29] Low, W. S., & Wan Abas, W. A. B. (2015). Benchtop technologies for circulating tumor cells separation based on biophysical properties. *BioMed Research International*, *2015*. https://doi.org/10.1155/2015/239362

[30] Park, S., Ang, R. R., Duffy, S. P., Bazov, J., Chi, K. N., Black, P. C., & Ma, H. (2014). Morphological differences between circulating tumor cells from prostate cancer patients and cultured prostate cancer cells. *PLoS ONE*, *9*(1). https://doi.org/10.1371/journal.pone.0085264

[31] Byun, S., Son, S., Amodei, D., Cermak, N., Shaw, J., Kang, J. H., ... Manalis, S. R. (2013). Characterizing deformability and surface friction of cancer cells. *Proceedings of the National Academy of Sciences of the United States of America*, *110*(19), 7580–7585. https://doi.org/10.1073/pnas.1218806110

[32] Byun, S., Son, S., Amodei, D., Cermak, N., Shaw, J., Kang, J. H., ... Manalis, S. R. (2013). Characterizing deformability and surface friction of cancer cells. *Proceedings of the National Academy of Sciences of the United States of America*, *110*(19), 7580–7585. https://doi.org/10.1073/pnas.1218806110

[33] A. Mohammadalipou, Y. E. Choi, F. Benencia, M. Burdick, and D. F. J. T. (2012). Investigation of mechanical properties of breast cancer cells using micropipette aspiration technique. *The Journal of the Federation of American Societies for Experimental Biology*, *26*, 905–909.

[34] Becker, F. F., Wang, X., Huang, Y., Pethigt, R., Vykoukal, J., & Gascoyne, P. R. C. (1995). Seperation of human breast cancer cells using micropipette aspiration technique. *Proceedings of the National Academy of Sciences of the United States of America*, *92*(3), 860–864.

[35] Qiao, G., Duan, W., Chatwin, C., Sinclair, A., & Wang, W. (2010). Electrical properties of breast cancer cells from impedance measurement of cell suspensions. *Journal of Physics: Conference Series*, *224*(1), 2–6. https://doi.org/10.1088/1742-6596/224/1/012081

[36] Hsieh, J. C.-H., & Wu, T. M.-H. (2016). The Selection Strategy for Circulating Tumor Cells (CTCs) Isolation and Enumeration: Technical Features, Methods, and Clinical Applications. *Tumor Metastasis*. https://doi.org/10.5772/64812

[37] Habli, Z., Alchamaa, W., Saab, R., Kadara, H., & Khraiche, M. L. (2020). Circulating tumor cell detection technologies and clinical utility: Challenges and opportunities. *Cancers*, *12*(7), 1–30. https://doi.org/10.3390/cancers12071930

[38] Cheng, J., Liu, Y., Zhao, Y., Zhang, L., Zhang, L., Mao, H., & Huang, C. (2020). Nanotechnology-assisted isolation and analysis of circulating tumor cells on microfluidic devices. *Micromachines*, *11*(8). https://doi.org/10.3390/MI11080774

[39] Cho, H., Kim, J., Song, H., Sohn, K. Y., Jeon, M., & Han, K. H. (2018). Microfluidic technologies for circulating tumor cell isolation. *Analyst*, *143*(13), 2936–2970. https://doi.org/10.1039/c7an01979c

[40] Rushton, A. J., Nteliopoulos, G., Shaw, J. A., & Coombes, R. C. (2021). A review of circulating tumour cell enrichment technologies. *Cancers*, *13*(5), 1–33. https://doi.org/10.3390/cancers13050970

[41] Sollier, E., Go, D. E., Che, J., Gossett, D. R., O'Byrne, S., Weaver, W. M., ... Di Carlo, D. (2014). Size-selective collection of circulating tumor cells using Vortex technology. *Lab on a Chip*, *14*(1), 63–77. https://doi.org/10.1039/c3lc50689d

[42] Ribeiro-Samy, S., Oliveira, M. I., Pereira-Veiga, T., Muinelo-Romay, L., Carvalho, S., Gaspar, J., ... Diéguez, L. (2019). Fast and efficient microfluidic cell filter for isolation of circulating tumor cells from unprocessed whole blood of colorectal cancer patients. *Scientific Reports*, *9*(1), 1–12. https://doi.org/10.1038/s41598-019-44401-1

[43] Lopes, C., Piairo, P., Chícharo, A., Abalde-Cela, S., Pires, L. R., Corredeira, P., ... Diéguez, L. (2021). Her2 expression in circulating tumour cells isolated from metastatic breast cancer patients using a size-based microfluidic device. *Cancers*, *13*(17). https://doi.org/10.3390/cancers13174446

[44] Sharma, S., Zhuang, R., Long, M., Pavlovic, M., Kang, Y., Ilyas, A., & Asghar, W. (2018). Circulating tumor cell isolation, culture, and downstream molecular analysis. *Biotechnology Advances*, *36*(4), 1063–1078. https://doi.org/10.1016/j.biotechadv.2018.03.007

[45] Hou, H. W., Warkiani, M. E., Khoo, B. L., Li, Z. R., Soo, R. A., Tan, D. S. W., ... Lim, C. T. (2013). Isolation and retrieval of circulating tumor cells using centrifugal forces. *Scientific Reports*, *3*, 1–8. https://doi.org/10.1038/srep01259

[46] Sarioglu, A. F., Aceto, N., Kojic, N., Donaldson, M. C., Hamza, B., Engstrom, A., ... Chase, C. (2015). A microfluidic device for label-free, physical capture of circulating tumor cell-clusters. *Nature Methods*, *12*(7), 685–691. https://doi.org/10.1038/nmeth.3404.A

[47] Miller, M. C., Robinson, P. S., Wagner, C., & O'Shannessy, D. J. (2018). The Parsortix™ Cell Separation System—A versatile liquid biopsy platform. *Cytometry Part A*, *93*(12), 1234–1239. https://doi.org/10.1002/cyto.a.23571

[48] Gross, A., Schoendube, J., Zimmermann, S., Steeb, M., Zengerle, R., & Koltay, P. (2015). Technologies for single-cell isolation. *International Journal of Molecular Sciences*, *16*(8), 16897–16919. https://doi.org/10.3390/ijms160816897

[49] Ye, F., Huang, W., & Guo, G. (2017). Studying hematopoiesis using single-cell technologies. *Journal of Hematology and Oncology*, *10*(1), 1–12. https://doi.org/10.1186/s13045-017-0401-7

[50] Heymann, D., & Téllez-Gabriel, M. (2018). Circulating tumor cells: The importance of single cell analysis. *Advances in Experimental Medicine and Biology*, *1068*, 45–58. https://doi.org/10.1007/978-981-13-0502-3_5

[51] Murphy, T. W., Zhang, Q., Naler, L. B., Ma, S., & Lu, C. (2018). Recent advances in the use of microfluidic technologies for single cell analysis. *Analyst*, *143*(1), 60–80. https://doi.org/10.1039/c7an01346a

[52] Lin, Jin-Ming (2019). *[Integrated Analytical Systems] Microfluidics for Single-Cell Analysis. 10.1007/978-981-32-9729-6().* doi:10.1007/978-981-32-9729-6

[53] Sohrabi, S., Kassir, N., & Keshavarz Moraveji, M. (2020). Droplet microfluidics: Fundamentals and its advanced applications. *RSC Advances*, *10*(46), 27560–27574. https://doi.org/10.1039/d0ra04566g

[54] Matuła, K., Rivello, F., & Huck, W. T. S. (2020). Single-Cell Analysis Using Droplet Microfluidics. *Advanced Biosystems*, *4*(1). https://doi.org/10.1002/adbi.201900188

[55] Zhu, P., & Wang, L. (2017). Passive and active droplet generation with microfluidics: a review. *Lab on a Chip*, *17*(1), 34–75. https://doi.org/10.1039/C6LC01018K

[56] Sinha, N., Subedi, N., Tel, J., & Systems, C. M. (2018). Integrating Immunology and Microfluidics for Single Immune Cell Analysis. *Front. Immunol*, *9*(2373). https://doi.org/10.3389/fimmu.2018.02373

[57] Mazutis, L., Gilbert, J., Ung, W. L., Weitz, D. A., Griffiths, A. D., & Heyman, J. A. (2013). Single-cell analysis and sorting using droplet-based microfluidics. *Nature Protocols*, *8*(5), 870–891. https://doi.org/10.1038/nprot.2013.046

[58] Wen, N., Zhao, Z., Fan, B., Chen, D., Men, D., Wang, J., & Chen, J. (2016). Development of Droplet Microfluidics Enabling. *Molecules*, *21*(7), 1–13. https://doi.org/10.3390/molecules21070881

[59] Shen, Y., Yalikun, Y., & Tanaka, Y. (2019). Recent advances in microfluidic cell sorting systems. *Sensors and Actuators, B: Chemical*, *282*(October 2018), 268–281. https://doi.org/10.1016/j.snb.2018.11.025

[60] Zhang, Y., Zheng, T., Wang, L., Feng, L., Wang, M., & Zhang, Z. (2021). From passive to active sorting in microfluidics : A review. *REVIEWS ON ADVANCED MATERIALS SCIENCE*, 313–324.

[61] Thomas, R. S. W., Mitchell, P. D., Oreffo, R. O. C., Morgan, H., & Green, N. G. (2019). Image-based sorting and negative dielectrophoresis for high purity cell. *Electrophoresis*, *40*, 2718–2727. https://doi.org/10.1002/elps.201800489

[62] Shang, L., Cheng, Y., & Zhao, Y. (2017). Emerging Droplet Microfluidics. *Chemical Reviews*, *117*(12), 7964–8040. https://doi.org/10.1021/acs.chemrev.6b00848

[63] Mazutis, L., & Griffiths, A. D. (2013). Preparation of monodisperse emulsions by hydrodynamic size fractionation Preparation of monodisperse emulsions by hydrodynamic size fractionation. *Applied Physics Letters*, *204103*(2009), 111–114. https://doi.org/10.1063/1.3250432

[64] Chang, Y., Chen, X., Zhou, Y., & Wan, J. (2020). Deformation-Based Droplet Separation in Microfluidics. *Industrial and Engineering Chemistry Research*, *59*(9), 3916–3921. https://doi.org/10.1021/acs.iecr.9b04823

[65] Diéguez, Lorena, Samy, Silvina, Oliveira,Marta , Gaspar, J. (2016). *Patent No. PCT/EP20 16/078406*.

[66] Xu, L., Mao, X., Imrali, A., Syed, F., & Mutsvangwa, K. (2015). Optimization and Evaluation of a Novel Size Based Circulating Tumor Cell Isolation System. *PLoS ONE*, 1–23. https://doi.org/10.1371/journal.pone.0138032

[67] Carneiro, A., Piairo, P., Teixeira, A., Ferreira, D., Cotton, S., Rodrigues, C., ... Di, L. (2022). Discriminating Epithelial to Mesenchymal Transition Phenotypes in Circulating Tumor Cells Isolated from Advanced Gastrointestinal Cancer Patients. *Cells*, *11*, 376.

[68] Lapierre, F., Wu, N., & Zhu, Y. (2011). Influence of flow rate on the droplet generation process in a microfluidic chip. *Smart Nano-Micro Materials and Devices*, *8204*, 82040H. https://doi.org/10.1117/12.903271

[69] Collins, J., & Lee, A. P. (2007). Control of serial microfluidic droplet size gradient by step-wise ramping of flow rates. *Microfluidics and Nanofluidics*, *3*(1), 19–25. https://doi.org/10.1007/s10404-006-0093-8

[70] Loizou, K., Wong, V. L., & Hewakandamby, B. (2018). Examining the effect of flow rate ratio on droplet generation and regime transition in a microfluidic t-junction at constant capillary numbers. *Inventions*, *3*(3). https://doi.org/10.3390/inventions3030054

[71] Rashid, Z., Erten, A., Morova, B., Muradoglu, M., Jonáš, A., & Kiraz, A. (2019). Passive sorting of emulsion droplets with different interfacial properties using laser-patterned surfaces. *Microfluidics and Nanofluidics*, *23*(5), 1–9. https://doi.org/10.1007/s10404-019-2236-8

[72] Li, M., Van Zee, M., Goda, K., & Di Carlo, D. (2018). Size-based sorting of hydrogel droplets using inertial microfluidics. *Lab on a Chip*, *18*(17), 2575–2582. https://doi.org/10.1039/c8lc00568k

[73] Clausell-Tormos, J., Lieber, D., Baret, J. C., El-Harrak, A., Miller, O. J., Frenz, L., ... Merten, C. A. (2008). Droplet-Based Microfluidic Platforms for the Encapsulation and Screening of Mammalian Cells and Multicellular Organisms. *Chemistry and Biology*, *15*(5), 427–437. https://doi.org/10.1016/j.chembiol.2008.04.004

[74] Best, Roshi, Abalde-Cela, Sara, Abell, Chris, G.Smith, A. (2016). Applications of Microdroplet Technology for Algal Biotechnology. *Current Biotechnology*, *4*, 109–117.

[75] Li, M., Liu, H., Zhuang, S., & Goda, K. (2021). Droplet flow cytometry for single-cell analysis. *RSC Advances*, *11*(34), 20944–20960. https://doi.org/10.1039/d1ra02636d

[76] Kang, D. K., Monsur Ali, M., Zhang, K., Pone, E. J., & Zhao, W. (2014). Droplet microfluidics for single-molecule and single-cell analysis in cancer research, diagnosis and therapy. *TrAC - Trends in Analytical Chemistry*, *58*, 145–153. https://doi.org/10.1016/j.trac.2014.03.006

Annex 1- Images of the set-up organisation of the various experiments

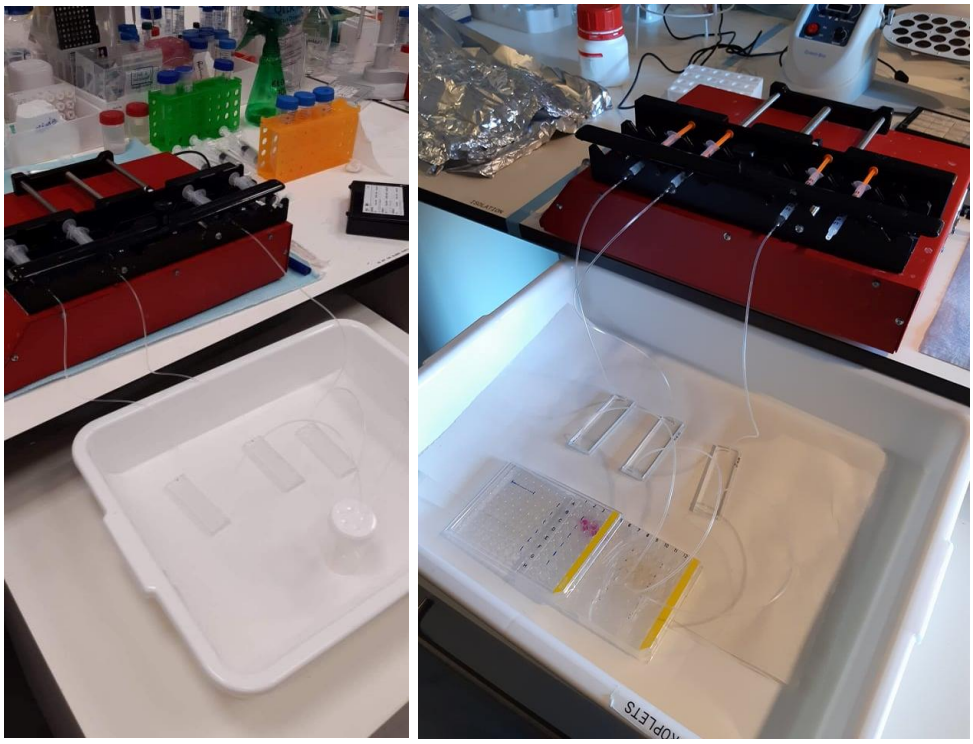

Figure 35 - Image depicting the actual aspect of the: A) processing and isolation experiments. B) recovery experiments.

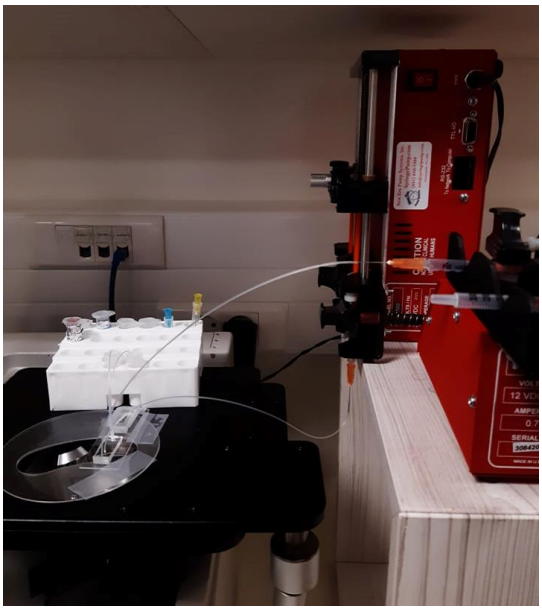

Figure 36- Image depicting the actual aspect of the cell encapsulation and sorting experiments.

Annex 2- Flow Rate and Number of Repetitions Optimisations

Table 7 - Results obtained in the experiment conducted under the microscope to monitor and evaluate the effect of increasing flow rates on the cells.

Flow Rate ($\mu L\ min^{-1}$)	200	220	240	260	280	300	Total
Well 1	182	8	0	1	1	1	190
Well 2	119	10	2	3	1	20	131
Well 3	126	13	21	2	2	7	160

Table 8 - Results obatined in the experiment carried out to determine the minimum number of pumps necessary to not observe the exit of cells.

Pump	**1st**	**2nd**	**3rd**	**4th**	**5th**	**6th**	**Total**
Well 1	40	11	16	1	6	1	67
Well 2	28	14	11	6	2	1	53
Well 3	21	14	11	4	2	1	46

Annex 3- First Attempts of Recovery in Blood

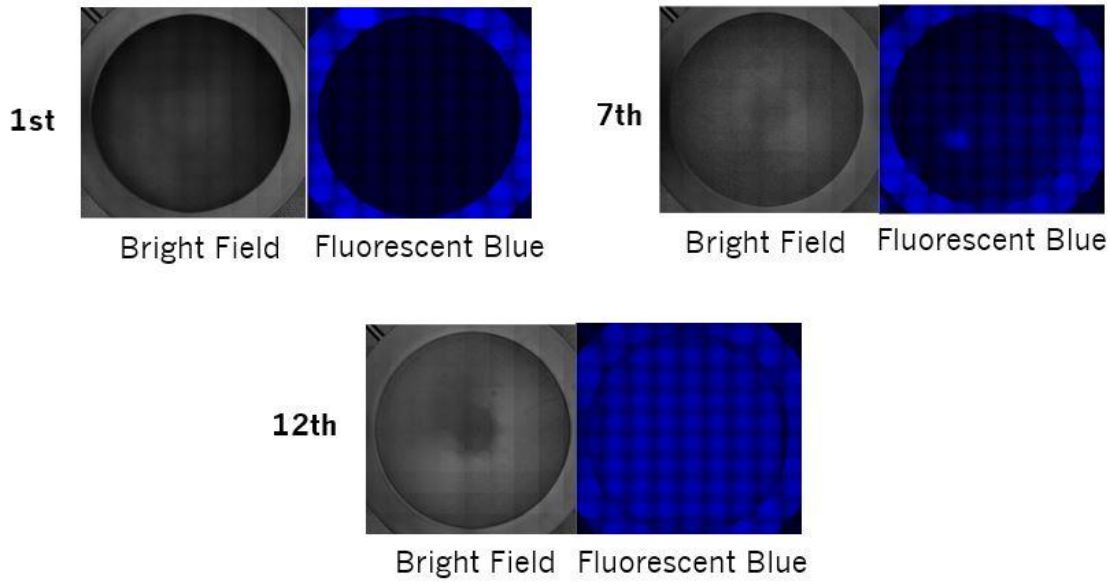

Figure 37 - Image captured of the wells after 12 pumps of 350 μL each for the recovery step in blood. In both Bright Field and Fluorescent Blue, we can see the wells full of red blood cells and no sight of SW480 cells

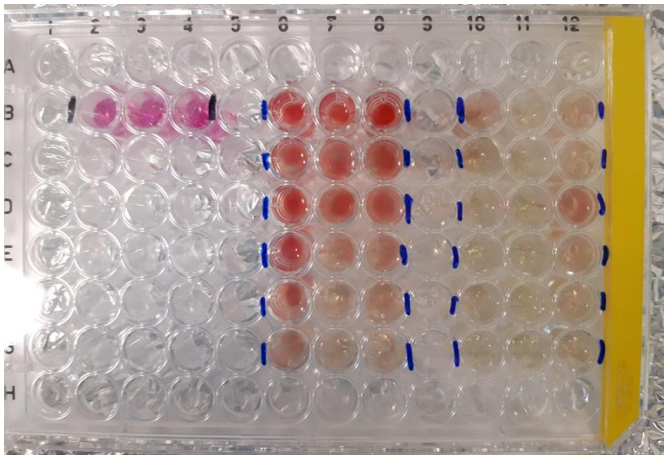

Figure 38 - Image captured of the wells after 12 pumps of 350 μL each for the recovery step in Blood.

Annex 4 – Recovery in Blood Optimisations – Washing Step and Connectors

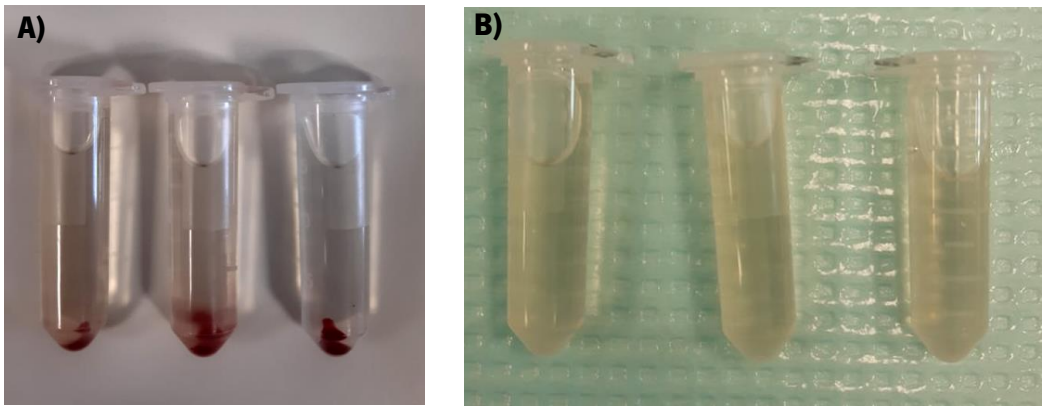

Figure 39 - Pictures of the Eppendorf utilised for the 2 mL BSA 10 % washing pump at 300 μL min^{-1}, previous to the recovery, without (A) and with (B) changing the connectors to new ones.

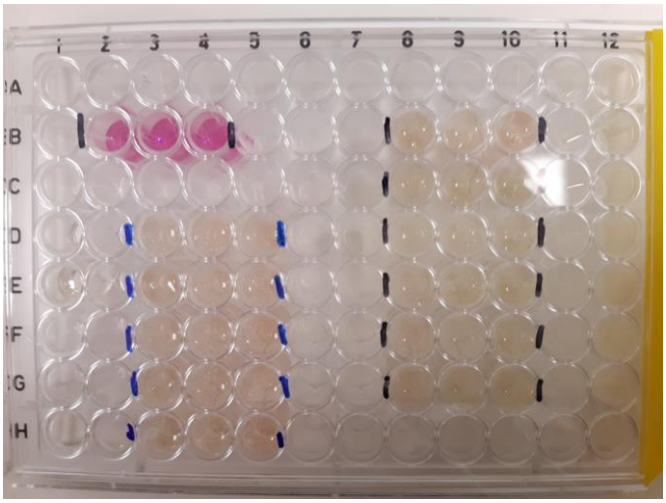

Figure 40 - Image captured of the wells the recovery step with the implementation of the change of the connectors to new ones, and the 2mL BSA 10 % washing pump. The wells on the right, marked in black, correspond to the 6 pumps of the recovery, while the ones in the left side, marked in blue, are relative to the Eppendorf with the 2mL BSA 10 % washing pump.

CONNECTORS CHANGE BEFORE STARTING RECOVERY

Initial total cells

	Total
Well 1	195
Well 2	234
Well 3	240

Total cells recovered

	Total
Well 1	34
Well 2	47
Well 3	35

Recovery Efficiency (%)	
Device 1	17.4
Device 2	20.1
Device 3	14.6

Average: 17.4%

CONNECTORS CHANGE BEFORE STARTING PBS WASHING STEP

Initial total cells

	Total
Well 1	174
Well 2	154
Well 3	180

Total cells recovered

	Total
Well 1	37
Well 2	55
Well 3	21

Recovery Efficiency (%)	
Device 1	21.3
Device 2	35.7
Device 3	11.6

Average: 22.8%

Figure 41 - Results depicting the comparison between the change of the connectors before the recovery and beforre starting the PBS washing step.

Annex 5- Droplets Size Experiments

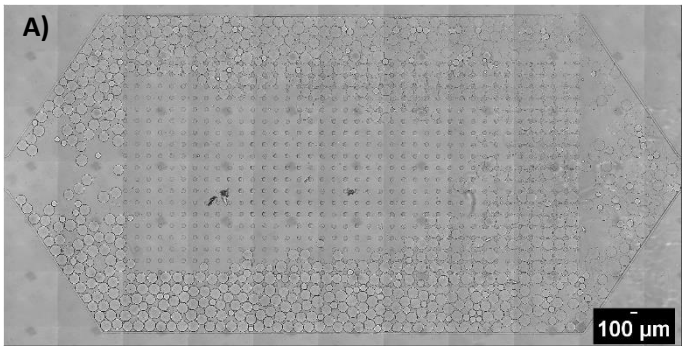

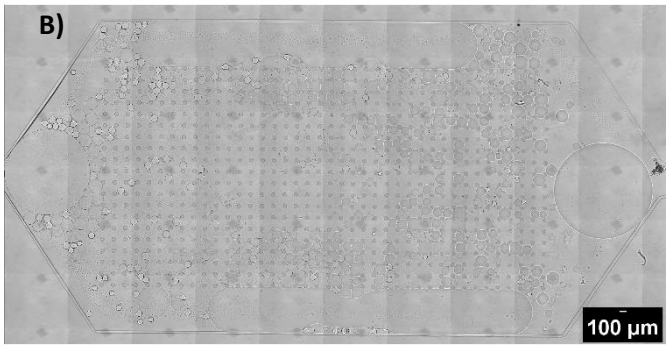

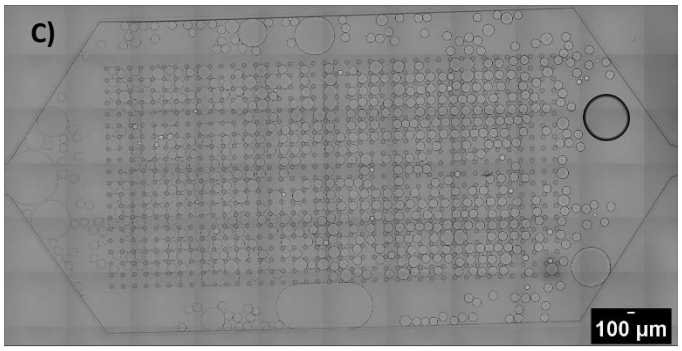

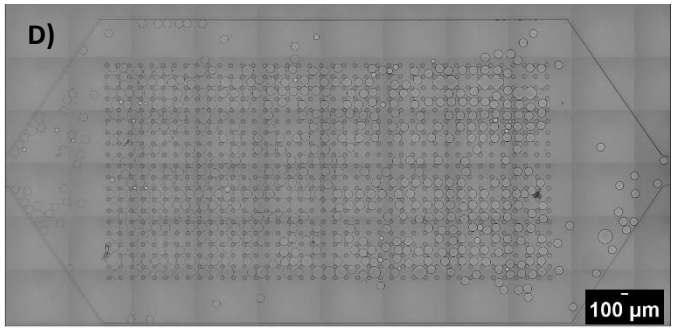

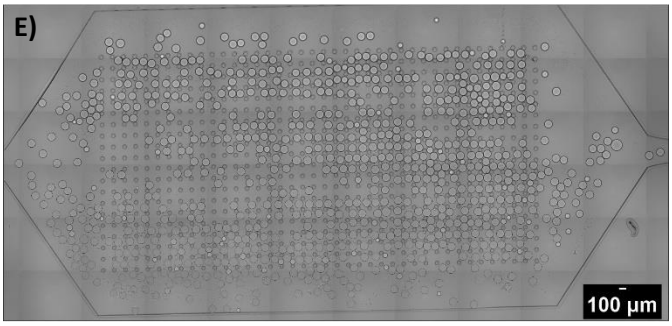

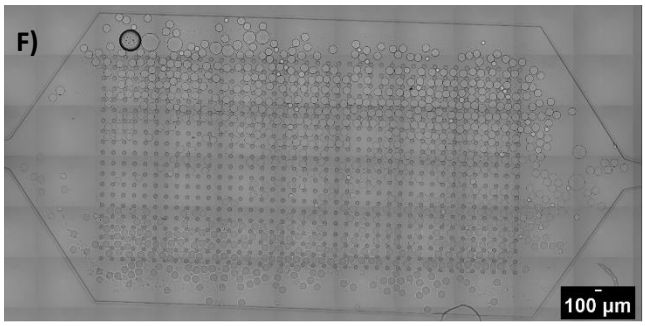

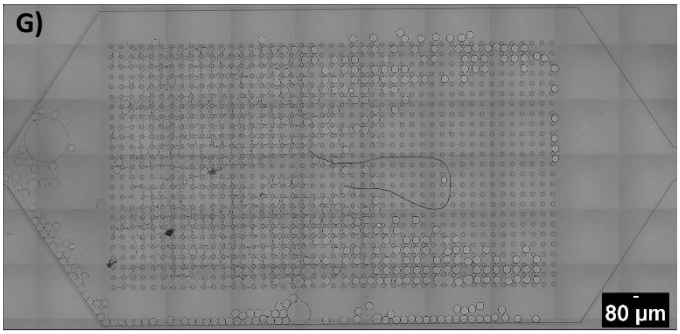

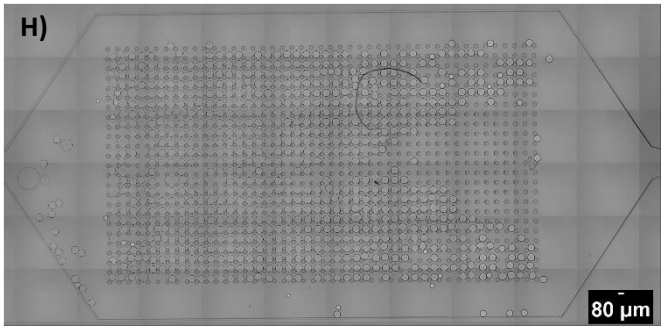

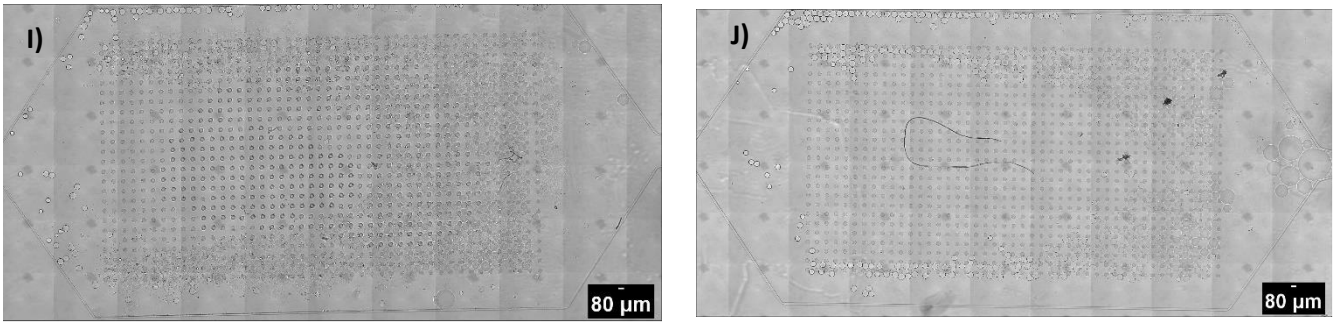

Figure 42- Scan images of the reservoirs used for the droplet size experiments at different flow rate ratio values. A) Reservoir 1 (100 µm) at Qc/Qd of 5; B) Reservoir 2 (100 µm) at Qc/Qd of 5; C) Reservoir 1 (100 µm) at Qc/Qd of 10; D) Reservoir 2 (100 µm) at Qc/Qd of 10; E) Reservoir 1 (100 µm) at Qc/Qd of 15; F) Reservoir 2 (100 µm) at Qc/Qd of 15; G) Reservoir 1 (80 µm) at Qc/Qd of 20; H) Reservoir 2 (80 µm) at Qc/Qd of 20; I) Reservoir 1 (80 µm) at Qc/Qd of 25 and J) Reservoir 2 (80 µm) at Qc/Qd of 25.

Table 9 - Summary of the minimum, maximum, and average size values of the droplets obtained at different flow rates ratio values (Qc/Qd).

$Q_{continuous}/Q_{dispersed}$	MINIMUM	MAXIMUM	AVERAGE
5	122.9	160.5	145.0
10	196.7	129.3	106.7
15	95.9	119.5	108.6
20	91.0	108.9	101.5
25	77.3	99.5	89.4

Table 10 - Summary of the minimum, maximum, and average size values of the droplets obtained at different flow rates ratio values (Qc/Qd).

$Q_{continuous}/Q_{dispersed}$	MINIMUM	MAXIMUM	AVERAGE
5	124.3	158.6	142.0
10	106.6	126.3	114.8
15	100.0	121.0	111.4
20	95.4	113.7	103.1
25	74.7	97.4	86.7

Annex 6 – Passive Sorting Experiments

6.1 First Set

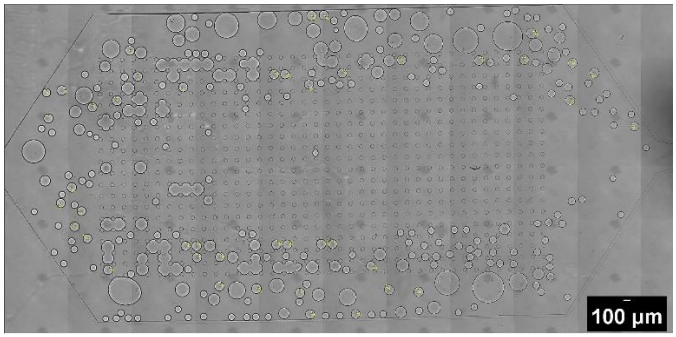

1500 µL_R1_100 µm_Waste

Droplets			
Size	Total	With cells	Empty
~110	44	11	33

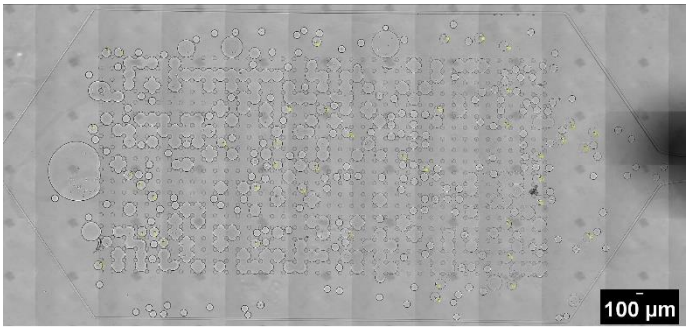

1500 µL_R2_100 µm_Sorting

Droplets			
Size	Total	With cells	Empty
~110	43	9	34

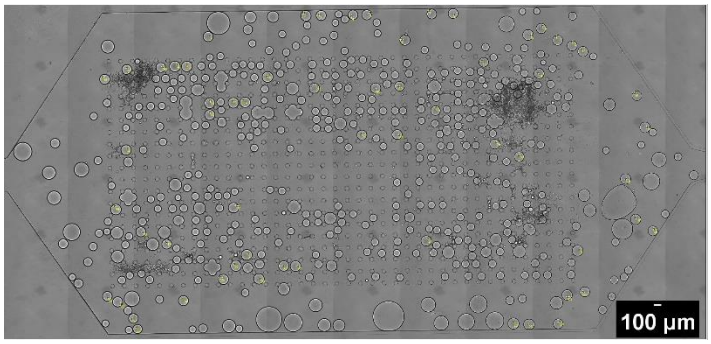

1500 µL_R3_100 µm_Waste

Droplets			
Size	Total	With cells	Empty
~110	62	11	51

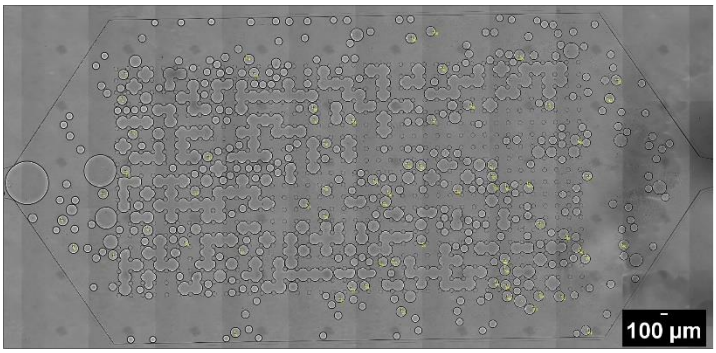

1500 µL_R4_100 µm_Sorting

Droplets			
Size	Total	With cells	Empty
~110	66	10	56

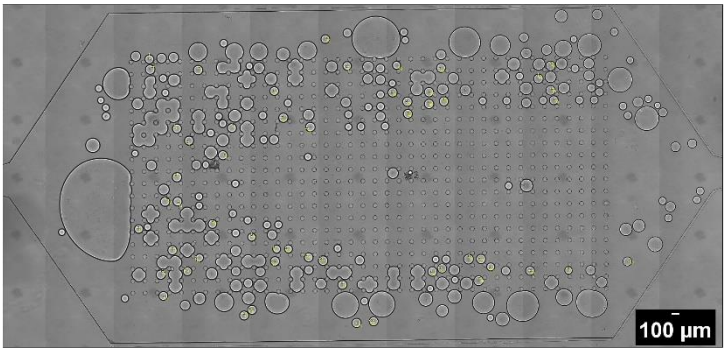

2000 µL_R1_100 µm_Waste

Droplets			
Size	Total	With cells	Empty
~100	54	7	47

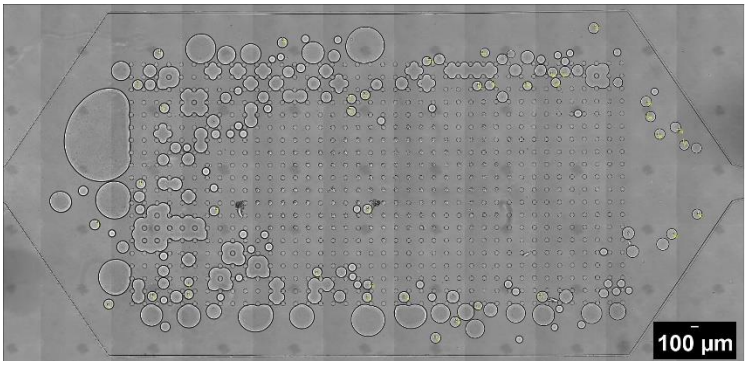

2000 µL_R2_100 µm_Sorting

Droplets			
Size	Total	With cells	Empty
~100	39	3	36

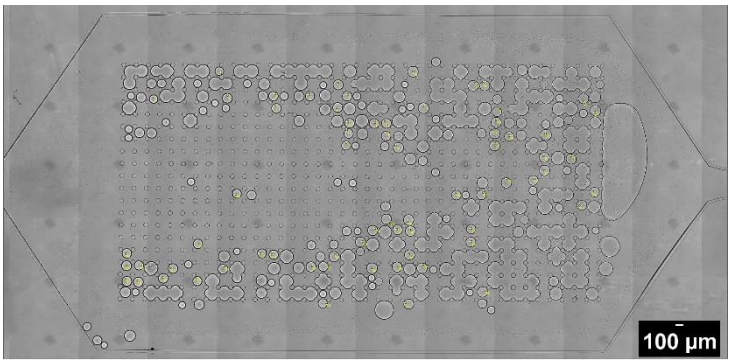

2000 µL_R3_100 µm_Waste

Droplets			
Size	Total	With cells	Empty
~100	68	4	64

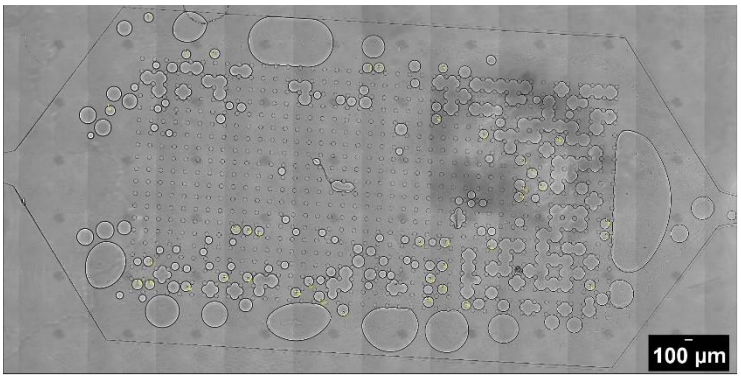

2000 µL_R4_100 µm_Sorting

Droplets			
Size	Total	With cells	Empty
~100	40	1	39

Figure 43 - Scan images of the reservoirs used for the passive sorting experiments with the cell density of 1×10^6 and respective tables with the total number of droplets analysed differentiating the number of droplets with cells and the number of empty droplets.

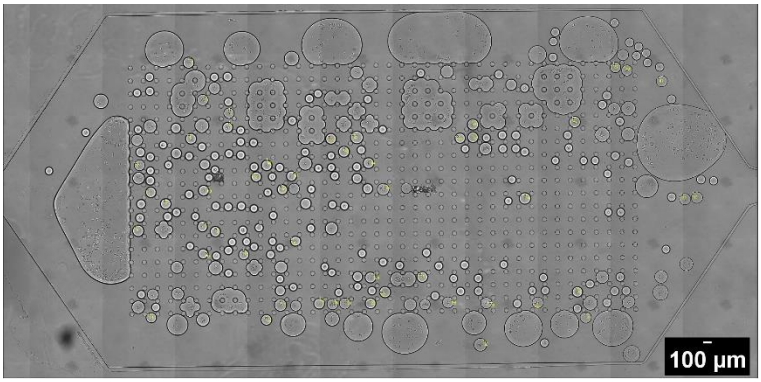

1500 µL_R1_100 µm_Waste

Droplets			
Size	Total	With cells	Empty
~110	50	43	7

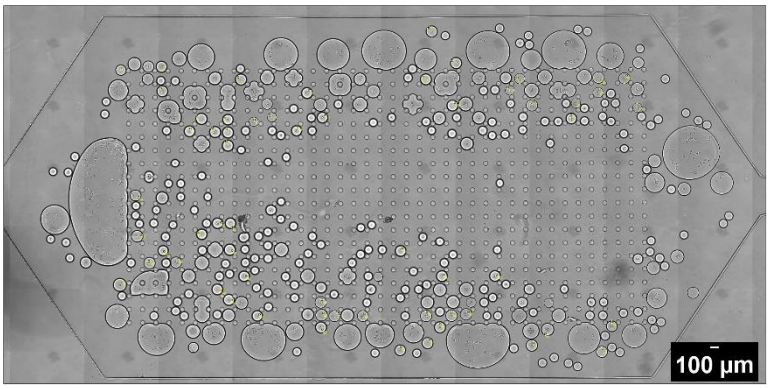

1500 µL_R2_100 µm_Sorting

Droplets			
Size	Total	With cells	Empty
~110	60	48	12

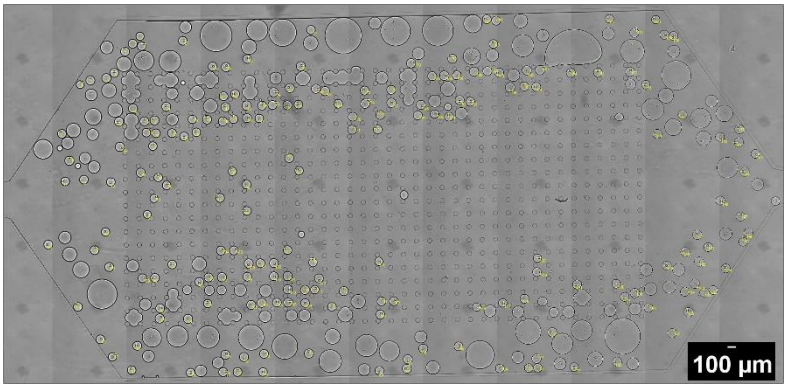

1500 µL_R3_100 µm_Waste

Droplets			
Size	Total	With cells	Empty
~110	197	26	171

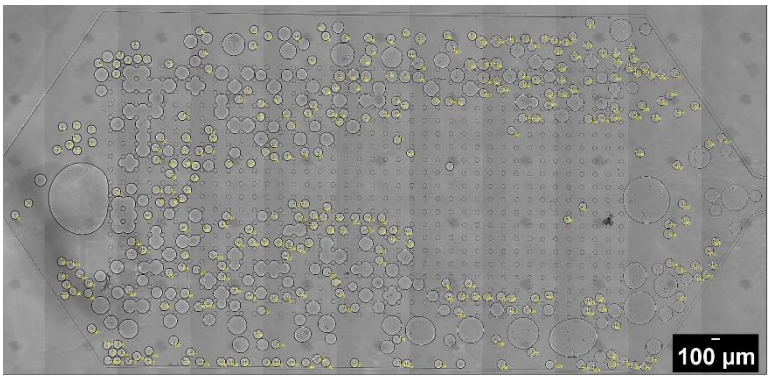

1500 µL_R4_100 µm_Sorting

Droplets			
Size	Total	With cells	Empty
~110	306	42	264

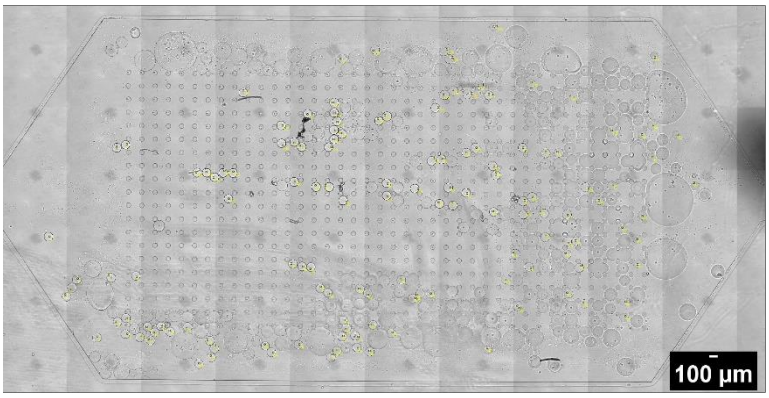

2000 µL_R1_100 µm_Waste

Droplets			
Size	Total	With cells	Empty
~100	135	10	125

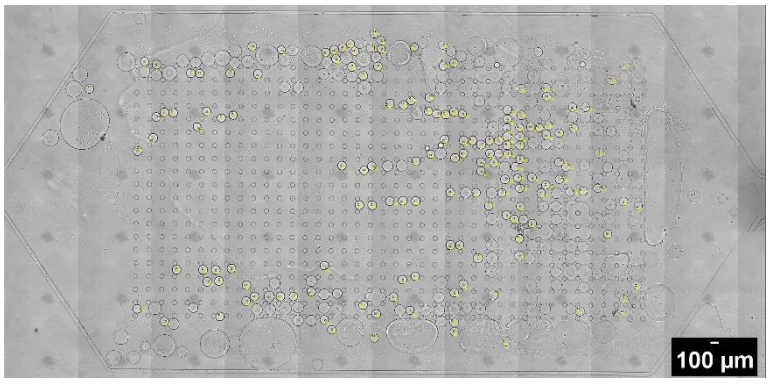

2000 µL_R2_100 µm_Sorting

Droplets			
Size	Total	With cells	Empty
~100	156	14	142

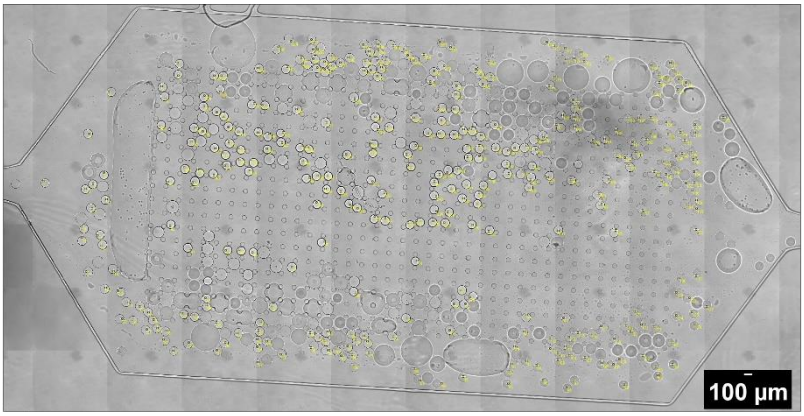

Droplets			
Size	Total	With cells	Empty
~100	356	2	354

2000 µL_R3_100 µm_Waste

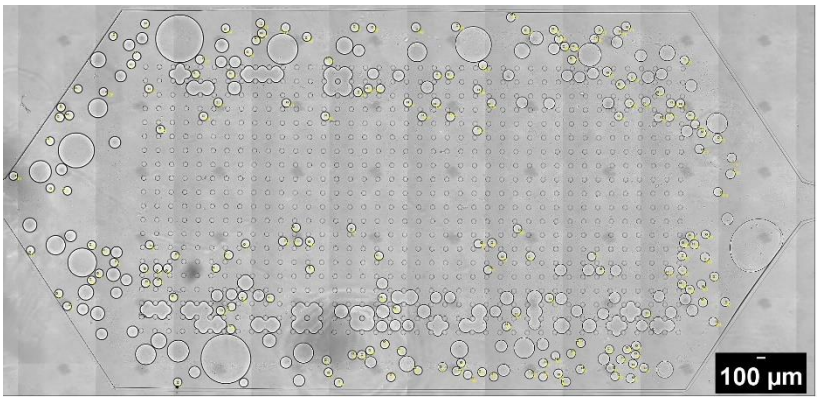

Droplets			
Size	Total	With cells	Empty
~100	175	1	174

2000 µL_R4_100 µm_Sorting

Figure 44 - Scan images of the reservoirs used for the passive sorting experiments with the cell density of 2×10^6 and respective tables with the total number of droplets analysed differentiating the number of droplets with cells and the number of empty droplets.

6.2 Second Set

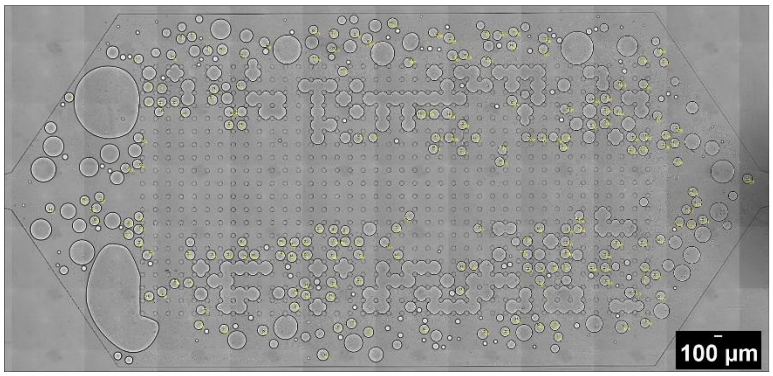

1000 µL_R1_100 µm_Waste

Droplets			
Size	Total	With cells	Empty
~110	188	26	162

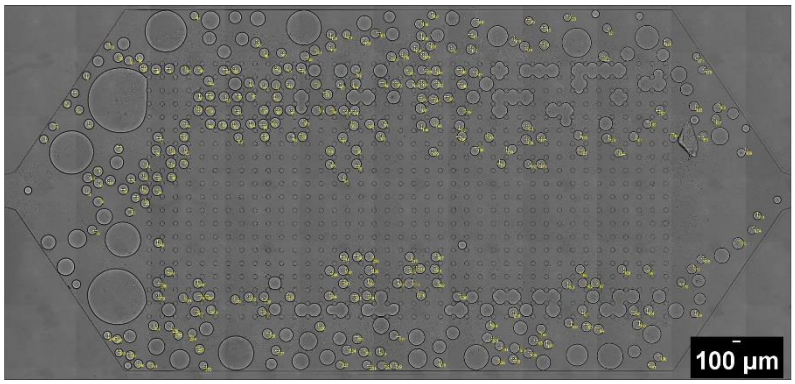

1000 µL_R2_100 µm_Sorting

Droplets			
Size	Total	With cells	Empty
~110	262	55	207

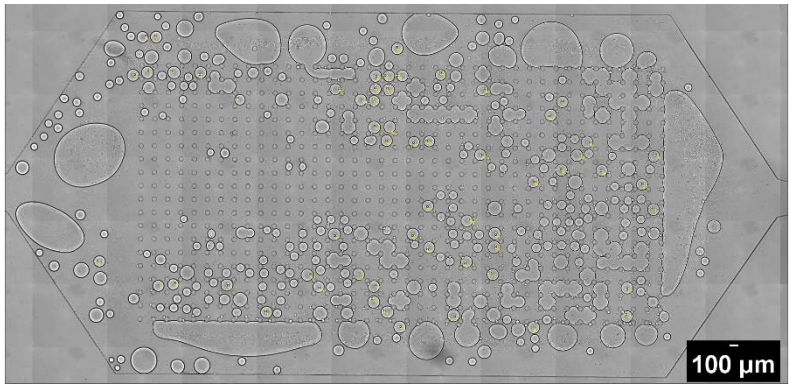

1500 µL_R1_100 µm_Waste

Droplets			
Size	Total	With cells	Empty
~110	59	9	50

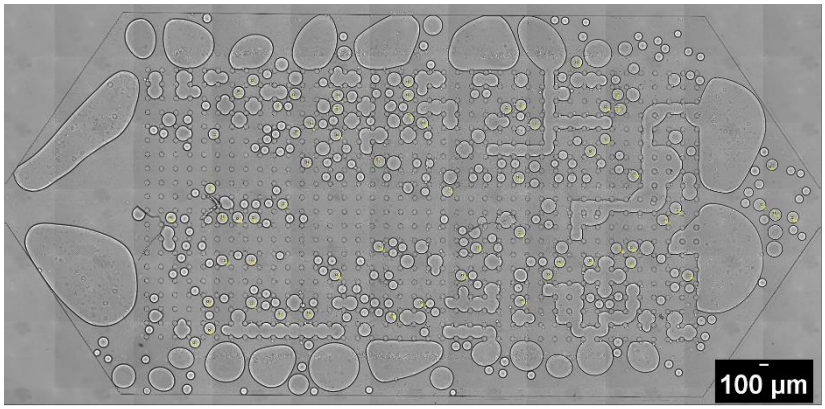

1500 µL_R2_100 µm_Sorting

Droplets			
Size	Total	With cells	Empty
~110	63	10	53

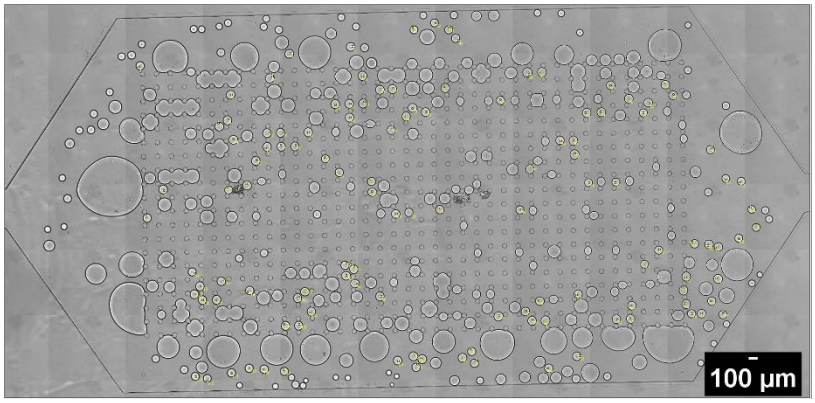

2000 µL_R1_100 µm_Waste

Droplets			
Size	Total	With cells	Empty
~100	121	8	113

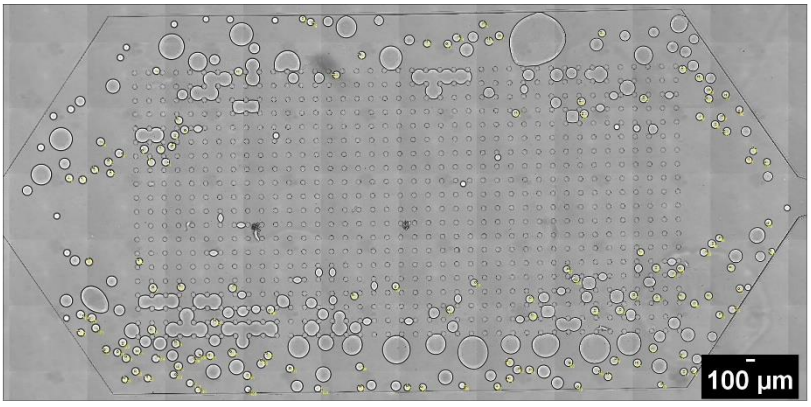

2000 µL_R2_100 µm_Sorting

Droplets			
Size	Total	With cells	Empty
~100	130	7	123

Figure 45 - Scan images of the reservoirs used for the passive sorting experiments with the cell density of 1×10^6 and respective tables with the total number of droplets analysed differentiating the number of droplets with cells and the number of empty droplets.

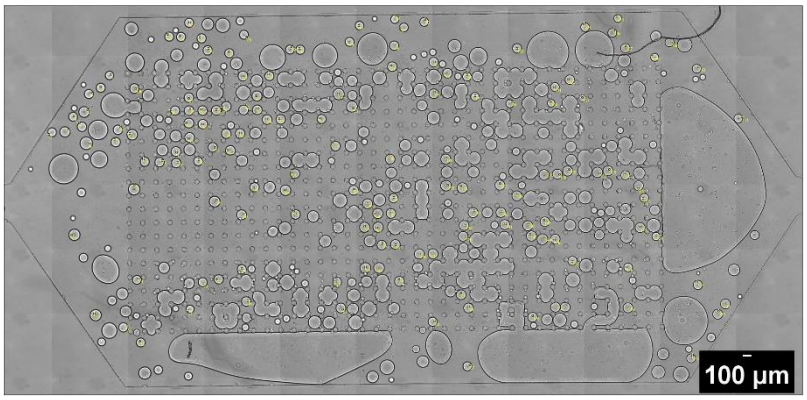

Droplets			
Size	Total	With cells	Empty
~110	153	68	85

1000 µL_R1_100 µm_Waste

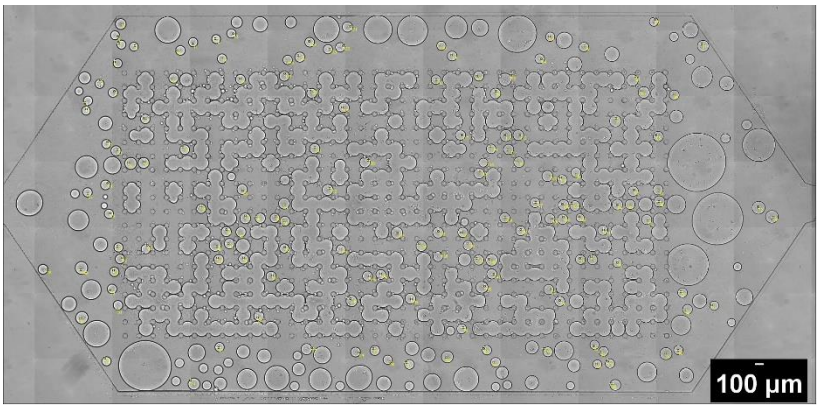

Droplets			
Size	Total	With cells	Empty
~110	150	50	100

1000 µL_R2_100 µm_Sorting

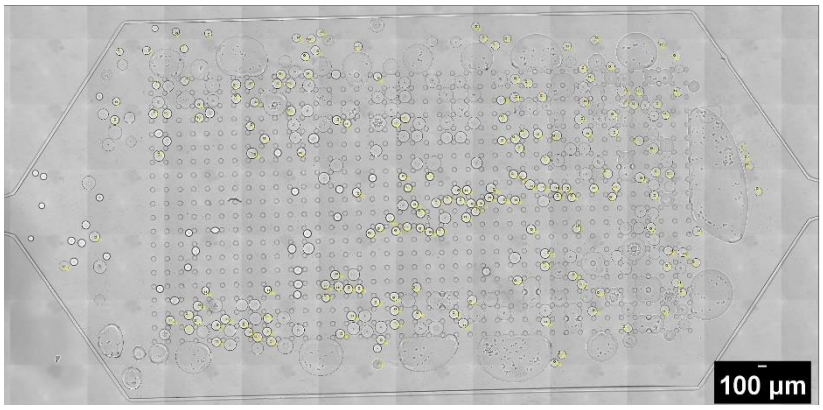

Droplets			
Size	Total	With cells	Empty
~110	183	37	146

1500 µL_R1_100 µm_Waste

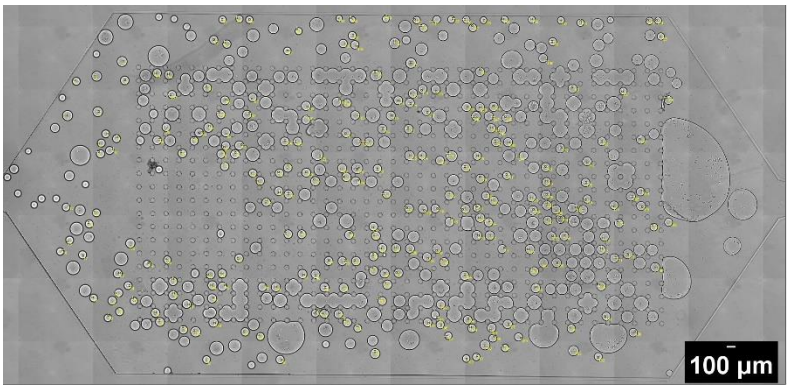

1500 µL_R2_100 µm_Sorting

Droplets			
Size	Total	With cells	Empty
~110	261	88	173

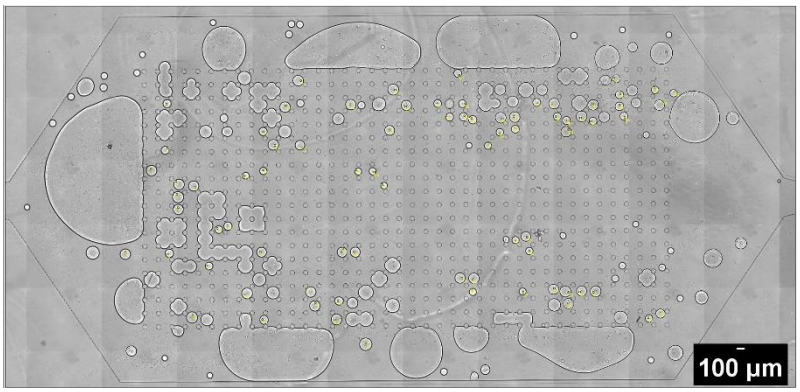

2000 µL_R1_100 µm_Waste

Droplets			
Size	Total	With cells	Empty
~100	80	23	57

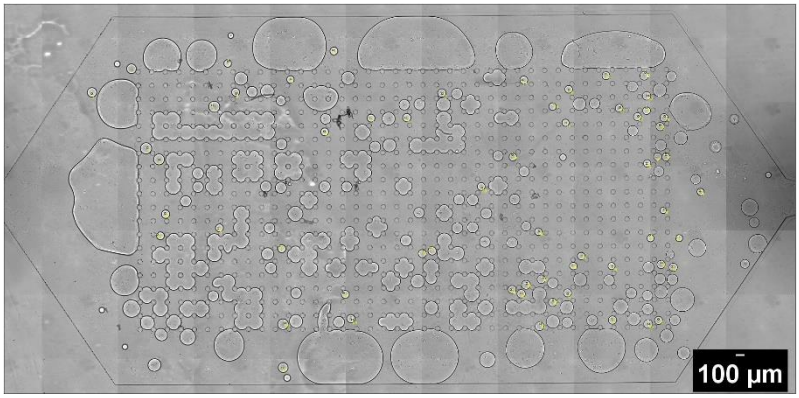

2000 µL_R2_100 µm_Sorting

Droplets			
Size	Total	With cells	Empty
~100	61	12	49

Figure 46 - Scan images of the reservoirs used for the passive sorting experiments with the cell density of 2×10^6 and respective tables with the total number of droplets analysed differentiating the number of droplets with cells and the number of empty droplets.

Annex 7 – Global Experiment

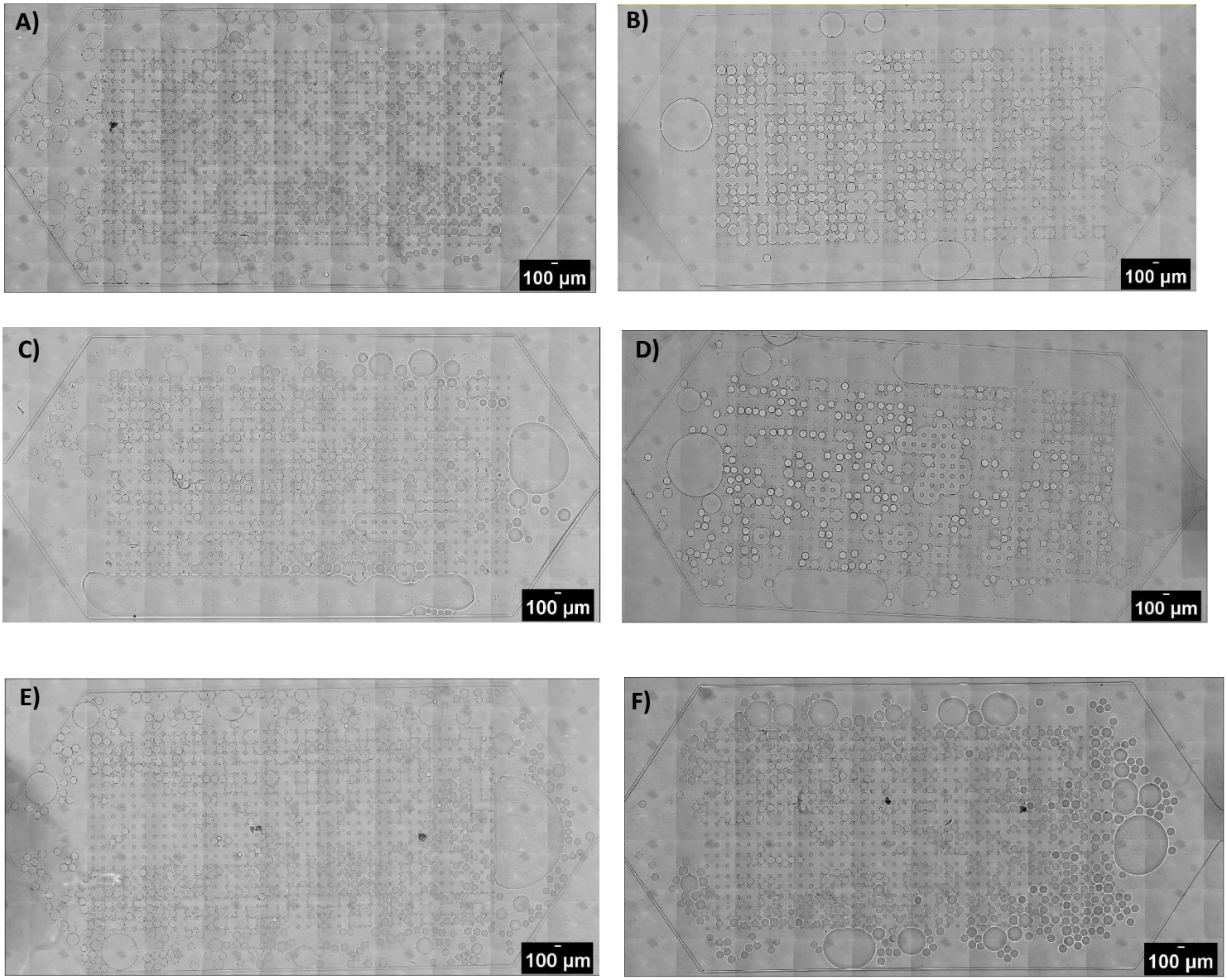

Figure 47 - Scan images of the reservoirs (100 µm) used for the droplet sorting experiments at flow rate ratio value of 10 and a target cells of 1000. A) Reservoir 1 (Waste) ; B) Reservoir 2 (Sorting) ; C) Reservoir 3 (Waste); D) Reservoir 4 (Sorting); E) Reservoir 5 (Waste); F) Reservoir 6 (Sorting).

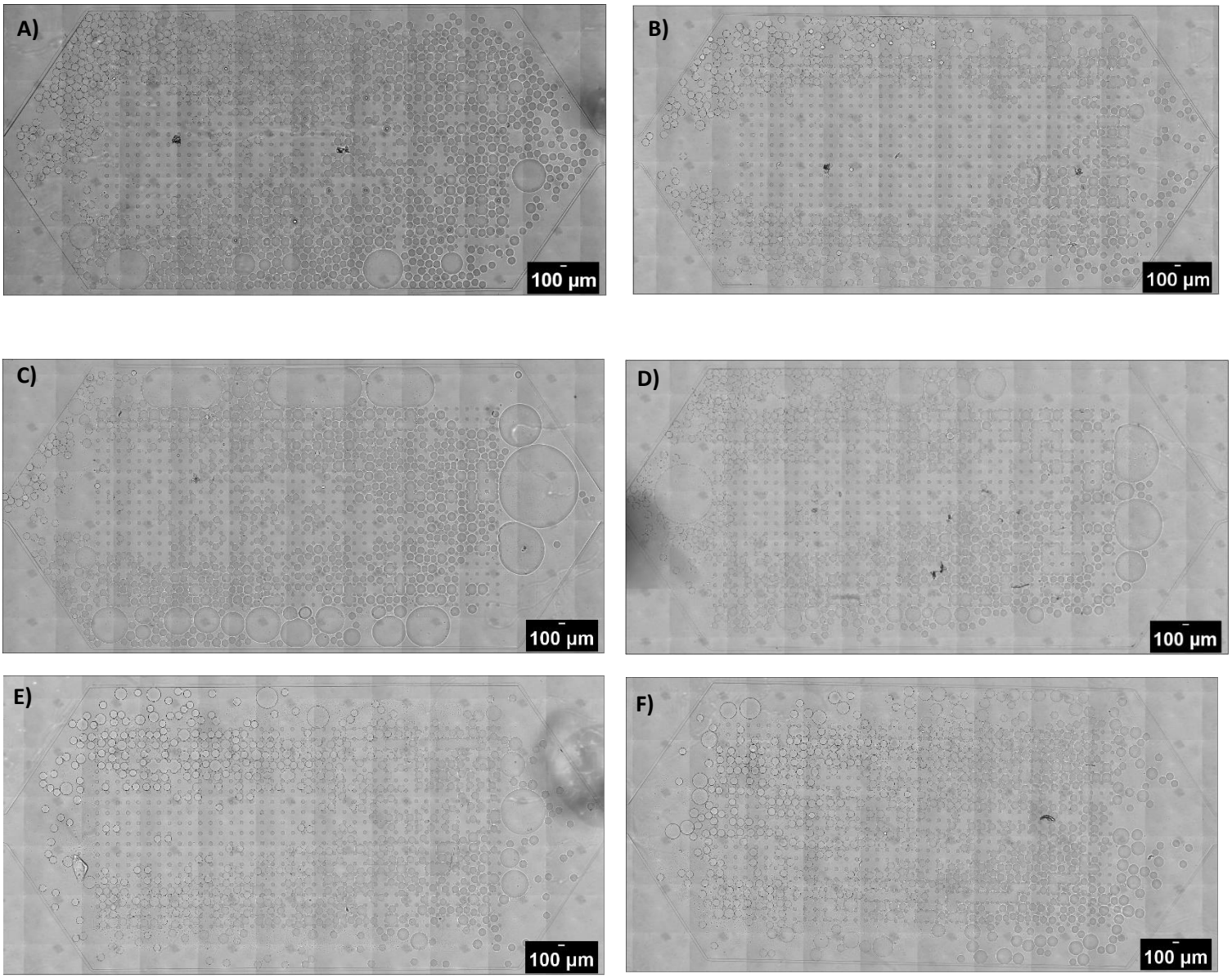

Figure 48 - Scan images of the reservoirs (100 µm) used for the droplet sorting experiments at flow rate ratio value of 10 and a target cells of 200. A) Reservoir 1 (Waste) ; B) Reservoir 2 (Sorting) ; C) Reservoir 3 (Waste); D) Reservoir 4 (Sorting); E) Reservoir 5 (Waste); F) Reservoir 6 (Sorting).